UNIVERSITY OF OKLAHOMA

GRADUATE COLLEGE

ECOSYSTEM RESPONSES TO CLIMATE VARIABILITY AND MANAGEMENT PRACTICES: DROUGHT ASSESSMENT (REMOTE SENSING), FIELD MEASUREMENTS (EDDY COVARIANCE) AND MODELING (DNDC)

A DISSERTATION

SUBMITTED TO THE GRADUATE FACULTY

in partial fulfillment of the requirements for the

Degree of

DOCTOR OF PHILOSOPHY

By

RAJEN BAJGAIN
Norman, Oklahoma
2017

ECOSYSTEM RESPONSES TO CLIMATE VARIABILITY AND MANAGEMENT PRACTICES: DROUGHT ASSESSMENT (REMOTE SENSING), FIELD MEASUREMENTS (EDDY COVARIANCE) AND MODELING (DNDC)

A DISSERTATION APPROVED FOR THE
DEPARTMENT OF MICROBIOLOGY AND PLANT BIOLOGY

BY

_____
Dr. Xiangming Xiao, Chair

_____
Dr. Jeffrey Basara

_____
Dr. Heather McCarthy

_____
Dr. Lara Souza

_____
Dr. Jean Steiner

This dissertation is dedicated to my parents and my wife for their unconditional love and support.

Acknowledgements

I especially thank to my major advisor, Dr. Xiangming Xiao, for his excellent guidance, encouragement, patience, and support during my research and study at The University of Oklahoma. This dissertation would not have been possible without the guidance and the support of several other individuals who in one way or another contributed and extended their valuable assistance for completion of the study. I would like to thank Dr. Jeffrey Basara, Dr. Heather McCarthy, and Dr. Lara Souza and Dr. Jean Steiner for serving on my committee. I owe a special thank you to several members of the crew in the Grazinglands Research Laboratory USDA-ARS, Drs. Prasanna Gowda, Pradeep Wagle, Patrick Starks, James Neel, and Brain Northup, for assisting in field data collection.

I extend my heartfelt thanks to my fellow colleagues in the Earth Observation and Modeling Facility group and in CHEWe group for their help and company during this work. I would like to express my full appreciation to the staffs of the Center for Spatial Analysis, especially Ms. Melissa Scott, and Ms. Leah Nash for their assistance. Thanks to the Department of Microbiology and Plant Biology for providing me the opportunity to continue my studies and research at the University of Oklahoma.

I would like to thank my wife, Rama Sapkota, for her support, encouragement, patience, and unwavering love. My deepest gratitude goes to my family members for their unflagging love and support throughout my life. I offer my regards and blessings to all of those who supported me in any respect during the completion of my Ph. D program.

Last but certainly not the least, I gratefully acknowledge research grants that made my Ph.D. work possible.

Table of Contents

List of Tables

List of Figures

Abstract

Climate variability and management practices in isolation or in combination influence the properties of ecosystems and the flows of energy and materials through them. The goal of this dissertation is to better understand the ecosystem responses to climatic variability and management practices using different approaches such as remote sensing, eddy covariance techniques and modelling. Remote sensing indices were tested and evaluated for developing better drought monitoring. Specifically, water related vegetation index (LSWI) was employed to assess the ecosystem responses to the drought events occurred in Oklahoma from 2000-2013. Field measurements data in combination with the EC system were used to understand how the sink-source potential of the ecosystem changes when grassland ecosystem is converted to winter wheat. DeNitrification- DeComposition (DNDC) model was used to analyze greenhouse gas emissions from pasture land amended with fertilizers compared to the native pastures in the scenario of climatic variability. We used 14 years of MODIS, Mesonet soil moisture and rainfall data at Marena and El Reno tallgrass prairie sites to study the impact of drought events on grassland phenology and growth through analyzing sensitivity differences of vegetation indices to drought. A new approach of drought assessment, counting number of days with LSWI < 0 and LSWI-based drought severity classification, is proposed in this study. The number of days with LSWI < 0 was found higher during the summer droughts of 2006 and 2012 and negative LSWI represented the higher intensity drought categories (D2, D3 and D4) defined by USDM, which demonstrated that it could be used to describe the hydrological condition of the ecosystem as an effective additional vegetation based indicator for drought assessment. This study also

investigates the potential of the LSWI-based algorithm, for agricultural drought monitoring under varying soil and land cover conditions of 113 Mesonet stations of Oklahoma. We compared LSWI and the number of days with negative LSWI (DNLSWI) to summer time precipitation, precipitation anomalies, and the U.S. Drought Monitor. Additionally, the assessment of the algorithm with USDM was performed separately for different land cover type and climate divisions. Therefore, results from this study will help in improving the capability of remote sensing vegetation drought monitoring by establishing LSWI as a complimentary tool to existing NDVI based drought products as well as help to identify the sensitivity of LSWI to the diversity of the ecosystems of Oklahoma.

We quantified and compared the carbon and water fluxes from winter wheat and tallgrass prairie ecosystems and discussed the possibility of change in carbon and water budgets of the southern plains under the land use change scenario (conversion of grassland into winter wheat). Both ecosystems were sinks of carbon during their respective growing seasons. At the annual scale, the wheat ecosystem was a net source of carbon (128 ± 46 g C m^{-2} yr^{-1}) when fluxes from summer fallow period were considered. Results suggest that the differences in magnitudes and patterns of CO_2 and H_2O fluxes between winter wheat and tallgrass prairie ecosystems can exert an influence on the carbon and water budgets of the whole region under land use change scenario. Another hypothesis tested in our study was that the application of fertilizers in the managed pasture would increase the primary productivity of the ecosystem for few years but this increase in carbon sink would be counteracted by the increasing rate of greenhouse gas emissions in the long run. Here we used DNDC, a process-based model that simulates the

emissions and consumption of gases within the ecosystem based on the interactions of local climate, local soils and on-site management practices. The fertilization of pasture increased the productivity that increased the roughages demands resulted by increased stocking density of cattle. Similarly, higher flux of N_2O from the managed pasture was resulted as the effect of fertilizer addition which amplified in magnitude in wet years than dry and normal years. The advantage from increased soil organic carbon due to the fertilizer application, measured in terms of global warming potential (GWP) was outweighed by the GWP calculated from the increased magnitude of N_2O fluxes thereby giving the positive net global warming potential (NGWP). Therefore, pasture management policies should consider maintaining emissions level as minimum as possible while optimizing the productivity.

Chapter 1: Introduction

1.1 Research background

Climate variability and management practices in isolation or in combination influence the properties of ecosystems and the flows of energy and materials through them (Fig 1.1). Models results shows large uncertainty in the estimates of plant productivity changes with the changes in temperature, moisture and rainfall that interact in influencing plant growth (Heinsch et al. 2006; Hilker et al. 2008). The effects of climate variability on ecosystems are likely to be exacerbated in ecosystems that are altered by anthropogenic interventions (Cramer et al. 1999; Huntzinger et al. 2012; Thebault et al. 2014). The question about how the change in patterns of weather elements will affect the complex interactions and feedbacks of ecosystems with diverse management activities is yet to be elucidated for addressing the uncertainties existed in model outputs.

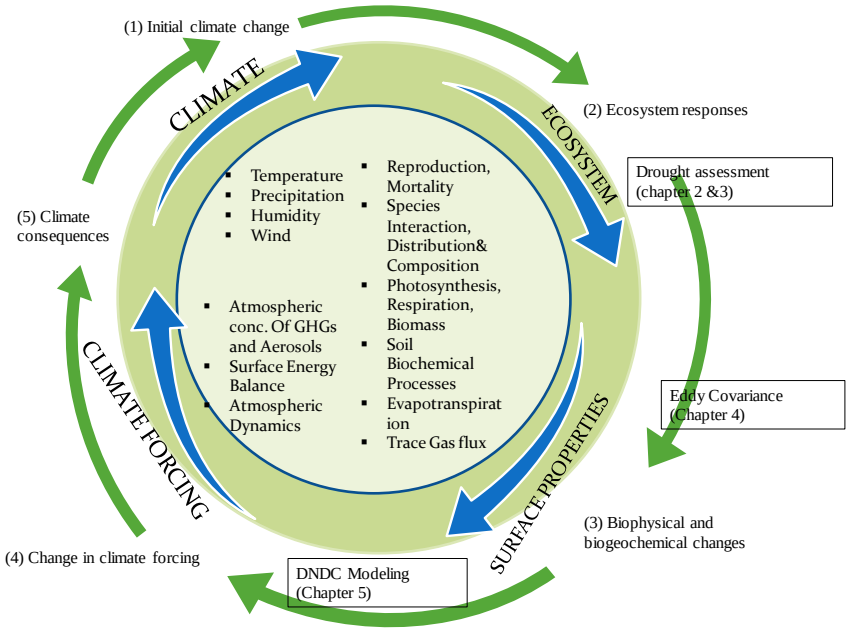

Figure 1.1. Two-way interactions between climate and ecosystem.

The Southern Great Plains (SGP) of the US is one of the most volatile region with respect to climatic variability especially rainfall. The ecosystems of this region have responded enormously to the dynamics of drought and wet events in the past (Basara et al. 2013b; Christian et al. 2015a). The ecosystem feedback in terms of productivity is generally positive in good rainfall year and is negative when it is impacted by drought. This kind of impact resulted from rainfall variability at the larger spatial extent have been monitored by using the vegetation indices derived from satellite observations. Yet, the repeated occurrence of drought events has highlighted the need to develop effective drought monitoring tools to assess the impacts of this phenomenon. It is well known that Normalized Difference Vegetative Index (NDVI) is related to leaf area index (LAI), and NDVI will decline when plant canopy defoliates due to drought, which often occur at late stage of severe agricultural drought. It is also well assumed that EVI is related to green and chlorophyll in the canopy, and Enhanced Vegetative Index (EVI) will decline when plant canopy starts to lose chlorophyll due to drought. When drought occurs, plant canopy will experience (1) loss of water in leaves, (2) loss of chlorophyll pigment in leaves (e.g., yellowing), and (3) loss of green leaves over time (dead leaves, defoliation). Land surface water index (LSWI) reflects the loss of water in leaves. EVI reflects the loss of chlorophyll in leaves. NDVI reflects the loss of green leaves. The hypothesis that the water related vegetation index LSWI computed based on Near infra-red (NIR) and Shortwave infra-red (SWIR) of electromagnetic spectrum is more sensitive to vegetation water content offers a new and improved capacity for drought monitoring, an approach to assess the ecosystem responses to drought.

Ecosystem responses to climatic variability and management practices causing altered species composition, productivity, vegetation phenology, canopy roughness and others may result in biophysical and/or biogeochemical feedbacks. Land use change as an example of a management practices impact the biophysical pathways that alter the exchange processes such as carbon, energy and water exchanges between the ecosystem and atmosphere. The eddy covariance (EC) systems provide continuous measurements of ecosystem-level net exchange of carbon, water, and energy between land surface and the atmosphere under different management scenario. Net Ecosystem Exchange is used to indicate whether the ecosystem is a carbon sink or source.

Biogeochemical feedbacks involve ecosystem changes when climate and management activities cause change in uptake and release rate of greenhouse gas (GHGs) emissions. Pasture grasslands used to graze livestock make up about 45% of land use southern Great Plains are also one of the most sensitive and important ecosystems of North America. Better Grassland management practices thus have the potential to mitigate climate change by shaping carbon sequestration and methane production (Smith et al. 2000). Native grasslands are often managed with the aim of enhancing Net Primary Production (NPP, the amount of plants dry matter produced per unit time through carbon fixation). But management activities like fertilizer application, deposition of manure by livestock, burning, tillage practices can have substantial influence on the fundamental biophysical processes such as mineralization and decomposition because addition of such managements inputs changes the soil Carbon (C) and Nitrogen (N) pool. This, in turn, can alter the soil environmental conditions such as moisture, temperature, pH and Eh (redox potential) thereby increasing the magnitude of the greenhouse gas (GHG) emission.

1.2 Overall research objectives

The goal of this dissertation is to better understand the ecosystem responses to climatic variability and management practices using different approaches such as remote sensing, eddy covariance techniques and modelling. Specifically, my dissertation focuses on three major topics: (1) Remote sensing indices were tested and evaluated for developing better drought monitoring. Water related vegetation index (LSWI) was employed to assess the ecosystem responses to the drought events occurred in Oklahoma from 2000-2013; (2) field measurements data in combination with the EC system to understand how the sink-source potential of the ecosystem changes when grassland ecosystem is converted to winter wheat; and (3) to model the greenhouse gas (GHGs) emissions from managed pasture amended with fertilizers compared to the native pastures in the scenario of climatic variability.

1.3. Organization of the dissertation

This dissertation consists of one introductory chapter, four main chapters, and one summary chapter. Chapters 2, 3 have been published in two peer-reviewed journals, chapter 4 is submitted to the peer-reviewed journal, and chapter 5 is in preparation and will be submitted to one of the peer-reviewed journals.

Chapter 2: This study aims to develop an LSWI-based drought monitoring algorithm based on two tallgrass prairie ecosystems in Oklahoma. This study describes an exploration of vegetation indices, both greenness related (NDVI and EVI) and water related (LSWI), as drought indicators. The key to this study is the site-specific analysis

and the comparison with the USDM index. We used 14 years of MODIS, Mesonet soil moisture and rainfall data at Marena and El Reno tallgrass prairie sites to study the impact of drought events on grassland phenology and growth through analyzing sensitivity differences of vegetation indices to drought. A new approach of drought assessment, counting number of days with LSWI < 0 and LSWI-based drought severity classification, is proposed in this study. The number of days with LSWI < 0 was found higher during the summer droughts of 2006 and 2012 and negative LSWI represented the higher intensity drought categories (D2, D3 and D4) defined by USDM, which demonstrated that it could be used to describe the hydrological condition of the ecosystem as an effective additional vegetation based indicator for drought assessment.

***Chapter 3*:** This study investigated the potential of the Land Surface Water Index (LSWI)-based algorithm developed in Chapter 2, for agricultural drought monitoring under varying soil conditions of 113 Mesonet stations of Oklahoma. We compared LSWI and the number of days with negative LSWI (DNLSWI) to summer time precipitation, precipitation anomalies, and the U.S. Drought Monitor. Additionally, the assessment of the algorithm with USDM was performed separately for different land cover type and climate divisions. Therefore, results from this study will help in improving the capability of remote sensing vegetation drought monitoring by establishing LSWI as a complimentary tool to existing NDVI based drought products as well as help to identify the sensitivity of LSWI to the diversity of the ecosystems of Oklahoma.

Chapter 4: This study quantified and contrasted the carbon and water fluxes from winter wheat and tallgrass prairie ecosystems and discussed the possibility of change in carbon and water budgets of the Southern Plains under the land use change scenario (conversion of grassland into winter wheat). We measured the exchange of carbon dioxide and water vapor fluxes from two major ecosystems, located very few kilometers away in OK using the eddy covariance technique. This study has a great significance in order to understand the impacts of land conversion from grassland to winter wheat since the Southern Plains of the United States has seen the dramatic land use change in the over the past century.

Chapter 5: The hypothesis tested in this chapter is that the application of fertilizers in the managed pasture would increase the primary productivity of the ecosystem for few years but this increase in carbon sink would be counteracted by the increasing rate of GHGs emissions in the long run. Here we used the De-Nitrification De-Composition (DNDC), a process-based model that simulates the emissions and consumption of gases within the ecosystem based on the interactions of local climate, local soils and on-site management practices. By combining field measurements and modeling simulations, we examined the effects of grassland management practices on the net carbon balance and GHGs emissions in the managed pasture amended with fertilizers. Fertilizer application increased the productivity and soil organic carbon (SOC) pool whereas grazing decreased the SOC pool. Farm management practices altered the soil moisture, temperature, redox potential, and SOC and available Nitrogen content. The change in these factors changed the rate and direction of nitrification, denitrification and decomposition either collectively or simultaneously and ultimately the GHGs emissions.

1.4 List of Publications from the dissertation

Chapter 2

Bajgain, R., X. Xiao, P. Wagle, J. Basara, and Y. Zhou. 2015. Sensitivity of Vegetation Indices to Drought over Two Tallgrass Prairie Sites. ISPRS International Journal of Photogrammetry and Remote Sensing (2015), 108: 151-160

Chapter 3

Bajgain, R., X. Xiao, P. Wagle, J. Basara, and Y. Zhou. 2016. Assessing agricultural drought in summer over Oklahoma Mesonet Sites using the water related vegetation index from MODIS. International Journal of Biometeorology (2016), 61:377 - 390

Chapter 4

Bajgain, R., X. Xiao, J. Basara, P. Wagle, Y. Zhou, M. Hayden, P. Gowda, H. McCarthy, B. Northup, J. Neel and J. Steiner. Contrasting carbon dioxide and water vapor fluxes between winter wheat and tallgrass prairie in central Oklahoma, Agricultural and Forest Meteorology (under review)

Chapter 5

Bajgain, R., X. Xiao, J. Deng, M. Arango, B. Peterson, S. Frolking and J. Steiner. Modeling of carbon sequestration and greenhouse gas dynamics in native and managed pasture, Nutrient Cycling in Agroecosystems (in preparation).

Chapter 2: Sensitivity analysis of vegetation indices to drought over two tallgrass prairie sites

Abstract

Vegetation growth is one of the important indicators of drought events. Greenness-related vegetation indices (VIs) such as Normalized Difference Vegetation Index (NDVI) and Enhanced Vegetation Index (EVI) are often used for the assessment of agricultural drought. There is a need to evaluate the sensitivity of water-related vegetation indices such as Land Surface Water Index (LSWI) to assess drought and associated impacts. Moderate-Resolution Imaging Spectroradiometer (MODIS) derived time series NDVI, EVI and LSWI data during 2000-2013 were compared for their sensitivity to drought at two tallgrass prairie sites in the Oklahoma Mesonet (Marena and El Reno). Each site has continuous soil moisture measurements at three different depths (5, 25 and 60 cm) and precipitation data for the study period (2000-2013) at 5-minute intervals. As expected, averaged values of vegetation indices consistently lower under drought conditions than normal conditions. LSWI decreased the most in drought years (2006, 2011 and 2012) when compared to its magnitudes in pluvial years (2007, 2013), followed by EVI and NDVI, respectively. Because green vegetation has positive LSWI values (> 0) and dry vegetation has negative LSWI values (< 0), much longer durations of LSWI < 0 were found in the summer periods of drought years rather than in pluvial years. A LSWI-based drought severity scheme (LSWI > 0.1; $0 <$ LSWI ≤ 0.1; $-0.1 <$ LSWI ≤ 0; LSWI ≤ -0.1) corresponded well with the drought severity categories (0; D0; D1: D2; D3 and D4) defined by the United States Drought Monitor (USDM) at these two study sites. Our results indicate that the number of days with LSWI < 0 during the

summer and LSWI-based drought severity scheme can be simple, effective and complementary indicator for assessing drought in tallgrass prairie grasslands at a 500-m spatial resolution.

2.1 Introduction

Drought is a recurring event of Oklahoma`s climate cycle (Basara et al. 2013b; Christian et al. 2015a) and poses significant impacts on various sectors of the economy (OWRB, 2010). Seasonal drought can occur at any time of the year and the summer drought that coincides with the growing season can cause ecological imbalances and influences surface biophysical parameters such as vegetation indices, land surface temperature, soil moisture and evapotranspiration (Ghulam et al. 2007; Reichstein et al. 2002). This ultimately impacts the productivity of the tallgrass prairie ecosystem, which can cause billions of dollars in damage to livestock's industries depending on its timing, duration and severity.

Several conceptual definitions of drought have been classified into four major categories: meteorological, agricultural, hydrological and socio-economic droughts (Wilhite and Glantz 1985). Understanding the need to quantify drought severity, researchers have developed several methods to assess and diagnose different droughts. Meteorological drought indices (Rainfall Anomaly Index, Bhalme and Mooley Drought Index, Drought Severity Index, Standardized Precipitation Index) were solely based on meteorological data such as precipitation and temperature (Bhalme et al. 1981; McKee et al. 1993; Van Rooy 1965). Agricultural drought indices (Crop Moisture Index, the Soil moisture Drought Index, Soil Moisture Deficit Index) considered soil moisture and

evapotranspiration deficit (Hollinger et al. 1993; Narasimhan and Srinivasan 2005; Palmer 1965), while hydrological drought indices (Palmer Hydrological Drought Index, Surface Water Supply Index, Reclamation Drought Index) were based on a water balance model (Shafer and Dezman 1982; Weghorst 1996).

With the advancement of Earth observations from satellite-based sensors, numerous recent studies have used remote sensing data for assessing drought impacts (Ghulam et al. 2007; Peters et al. 2002; Tadesse et al. 2005; Wan et al. 2004). Over the period of more than 20 years, a number of remote sensing based vegetation indices (VIs) have been developed from various spectral band combinations to monitor vegetation (Table 2.1). While greenness-related VIs retrieved from remote sensing land surface reflectance such as Normalized Difference Vegetation Index (NDVI) and Enhanced Vegetative Index (EVI) have often been used for vegetation condition monitoring (Diodato and Bellocchi 2008; Herrmann et al. 2005; Song and Ma 2011), NDVI derived indices such as Anomaly Vegetation Index (Weiying et al. 1994) and the Vegetation Condition Index (VCI) (Kogan 1995) were used to relate vegetation dynamics to drought patterns. Similarly, several water related satellite-based vegetation indices that estimate vegetation water content have been used for drought detection (Chen et al. 2005; Fensholt and Sandholt 2003; Gao 1996; Kimes et al. 1981). Shortwave infrared reflectance (SWIR) and leaf water content are negatively related due to the large absorption (Hunt and Rock 1989; Tucker 1980) and is contrasted with near infrared (NIR) band to normalize the effects of other leaf parameters such as internal leaf structure for proper estimation of vegetation water content (Ceccato et al. 2001; Gao 1996). Based on the analysis of reflectance spectra, combination of SWIR and NIR bands have been reported

by numerous studies under different names: Normalized Difference of Landsat TM bands 4 and 5, ND45 (Kimes et al. 1981); Normalized Difference Infrared Index, NDII (Hardisky et al. 1983); Shortwave Water Stress Index, SWIS (Fensholt and Sandholt 2003); Normalized Difference Water Index, NDWI (Jackson et al. 2004; Maki et al. 2004) and Land Surface Water Index, LSWI (Qin et al. 2015; Xiao et al. 2002; Zhang et al. 2015).

Table 2.1. Drought indices based on different spectral bands and their combination.

Name of Vegetation indices	Full name	Formula	References
NDVI	Normalized Difference Vegetation Index	*(ρ858 – ρ650)/(ρ858+ρ650)*	Tucker, 1979; Kogan, 1991; Kogan, 1995
EVI	Enhanced Vegetation Index	*2.5*(ρ858 – ρ650)/(ρ858+6* ρ650-7*ρ469+1)*	Huete et al. 2002; Saleska et al. 2007
WI	Water Index	*ρ900/ρ970*	Peñuelas et al. 1993, 1997
$NDWI_{1240}$	Normalized Difference Water Index	*(ρ858– ρ1240)/(ρ858+ρ1240)*	Gao, 1996
NDII	Normalized Difference Infrared Index	*(ρ850 – ρ1650)/(ρ850+ρ1650)*	Kimes et al. 1981; Hardisky et al. 1983
MSI	Moisture Stress Index	*ρ1600/ρ820*	Hunt et al. 1989
SRWI	Simple Ratio Water Index	*ρ858 /ρ1240*	Zarco-Tejada et al. 2001, 2003
LSWI	Land Surface Water Index	*(ρ858– ρ1640)/(ρ858+ρ1640)*	Xiao et al. 2002
SWISI	Shortwave Infrared Water Stress Index	*(ρ1640-ρ850)/(ρ1640+ρ850) or (ρ1240-ρ850)/(ρ1240+ρ850)*	Fensholt and Sandholt 2003
$NDWI_{2130}$	Normalized Difference Water Index	*(ρ858– ρ2130)/(ρ858+ρ2130)*	Chen and Huang, 2005
NMDI	Normalized Multiband Drought Index	*(ρ860–(ρ1640-ρ2130))/ (ρ860+(ρ1640- ρ2130))*	Wang et al. 2007
VTCI	Vegetation Temperature Condition Index	*NDVI, Land Surface Temperature(LST)*	Morgan et al. 1995; Wan et al. 2004
TVDI	Temperature Vegetation Dryness Index	*NDVI, LST*	Sanholt et al. 2002
SDCI	Scaled Drought Condition Index	*LST, NDVI, Precipitation*	Rhee et al, 2010
VCI	Vegetation Condition Index	$(NDVI - NDVI_{MIN}) / (NDVI_{MAX} - NDVI_{MIN})$	Kogan, 1995
VHI	Vegetation Health Index	*NDVI, LST*	
NDDI	Normalized Difference Drought Index	*(NDVI-NDWI)/(NDVI+NDWI)*	Gu et al.2007

These indices have proven to be effective in monitoring the water content of vegetation. However, NDVI has been the most popular and extensively used satellite-based index for drought monitoring over the past decades. Numerous studies have analyzed the relationships between NDVI and rainfall across geographical areas and vegetation types (Bhalme et al. 1981; Boschetti et al. 2013; McKee et al. 1993; Van Rooy 1965). In the central and northern Great Plains grasslands, growing season rainfall, growing degree days and potential evapotranspiration exerted strong control over grassland productivity (Yang et al. 1998). There was a stronger relationship between NDVI and rainfall than between NDVI and temperature for the grassland located in the central and northern Great Plains of the US (Wang et al. 2001). Like other drought monitoring algorithms (Ji and Peters 2003; Liu and Kogan 1996; Nemani and Running 1989; Pettorelli et al. 2005), the Vegetation Drought Response Index (VegDRI) introduced by the United States Drought Monitor (USDM) also used NDVI in monitoring droughts (Brown et al. 2008). A few recent publications have reported that water-related vegetation indices such as LSWI are relatively more sensitive to drought than greenness related VIs and presented as a potential drought monitoring tool (Chandrasekar et al. 2010; Gu et al. 2008; Wagle et al. 2015c; Wagle et al. 2014; Zhang et al. 2013). Long term analysis of LSWI over pluvial, dry and normal years can provide better insight into vegetation response to climate variations and complement current drought monitoring tools to incorporate water related vegetation index into their models and algorithms.

In this pilot and site-level study, we chose two tallgrass prairie sites in Oklahoma, which are the part of the Oklahoma Mesonet (McPherson et al. 2007). The objectives of this study were to: a) explore the relationship between seasonal and inter-annual rainfall

variability and dynamics of grassland vegetation growth, and b) ascertain the sensitivity of VIs (NDVI, EVI and LSWI) to rainfall variations. This study further investigates additional drought information rendered by LSWI, based on episodic drought events over time series (2000-2013). Using the drought information generated from LSWI, a new approach (the number of days with LSWI < 0 during the plant growing season and LSWI-based drought severity classification) for an assessment of the drought impacts over grasslands is proposed in this study. This LSWI-based approach can potentially provide more insights into drought monitoring over tallgrass prairie grasslands.

2.2 Materials and Methods

2.2.1 Site description

The Marena site is located near Stillwater, OK (97.21694° W, 36.063493° N). This site is collocated with the Marena Oklahoma In-Situ Sensor Test bed (MOISST), a core calibration/validation site for NASA`s soil moisture active passive (SMAP) satellite mission. The site contains relatively homogenous distribution of tallgrass prairie in sandy clay loam soil with similar grazing management practices over the years.

The El Reno site is located near El Reno, OK (98.0401°W, 35.5465° N) at the United States Department of Agriculture-Agriculture Research Service (USDA-ARS) Grazing Research laboratory (GRL). The site is an open terrain, slightly sloped from east to west and is covered by natural tallgrass prairie in silty clay loam soil. The location and the landscape features of the study sites are shown in Fig. 2.1 while the biophysical features of the sites are presented in Table 2.1.

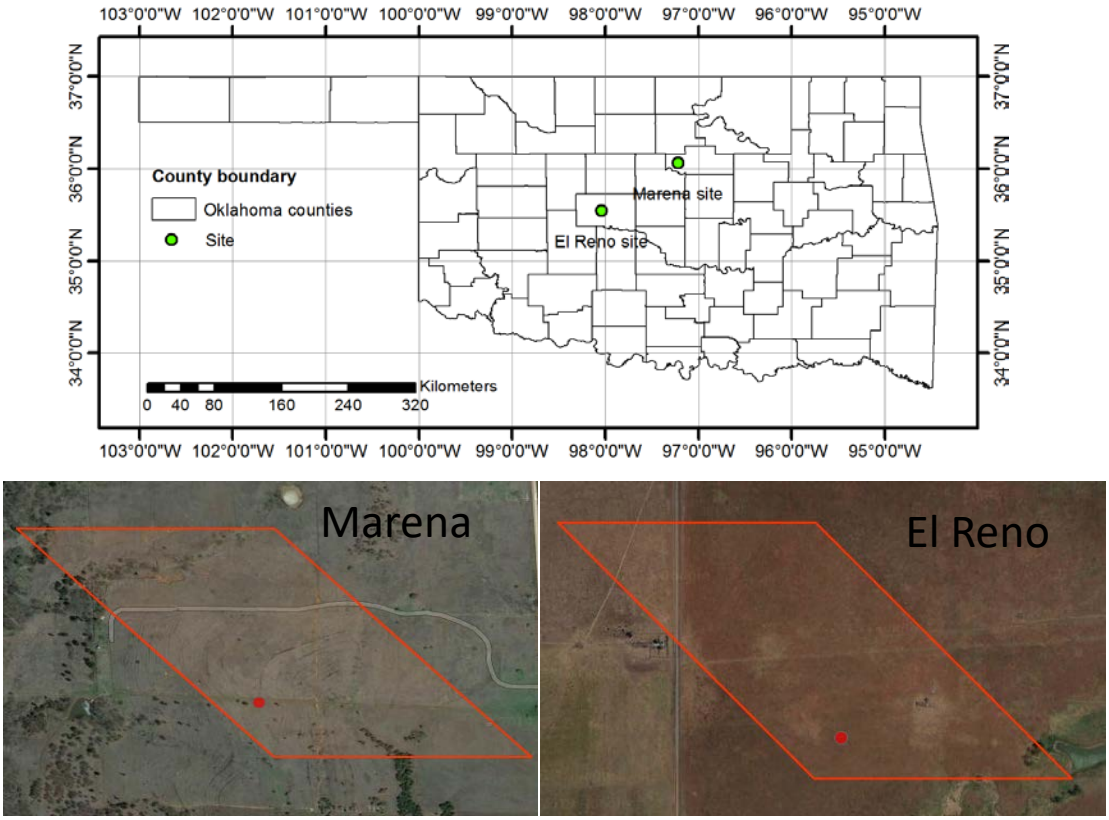

Figure 2.1. The location (Oklahoma map) and the landscape features of the study sites. The red boarder line represents the size of a MODIS pixel at 500-m spatial resolution.

Table 2.2. Overview of the study sites.

Site	Lat	Long	Elevation (m)	Mean annual rain (mm)	Mean annual temp (° C)	Major vegetation	Soil type
Marena	36.063 °N	97.216 °W	327	802	14	Tallgrass prairie	Sandy clay loam
El Reno	35.546 °N	98.040 °W	419	794	15	Tallgrass prairie	Silty clay loam

2.2 Rainfall and soil moisture data during 2000-2013 from the Oklahoma Mesonet

The Oklahoma Mesonet is a system designed to measure the environmental parameters by a network of instruments deployed on or near a 10-meter-tall tower. The recorded measurements are aggregated into observations every five minutes and the observations are sent out to a central facility every five minutes, 24 hours per day year-round (McPherson et al. 2007). Daily precipitation and soil moisture data from 2000-2013 at the Oklahoma Mesonet Marena and El Reno stations were downloaded from the Oklahoma Mesonet website (http://www.mesonet.org/index.php/weather/daily_data_retrieval). The daily data were aggregated into 8-day periods to match with the temporal resolution of the Moderate-Resolution Imaging Spectroradiometer (MODIS) derived VIs. Three different soil moisture data products (soil water potential, fractional water index and volumetric water content) are available at the Mesonet website. These soil moisture data products were derived based on the calibrated change in soil temperature over time after a heat pulse is introduced (Illston et al. 2008). In our analysis, we used volumetric soil water content (SWC) collected at three different soil profiles (5, 25, and 60 cm depth). The SWC measured by Mesonet is a point measurement, but it is representative from a magnitude and temporal variability standpoint at scales of up too several hundred meters or field scale (Basara and Crawford 2002a; Illston et al. 2008).

2.2.3 MODIS images and vegetation indices during 2000-2013

Daily images are acquired by the MODIS sensors on-board the Terra and Aqua satellites. Seven spectral bands: red (620-670 nm), NIR_1 (841-876 nm), blue (459-479 nm), green (545-565 nm), NIR_2 (1230-1250 nm), $SWIR_1$ (1628-1652 nm), and $SWIR_2$

(2105-2155 nm) are available for the study of vegetation. In this study, we used the 8-day composite land surface reflectance (MOD09A1) data from Feb 2000 to Dec 2013 for one MODIS pixel (500 m × 500 m spatial resolution) centered on the study sites. The dataset was extracted from the data portal at the Earth Observation and Modeling Facility (EOMF) at the University of Oklahoma (http://eomf.ou.edu/visualization/gmap/). Land surface reflectance (ρ) from blue, green, red, NIR_1, and $SWIR_1$ bands were used to calculate three spectral indices as follows:

$$NDVI = \frac{\rho\ NIR1 - \rho red}{\rho\ NIR1 + \rho red} \quad (1)$$

$$EVI = \frac{\rho\ NIR1 - \rho red}{\rho\ NIR1 + 6 * \rho red - 7.5\ \rho blue + 1} \quad (2)$$

$$LSWI = \frac{\rho\ NIR1 - \rho SWIR1}{\rho\ NIR1 + \rho SWIR1} \quad (3)$$

To understand the relative sensitivity of these three VIs to drought, we computed the deviation (absolute values) of the maximum values ($NDVI_{max}$, EVI_{max}, and $LSWI_{max}$) of VIs each year with reference to 14-year mean maximum VIs.

2.2.4 United States Drought Monitoring (USDM) Data

The USDM is a composite drought index that includes many indicators based on measurements of climatic, hydrologic and soil conditions in order to provide weekly maps of drought conditions (Svoboda et al. 2002). The drought categories (D0, D1, D2, D3 and D4) for the study sites were extracted from the weekly drought maps published by the USDM (http://droughtmonitor.unl.edu/MapsAndData/). The corresponding NDVI and LSWI values to the USDM defined drought categories were identified from MODIS data and plotted against each other to define the LSWI-based drought classifications. This

relationship between the USDM classified drought categories and MODIS-derived VIs were analyzed only for the Summer months (Jun- Aug) of each year from 2000-2013.

2.3 Results

2.3.1. Inter-annual variation of rainfall, soil moisture and vegetation indices- identifying drought years

Annual precipitation varied substantially during 2000-2013 at both sites with an annual average precipitation of 802 mm (± 220) at the Marena site and 794 mm (± 182) at the El Reno site. Dry and pluvial years were determined based on the 14-year (2000-2013) average annual precipitation and the associated standard deviation. Years with standardized score values greater than sum of its average and one standard deviation (negative side) were labeled as drought years, whereas years with standardized score greater than sum of its average and one standard deviation (positive side) were identified as pluvial years (Fig. 2.2).

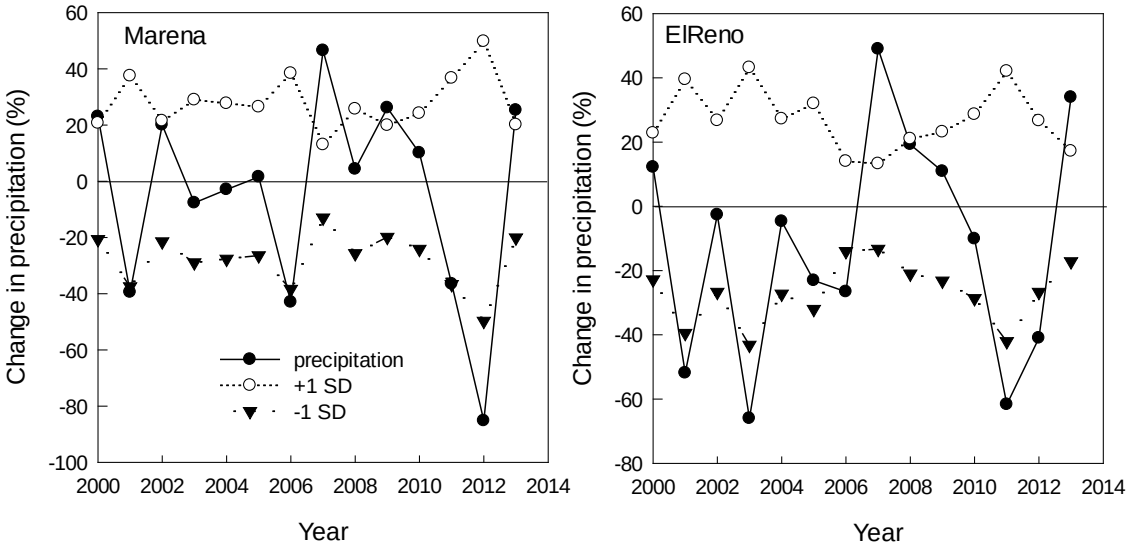

Figure 2.2. The variability of annual rainfall at study sites over time (2000-2013). The anomaly of rainfall is calculated as percentage change from a 14- year average rainfall.

From this analysis, the years 2001, 2006, 2011, and 2012 were identified as drought years at both Marena and El Reno sites. In addition, 2003 also was a drought year at the El Reno site. Additionally, 2007 and 2013 were identified as pluvial years for both sites. For both sites, two episodic drought years (2006 and 2012) were compared with two episodic pluvial years (2007 and 2013).

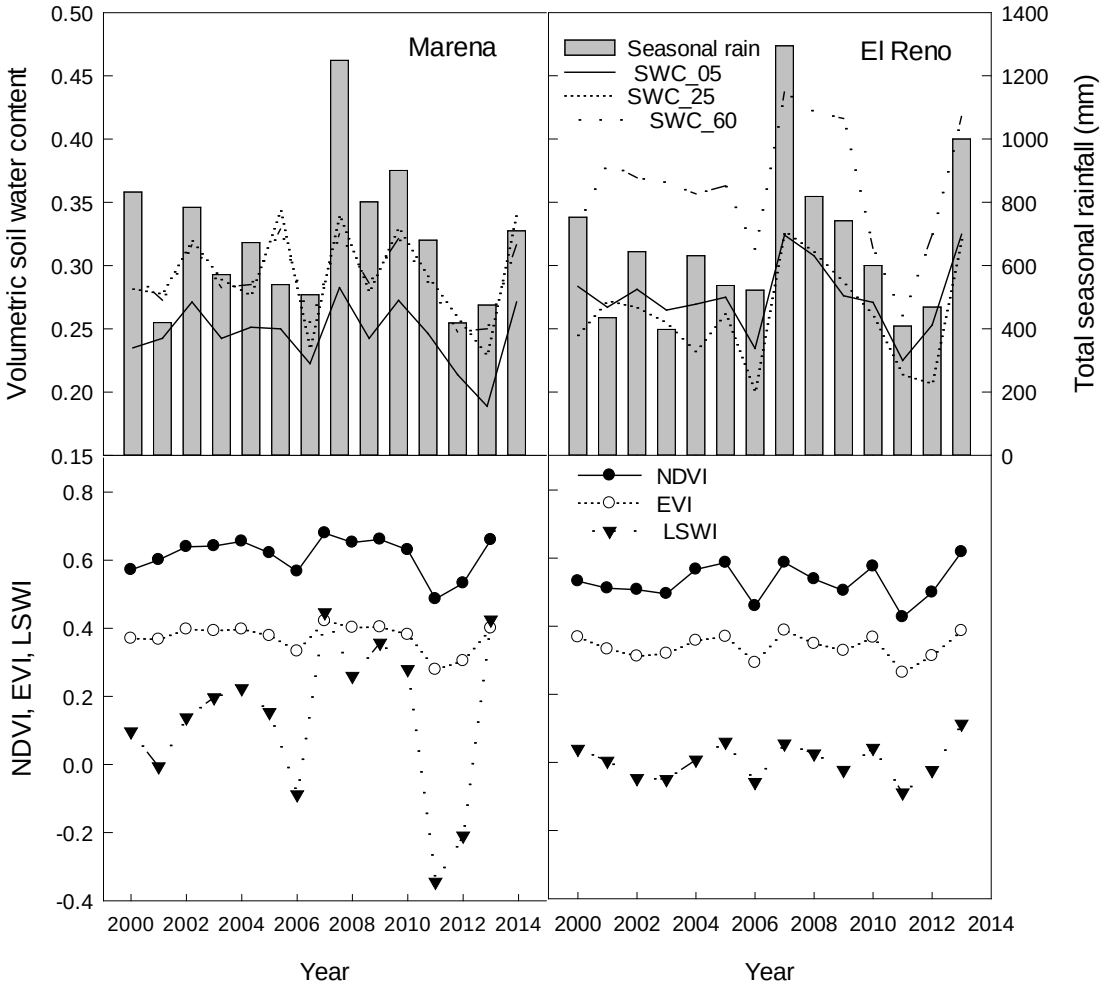

Figure 2.3. Inter-annual variation of: soil water content at different soil depths (a, b) and growing season (March- October) vegetation indices (c, d). The vertical bars represent the total growing season rainfall.

Figure 2.3 (a, b) shows SWC at various depths (5, 25, and 60 cm). The growing season average SWC of drought years (2006 and 2012) was approximately 20-25 % (5 and 25 cm depths) and 25-30 % at 60 cm whereas SWC at three depths ranged from 27-44% in pluvial years (2012 and 2013). At El Reno, SWC at the 60-cm depth was relatively higher than that of Marena for all years.

Figure 2.3 (c, d) shows inter-annual variation of seasonal mean VIs (NDVI, EVI, and LSWI). NDVI and EVI had relatively smaller variations compared to the variation observed in LSWI. The average NDVI, EVI and LSWI values during the growing season were consistently lower ($NDVI_{avg}<0.55$, $EVI_{avg}<0.35$ and $LSWI_{avg}<0$) in drought years (2006 and 2012) in comparison with pluvial years (2007 and 2013). Both sites showed consistently lower values of VIs in drought years. However, VIs at the Marena site were more sensitive to drought than those at the El Reno site.

To understand the relative sensitivity of VIs to drought, the deviation in the maximum values of VIs ($NDVI_{max}$, EVI_{max} and $LSWI_{max}$) for each year were compared to long term (2000-2013) mean of maximum VIs (Fig. 2.4). The largest negative LSWI anomaly was observed in drought years (2006 and 2012) at both sites, although the magnitudes of decrease varied between sites. LSWI showed the largest deviations in drought and pluvial years compared to NDVI and EVI. For Example, $LSWI_{max}$ was reduced by -0.36 (66%) and-0.32 (59%) at the Marena site, and by -0.18 (43%) and -0.2 (62%) at the El Reno site in 2006 and 2012, respectively. The change in EVI_{max} in drought years was greater than that of $NDVI_{max}$. In 2006 and 2012, drought reduced the

EVI_{max} by almost two folds compared to $NDVI_{max}$. At the Marena site, the drought reduced $NDVI_{max}$ by -0.04 (7%) whereas EVI_{max} was reduced by -0.09 (17%) and -0.07 (14%) in 2006 and 2012, respectively. Similarly, at the El Reno site, $NDVI_{max}$ was reduced only by -0.02 (4%) and -0.06 (10%) whereas EVI_{max} was reduced by -0.04 (10%) and -0.09 (19%) in 2006 and 2012, respectively.

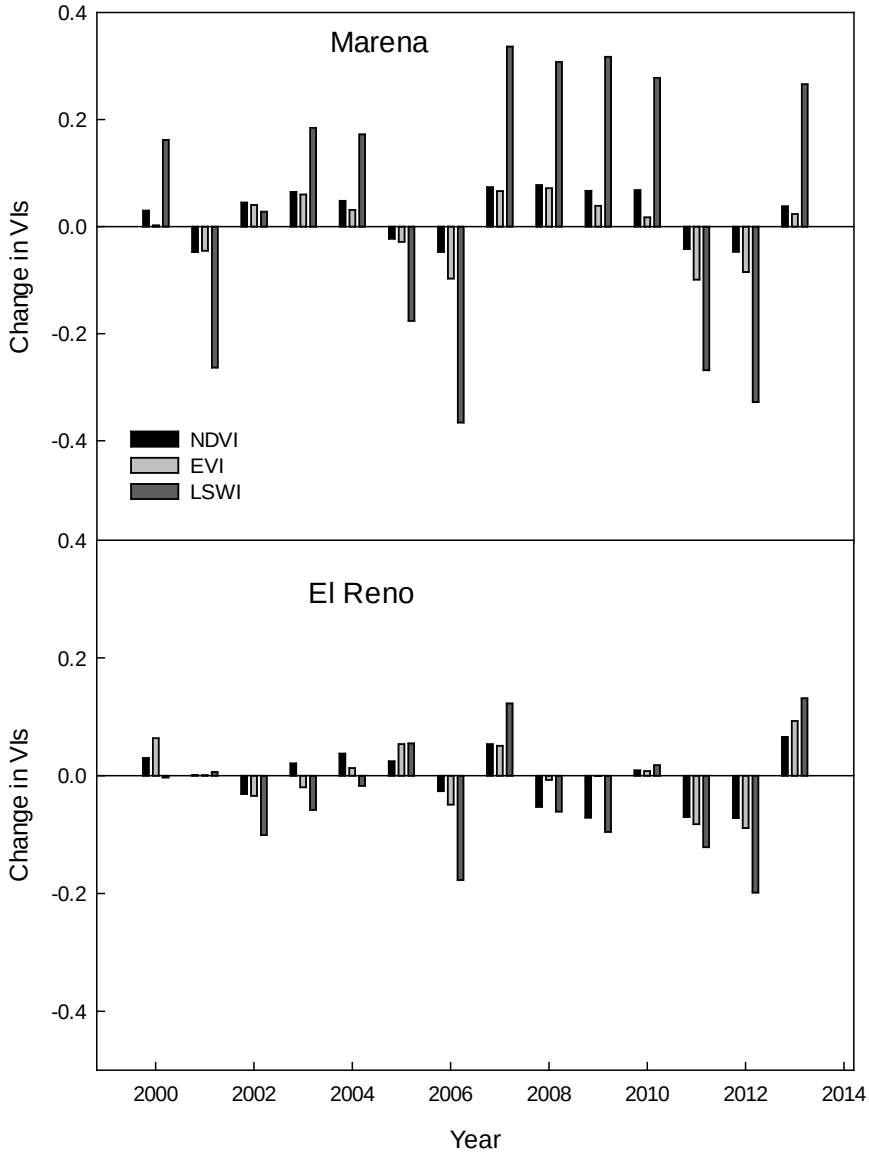

Figure 2.4. Sensitivity analysis of three vegetation indices (NDVI, EVI, and LSWI) to drought. The change in absolute values of vegetation indices (maximum values) is computed based on 14-year average values deviated from mean.

2.3.2. Seasonal dynamics of rainfall, soil moisture and vegetation indices – identifying spring drought and summer drought within a year

During pluvial years, the duration of LSWI > 0 period was longer and LSWI values were positive throughout the growing season. Air temperature over a certain threshold (> 5 °C) in the spring determines the start of the growing season (late Mar-early Apr). After greening up in spring, the rate of vegetation growth depends on available SWC. If the plant available SWC is not sufficient then the vegetation experiences stress. As such, LSWI< 0 during the Mar-May period was designated as Spring drought. LSWI < 0 during the Summer period (Jun-Aug) was defined as Summer drought, while LSWI< 0 during the late growing season (Sep-Oct) was defined as Fall drought (Fig. 2.5 inset Table). Thus, a year could have Spring, Summer and/or Fall droughts as per the rainfall received for that period of that year.

Duration of negative LSWI (LSWI < 0) during Summer (Jun, Jul and Aug) was longer in drought years than pluvial and normal years (Table 2.3). For example, LSWI values were negative for 56 and 42 days during summer months in 2006 at the Marena and El Reno sites, respectively. Further, LSWI values were negative for 72 days during the summer of 2011 at the Marena site. In contrast, LSWI values never fell below zero in the summer of pluvial years (2007 and 2013) at both sites. These results indicate the potential of LSWI to track water status of vegetation during dry summers. Interestingly, the duration of negative LSWI values during summer showed a definite pattern when plotted with the cumulative summer rainfall (Fig. 2.6). For those years with summer rainfall less than certain thresholds (230 mm for Marena site and 250 mm for El Reno

site), duration of negative LSWI values increased linearly as the cumulative summer rainfall decreased. However, the relationship collapsed when the summer rainfall exceeded the threshold.

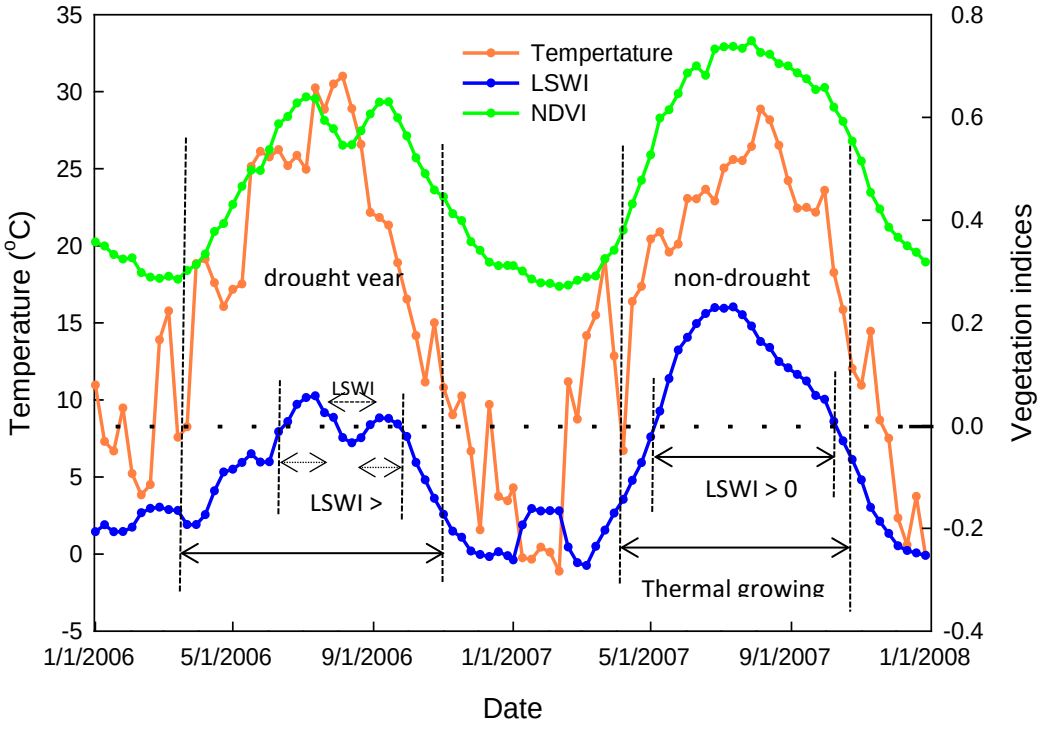

Season	Months	LSWI values	Drought
spring	Mar-May	if LSWI < 0 after green-up during April- May	spring drought
summer	Jun-Aug	if LSWI < 0 during Jun-Aug	summer drought
fall	Sep-Nov	if LSWI < 0 during Sep-Oct before senescence	fall drought

Figure 2.5. Schematic diagram showing seasonal dynamics of daily air temperature, NDVI and LSWI in drought (2006) and non-drought year (2007). The inset table (below) presents the designation of drought types based on LSWI values and seasons.

The years with summer rainfall over the threshold had zero or only one 8-day period with LSWI < 0. The relationship between NDVI and LSWI for summer months (Jun- Aug) over the 14-years is presented in Fig. 2.7. Each point in the plot represents the weekly observation of drought severity designation for the study area as determined from USDM drought maps (http://droughtmonitor.unl.edu/MapsAndData/). The descriptions

of the drought intensity defined by the USDM are listed Fig. 2.7 inset table. Results illustrated that VIs values were much lower (NDVI < 0.6 and LSWI < 0) during higher intensity droughts, identified as D2, D3 and D4 by the USDM, whereas NDVI and LSWI values were higher (NDVI > 0.6 and LSWI > 0) in lower intensity and non-drought conditions, identified as D1 (moderate) and D0 (dry) by the USDM. Based on LSWI values during the summer months, drought was classified into non-drought or dry (LSWI > 0.1), moderate ($0 < LSWI \leq 0.1$), severe ($-0.1 < LSWI \leq 0$) and extreme-exceptional drought ($LSWI \leq -0.1$) corresponding to USDM`s 0 or D0, D1, D2 and D3 or D4 categories, respectively.

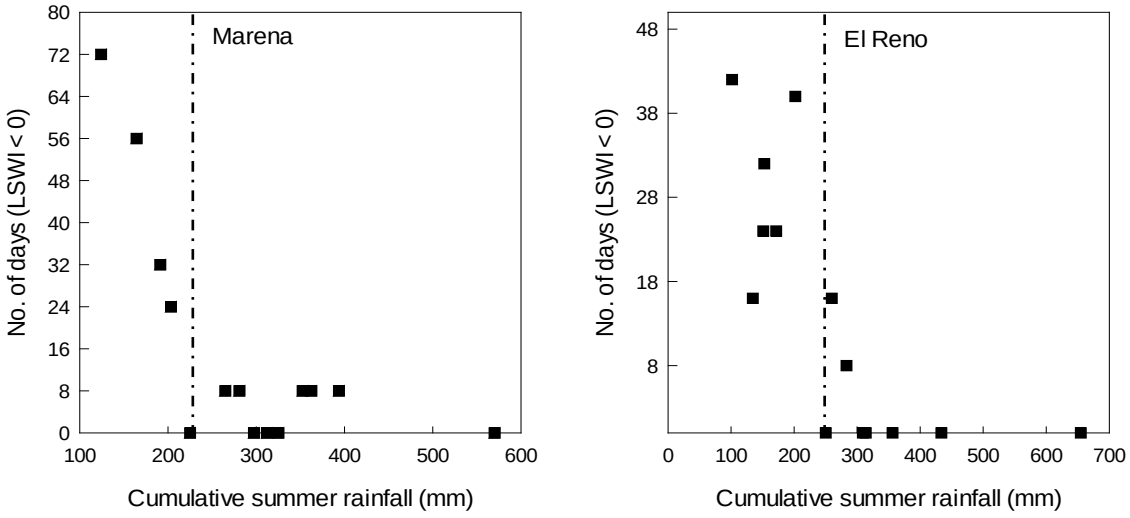

Figure 2.6. Relationship between duration of negative LSWI and cumulative rainfall during summer (June-August).

Table 2.3. Summary of the start of growing season (SOS), ending of growing season (EOS), duration (in days) of land surface water index (LSWI < 0) during spring and summer for the study sites over the study period (2000 – 2013).

	Marena					El Reno				
Year	SOS (T_{min} >5°C)	duration of LSWI <0 (spring)	duration of LSWI <0 (summer)	Summer rainfall (mm)	EOS (T_{min}< 5°C)	SOS (T_{min} >5°C)	duration of LSWI <0 (spring)	duration of LSWI <0 (summer)	Summer rainfall (mm)	EOS (T_{min}< 5°C)
2000	21-Mar	24	10	394	07-Oct	21-Mar	42	0	250	05-Oct
2001	02-Apr	40	23	203	09-Oct	02-Apr	42	16	135	13-Oct
2002	10-Apr	40	8	281	11-Oct	06-Apr	56	24	151	10-Oct
2003	11-Apr	32	0	225	24-Oct	13-Apr	80	24	172	24-Oct
2004	15-Apr	16	0	312	29-Oct	15-Apr	56	8	283	02-Nov
2005	04-Apr	48	8	362	20-Oct	13-Apr	16	0	309	22-Oct
2006	29-Mar	56	53	164	17-Oct	29-Mar	56	40	214	17-Oct
2007	18-Apr	24	0	570	20-Oct	17-Apr	24	0	655	20-Oct
2008	16-Apr	24	0	297	14-Oct	20-Apr	24	0	356	21-Oct
2009	15-Apr	32	8	353	07-Oct	21-Apr	24	16	260	21-Oct
2010	10-Apr	16	8	265	27-Oct	10-Apr	24	0	314	25-Oct
2011	17-Apr	24	76	124	17-Oct	06-Apr	88	32	153	18-Oct
2012	11-Mar	56	34	191	24-Oct	11-Mar	72	42	102	24-Oct
2013	26-Apr	24	0	325	15-Oct	26-Apr	8	0	434	15-Oct

2.4 Discussions

Globally, all ecosystems will be impacted to a greater extent by the climatic extremes in future because most of the global climate models predicted more extremes in the climates such as multi-year droughts (Field et al. 2014). Previous studies reported the sensitivity of the U.S. Southern Great Plains grassland to extreme drought events during the historic droughts of the 1930`s and 1950`s (Albertson et al. 1957; Albertson and Weaver 1944). Both pure and mixed prairies were seriously depleted by those historic droughts and a long delay occurred in the recovery of the vegetation. The negative impacts of two episodic droughts of 2006 and 2012 over tallgrass prairie were apparent in our study as documented by the lower values of NDVI, EVI and LSWI (Fig. 3). Sensitivity of grassland vegetation to drought, when monitored through several VIs,

showed varied degrees of response. LSWI was the most sensitive indicator of vegetation condition followed by EVI and NDVI. For example, $NDVI_{max}$ was 0.63 (7 % less than 14-year average, 0.69), the EVI_{max} was 0.39 in 2012 (14% less than 14-year average, 0.45) and the $LSWI_{max}$ was 0.22 (59% less than 14-year average, 0.56) in 2012 at the Marena site.

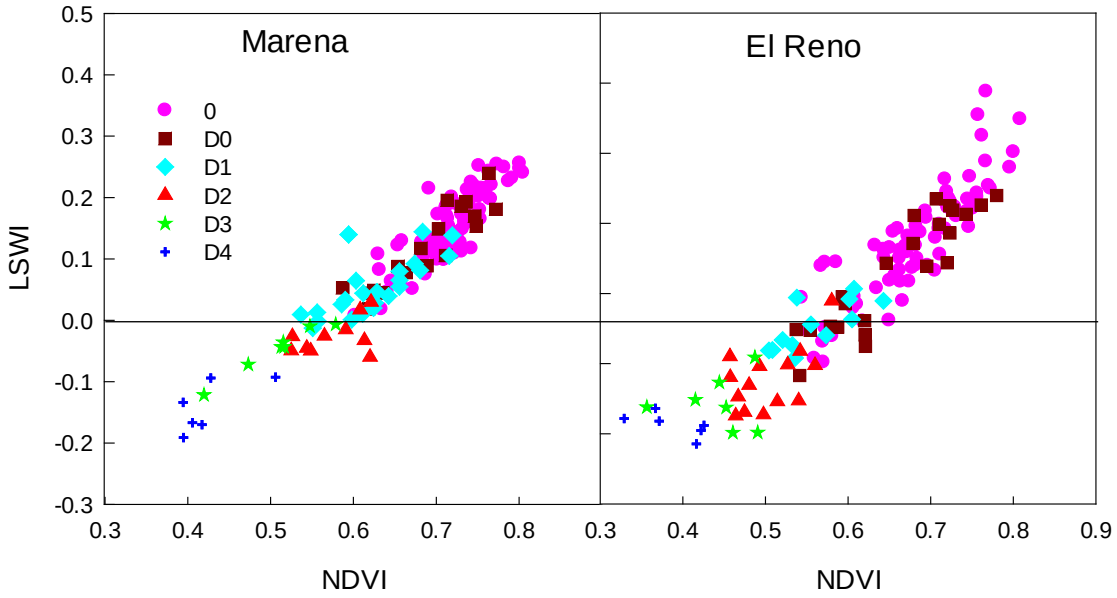

Drought Class	Description	PDSI	LSWI-D values and drought class
0	non-drought	-0.49 or more	
D0	abnormally dry	-0.5 to -1.99	LSWI > 0.1
D1	drought-moderate	-2.0 to -2.99	0 < LSWI ≤ 0.1
D2	drought-severe	-3.0 to -3.99	-0.1 < LSWI ≤ 0
D3 D4	drought-extreme drought- exceptional	-4.0 or less	LSWI ≤ -0.1

Figure 2.7. Relationship between: NDVI, EVI and LSWI for individual pixels of the grassland study sites for June – August over a 14-year study period (2000-2013). Drought severity categories defined by USDM, Palmer Drought Severity Index (PSDI) and LSWI-based drought categories (inset table).

Years with abundant rainfall (2007 and 2013) were characterized by the positive LSWI throughout the entire season, while LSWI values decreased below zero and remained negative during the summer droughts in 2006 and 2012.This finding is in agreement with the results reported by Wagle et al. (2014) for El Reno tallgrass prairie sites in Oklahoma. The sharper drop in LSWI values in drought years revealed that the grassland vegetation had lost a greater amount of water than the greenness because loss of chlorophyll and leaves is a rather slow process compared to water loss from stomata via transpiration during drought (Chaves et al. 2003). Therefore, LSWI can give a stronger vegetation drought signal than that of NDVI or EVI. Chandrasekar et al. (2010) also reported that LSWI responded more directly to the water status of the vegetation than did NDVI and EVI. Negative LSWI during the summer not only indicated the drought but also reflected the relative persistency of summer droughts. The longer the period of LSWI< 0, the lesser the amount of rainfall was received by the ecosystem and vice-versa, indicating relative drought persistency or duration (Fig. 2. 6). For example, LSWI < 0 in 2011 (Marena site) lasted for a longer period than in 2006 (72 and 32 days, respectively), which indicates more persistent summer drought in 2011 than in 2006. Rainfall events correlate with the soil moisture regimes and LSWI being the sensitive index provided an earlier signal of declining SWC than did NDVI and EVI. For instance, at the Marena site, LSWI dropped below zero indicating droughts during late June (DOY 170) of 2006 (Fig. 2.8e) when the SWC dropped below 12% whereas the NDVI reduced late during mid-July (DOY 200) only when SWC dropped below 12% for a substantial period of time (Fig. 2.8a). However, most of the models and drought monitoring algorithms for the last two decades (Hartmann et al. 2003; Ji and Peters 2003; Liu and

Kogan 1996; Nemani and Running 1989; Pettorelli et al. 2005) have widely used NDVI as a drought index.

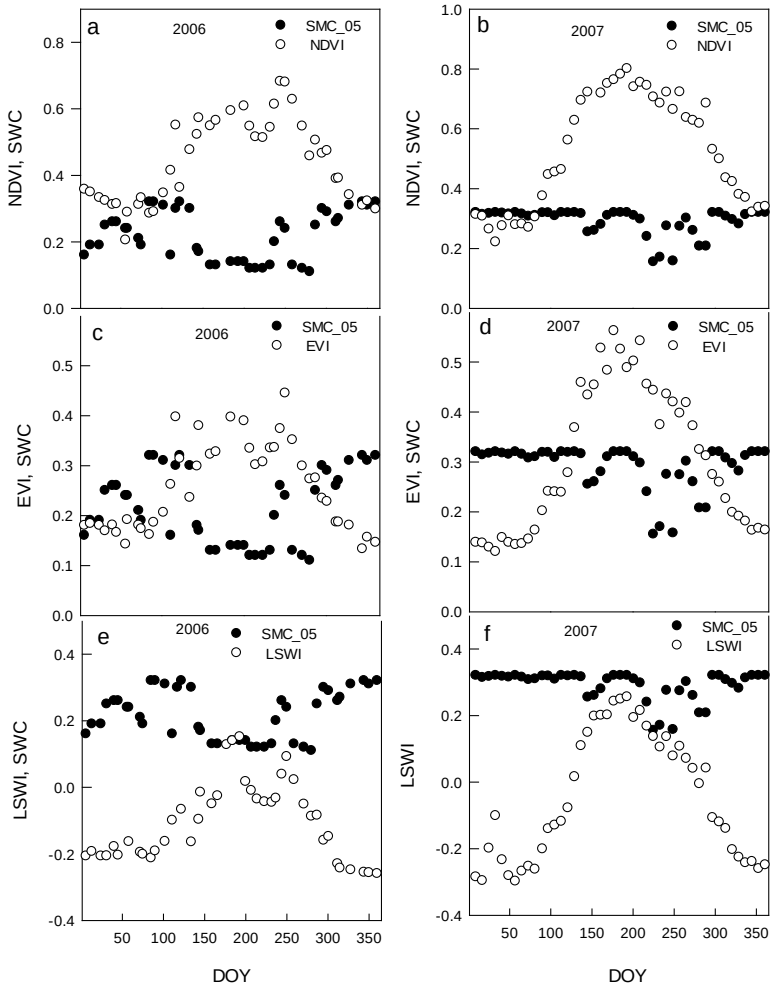

Figure 2.8. Seasonal soil moisture dynamics between dry and wet years and sensitivity of NDVI (a,b) EVI (c,d) and LSWI (e,f) to declining soil moisture at 5 cm depth (Marena).

Updating the climate based drought indicators such as Palmer Drought Severity Index (PDSI) and Standardized Precipitation Index (SPI), USDM has introduced the VegDRI in 2007 (Brown et al. 2008).This drought-monitoring indicator provides a measure of drought severity by integrating satellites observation, local weather report and

experts reviews. The USDM employs NDVI observations that are more characteristic features of plant greenness and was found to be relatively less sensitive to drought compared to EVI and LSWI in our study. Our study (14 years) over the grassland based on sensitivity of VIs to past drought revealed that LSWI could not only monitor the drought occurrence but also designate drought into different intensity categories (Fig. 2.7). Traditionally, USDM has used PDSI to classify drought into different classes (D0, D1, D2, D3 and D4). Such climate based drought monitoring and classification approaches have coarse spatial resolutions and do not better represent vegetation status since the interpretation depends heavily on point based meteorological measurements (Brown et al. 2008). We attempted to describe drought severity categories quantitatively based on LSWI values of vegetation which is relatively more precise and useful because it is a pixel based finer resolution and vegetation specific calculation and is more related to water status of vegetation than greenness. The classification of drought categories is simply grouped based on two dimensional spaces of NDVI and LSWI plots where each point represents the weekly observation of drought severity designation for the study area as determined from USDM (Fig. 2.7). In our study, we found that higher negative values of LSWI represent a higher intensity drought. For example, when LSWI was -0.1 or smaller we defined it as extreme drought, comparable to D3 and D4 (extreme and exceptional) categories by USDM, while moderate-severe droughts were identified when LSWI values ranged greater or equal to zero to less than -0.1 corresponding to D1 and D2 drought categories of USDM classification. Overall, good vegetation growth exhibited higher LSWI values, which decreased with drought and ultimately became negative when drought became more extreme. Therefore, by using the information rendered by LSWI

during the drought, we can quantitatively investigate the drought impacts on vegetation that can contribute toward the development of more robust tools for monitoring drought stress in vegetation.

2.5 Conclusion

We used 14 years of MODIS-derived VIs, Mesonet soil moisture and rainfall data at Marena and El Reno tallgrass prairie sites to study the impact of drought events on grassland phenology and growth through analyzing sensitivity differences of vegetation indices to drought. Specifically, the drought events (2006 and 2012) that occurred in the last 14 years negatively impacted the growth of the vegetation. When three VIs were compared, LSWI decreased the most in drought years followed by EVI and NDVI, indicating that LSWI was the most sensitive indicator to the drought events. The number of days with LSWI < 0 was found higher during the summer droughts of 2006 and 2012, showing the ability of LSWI to track drought. Based on this finding, a new approach of drought assessment, counting number of days with LSWI < 0 and LSWI-based drought severity classification, is proposed in this study. LSWI values were more negative for the period of intensity drought categories (D2, D3 and D4) defined by USDM, demonstrating that LSWI could be used to describe the hydrological condition of the tallgrass prairie as an effective additional VI for drought assessment. However, a more thorough evaluation of this approach as a drought monitoring tool for widely distributed grasslands and other vegetation types is required and will be the subject of future research.

Chapter 3: Assessing agricultural drought in summer over Oklahoma Mesonet sites using the water related vegetation index from MODIS

Abstract

Agricultural drought, a common phenomenon in most parts of the world, is one of the most challenging natural hazards to monitor effectively. Land surface water index (LSWI), calculated as a normalized ratio between near infra-red (NIR) and short wave infra-red (SWIR), is sensitive to vegetation and soil water content. This study examined the potential of a LSWI- based drought monitoring algorithm to assess summer drought over 113 Oklahoma Mesonet stations comprising various land cover and soil types in Oklahoma. Drought duration in a year was determined by the number of days with LSWI < 0 (DNLSWI) during summer months (Jun-Aug). Summer rainfall anomalies and LSWI anomalies followed a similar seasonal dynamic and showed strong correlations (R^2= 0.62 – 0.73) during drought years (2001, 2006, 2011, and 2012). The DNLSWI tracked the East-West gradient of summer rainfall in Oklahoma. Drought intensity increased with increasing duration of DNLSWI, and the intensity increased rapidly when DNLSWI was more than 48 days. The comparison between LSWI and the United States Drought Monitor (USDM) showed a strong linear negative relationship i.e, higher drought intensity tends to have lower LSWI values and vice-versa. However, the agreement between LSWI-based algorithm and USDM indicators varied substantially from 32% (D2 class, moderate drought) to 77 % (0 and D0 class, no drought) for different drought intensity classes and varied from and ~ 30% (western Oklahoma) to >80 % (eastern Oklahoma) across regions. Our results illustrated that drought intensity thresholds can be established by counting DNLSWI (in days) and used as a simple complementary tool in

several drought applications for semi-arid and semi-humid regions of Oklahoma. However, larger discrepancies between USDM and the LSWI-based algorithm in arid regions of western Oklahoma suggest the requirement of further adjustment in the algorithm for its application in arid regions.

3.1 Introduction

Drought is a recurrent and inevitable threat in several parts of the world (Hulse and Escott 1986; Shahid and Behrawan 2008; Sönmez et al. 2005). Southern Great Plains of the United States experience drought on varying spatial and temporal scales (Basara et al. 2013a; Christian et al. 2015b). Drought is also among the most difficult of all natural hazards to monitor effectively.

Yet, the repeated occurrence of drought events has highlighted the need to develop effective drought monitoring tools to assess the impacts of this phenomenon. Research to retrieve leaf water content from the reflectance acquired from satellite sensors has progressed for more than three decades. Tucker 1980 first suggested that the 1550–1750 nm spectral intervals were the best-suited band in the 700–2500 nm region for monitoring plant canopy water status from space. A number of broad-band ratio and combination techniques using Thematic Mapper (TM) channel 4 (760–900 nm, near infrared) and TM channel 5 (1550-1750nm, shortwave infrared) were proposed for remote sensing of plant water status (Hunt et al. 1987; Jackson et al. 1983). The combination of the near infra-red (NIR) and short wave infra-red (SWIR) bands has the potential of retrieving vegetation canopy water content (Ceccato et al. 2002; Ceccato et al. 2001; Maki et al. 2004). The water related vegetation index computed from the

combination of NIR and SWIR has different nomenclatures by different authors. Gao 1996 and Chen et al. 2005 referred it the Normalized Difference Water Index (NDWI. Kimes et al. 1981 used the terms Normalized Difference Infrared Index (NDII). Similarly, Jurgens 1997 and Xiao et al. 2002a, b called the same combination of NIR and SWIR bands as the Land Surface Water Index (LSWI). Despite known by different names, the features they have in common is that the NIR spectral region serves as a moisture reference band and the SWIR spectral domain is used as the moisture measuring band. The water related vegetation index is a measurement of liquid water in vegetation canopies and hence is sensitive to the total amount of liquid water contained in vegetation when the vegetation cover is high. Some recent studies (Bajgain et al. 2015; Chandrasekara et al. 2011; Wagle et al. 2014) have identified LSWI as an index in extracting the vegetation water status and in drought detection.

Because agricultural drought occurs due to lack of soil moisture and the consequent water stress in the vegetation, a water-based index should also be used along with the greenness related indices such as Normalized Difference Vegetative Index (NDVI) and Enhanced Vegetative Index (EVI) to develop systematic and effective method of agriculture drought assessment (Bajgain et al. 2015; Chandrasekara et al. 2011; Tian et al. 2013; Wagle et al. 2014).The Moderate Resolution Imaging Spectrometer (MODIS) sensor onboard the NASA Terra satellite platform provides continuous daily observations of the land surface. Our hypothesis is that the water related vegetation index LSWI computed from time series MODIS images, offers a new and improved capacity for drought monitoring. In this study, we evaluated the hypothesis over 113 Mesonet sites across Oklahoma under different land cover and soil types. Also,

the drought intensity class classified based on LSWI values corresponding to United States Drought Monitor (USDM) drought intensity classes are further linked to the duration of LSWI < 0 (DNLSWI) to establish a certain threshold of DNLSWI (in days) to define drought intensity classes. Therefore, results from this study will help in improving the capability of remote sensing vegetation drought monitoring by establishing LSWI as a complimentary tool to existing NDVI based drought products. Specifically, we addressed the following research questions:

1) Is LSWI anomaly able to capture the drought events across multiple sites over years?

2) Is LSWI-based drought monitoring algorithm developed for two tallgrass prairie sites (Bajgain et al., 2015) applicable to quantify drought intensity over 113 Mesonet sites comprising various land cover and soil types in Oklahoma?

3) What is the relationship between the DNLSWI and drought intensity classified by USDM?

3.2 Materials and Methods

3.2.1 Data

3.2.1.1 Oklahoma Mesonet Stations and rainfall data

An extensive environmental observation network is well established and distributed over Oklahoma, known as the Oklahoma Mesonet (Brock et al. 1995). The Oklahoma Mesonet is a network of 120 automated stations with at least one in each 77 counties of Oklahoma. The Mesonet provides quality-controlled measurements of meteorological and land-surface variables such as precipitation, temperature, and soil

moisture at intervals spanning 5-30 minutes depending on the variables (http://www.Mesonet.org/).

In this study, we used 113 Mesonet stations that have continuous measurements of meteorological parameters from 2000-2013. Retired and replaced Mesonet stations were not considered because site replacements were on different MODIS pixels. The locations of the selected sites are presented in Fig. 3.1; biophysical features are presented in Table S1. In this study, we used the precipitation and soil water content (SWC) data for three summer months (Jun-Aug) and calculated the rainfall and SWC anomalies from the 14-year mean (2000-2013). Additionally, the anomalies in rainfall calculated from 30-year rainfall data (climatological normal) from COOP (Cooperative Observer Program, National Weather Service) sites were compared with the rainfall anomalies computed from a 14-year data from Mesonet stations, two from each climate division of Oklahoma.

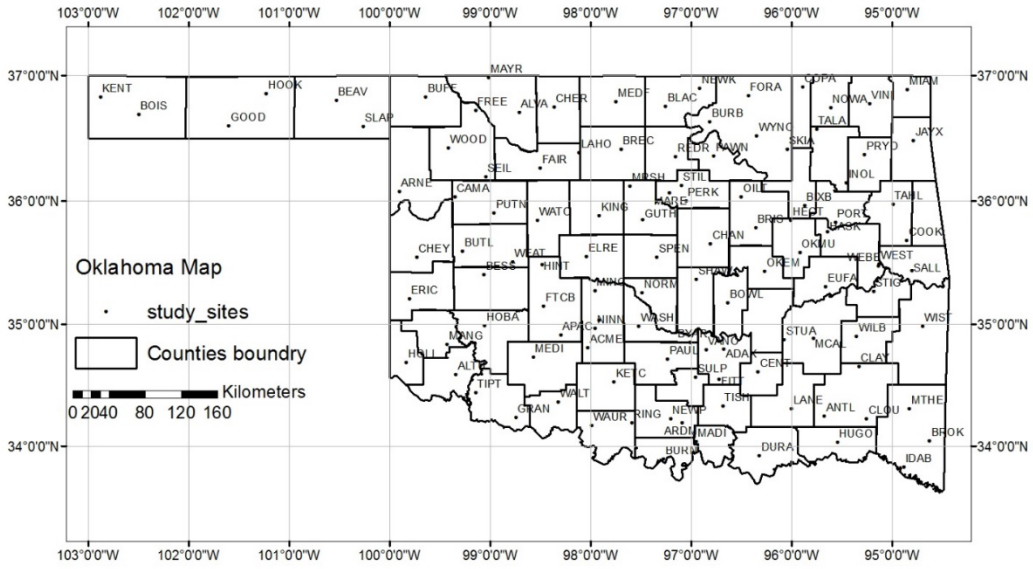

Figure 3.1. The location and distribution of the Mesonet sites (113 Mesonet stations) in Oklahoma, USA.

3.2.1.2 MODIS surface reflectance and vegetation index data

The MODIS is an instrument on board the NASA's Terra (EOS am) and Aqua (EOS pm) spacecraft. This sensor provides simultaneous observations of the atmosphere, terrestrial surface, and oceans. The MODIS instrument has a temporal resolution of one to two days with high radiometric resolution images (12 bit). It collects data for 36 spectral bands, and seven of these bands are designated mainly for land surface and vegetation studies: blue (459-479 nm), green (545-565 nm), red (620-670 nm), near infrared (nir1: 841-875 nm and nir2: 1230-1250 nm), and shortwave infrared (swir1: 1628-1652 nm, and swir2: 2105-2155 nm) (Lillesand et al. 2014).

The 8-day MODIS land surface reflectance product (MOD09A1) at a 500-m spatial resolution, was used in this study. The MOD09A1 time series datasets for individual Mesonet sites were downloaded from the data portal managed by the Earth Observation and Modeling Facility at the University of Oklahoma (http://eomf.ou.edu/visualization). The geographic locations of the Mesonet sites were used to retrieve MODIS data at pixel level. For each MODIS 8-day composite, surface reflectance (ρ) values for visible, NIR and SWIR bands were used to calculate NDVI, EVI and LSWI as:

$$\mathrm{NDVI} = \frac{\rho\ \mathrm{NIR1} - \rho\mathrm{red}}{\rho\ \mathrm{NIR1} + \rho\mathrm{red}} \quad (1)$$

$$\mathrm{EVI} = \frac{\rho\ \mathrm{NIR1} - \rho\mathrm{red}}{\rho\ \mathrm{NIR1} + 6 * \rho\mathrm{red} - 7.5\ \rho\mathrm{blue} + 1} \quad (2)$$

$$\mathrm{LSWI} = \frac{\rho\ \mathrm{NIR1} - \rho\mathrm{SWIR1}}{\rho\ \mathrm{NIR1} + \rho\mathrm{SWIR1}} \quad (3)$$

3.2.1.3 United States Drought Monitor (USDM) data

The USDM map is a weekly drought product developed by a partnership of various agencies including National Oceanic and Atmospheric Administration (NOAA), the United States Department of Agriculture (USDA), and the National Drought Mitigation Center (NDMC) (http://www.drought.unl.edu/MonitoringTools/USDroughtMonitor.aspx). The USDM includes a weekly national map displaying dryness divided into five categories, or levels of intensities, from D0 to D4, based on a percentile ranking of numerous indicators or indices (Svoboda et al. 2002). The D levels are based on a blend of different indices including: the Palmer drought index, CPC soil moisture model, United States Geological Survey (USGS) weekly streamflow, standardized precipitation index (SPI), and satellite vegetation health index (Kogan 2002; Kogan et al. 2004). The D levels are labeled by drought intensity or severity, with D1 being the least intense and D4 is the most intense. The D0 classification or drought watch areas, are abnormally dry and may be heading into drought or recovering from drought but conditions have not yet returned to normal (Svoboda et al. 2002). The USDM archived weekly maps are available at http://droughtmonitor.unl.edu/archive.html.

For this study, weekly USDM drought maps for Jun-Aug (2000 to 2013) were provided by the National Drought Mitigation Center (NDMC) in shape file format and then rasterized to the 10-km ALEXI CONUS grid. Numerical values were assigned to each drought category, with no drought conditions set to 0, abnormally dry conditions (D0) to 1, moderate drought (D1) to 2, severe drought (D2) to 3, extreme drought (D3) to 4, and exceptional drought (D4) to 5.

3.2.2 Methods

3.2.2.1 LSWI-based agricultural drought monitoring algorithm

The LSWI-based algorithm uses LSWI as an indicator to assess agricultural drought in tallgrass prairie (Bajgain et al. 2015). Generally, green vegetation has positive LSWI values (> 0) and dry vegetation has negative LSWI values (< 0). Therefore, LSWI < 0 during growing season indicates drought in tallgrass prairie in Oklahoma (Bajgain et al. 2015; Wagle et al. 2014). The duration of LSWI < 0 (DNLSWI) during the summer months (Jun-Aug) was used to estimate the drought duration and drought intensity. To illustrate the algorithm at single site, the dynamics of rainfall and LSWI in drought (2006) and pluvial year (2007) at Marena Mesonet station is presented in Fig. 3.2. The LSWI was greater than zero throughout the growing season in 2007 when ecosystem received well distributed rainfall, while the LSWI was less than zero for substantial number of days in 2006 due to rainfall associated with drought (Dong et al. 2011). Therefore, we used DNLSWI during the summer months (Jun-Aug) to reflect the duration (length) of drought period as an algorithm to assess summer drought of the ecosystem.

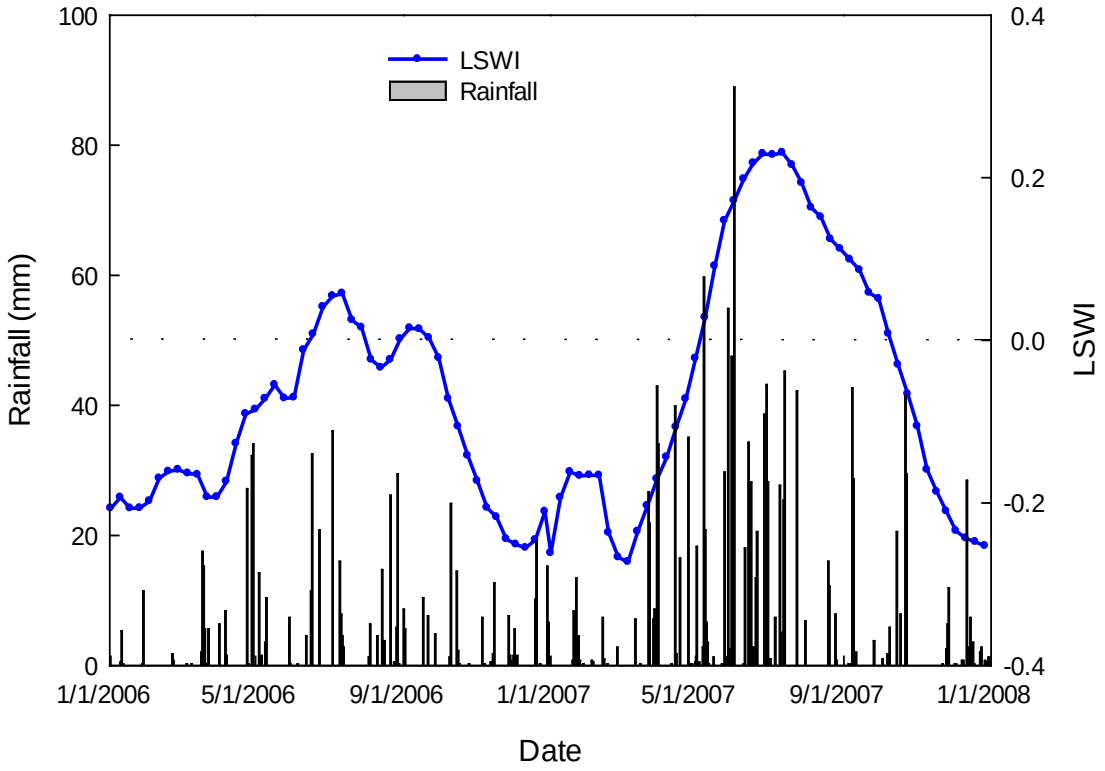

Figure 3.2. Seasonal dynamics and interannual variations of daily rainfall and land surface water index (LSWI) in drought (2006) and pluvial (2007) years at Marena, Oklahoma.

3.2.2.2 Anomaly analysis of summer rainfall and LSWI

Mean LSWI was computed for the summer months and anomalies were determined for each station during drought years (2001, 2006, 2011 and 2012) from the 14-year mean (2000-2013). Similarly, summer rainfall anomalies were computed for each station during drought years based on the 14-year mean. The similarity between the LSWI anomaly and summer rainfall anomaly for each station was determined by evaluating the correlation between them. This method identified the stations where LSWI anomalies followed the trends of summer rainfall anomalies, thus providing a direct method to assess ecosystem drought.

3.3 Results

3.3.1 Characteristics of summer rainfall over 113 Mesonet sites and identification of drought years based on summer rainfall

Figure 3.3a shows the box plots of the total summer rainfall that occurred in each year over the113 Mesonet sites. The dispersion in the rainfall among the 113 stations is compared for each year and the line in the box represents the median summer rainfall amount which is equivalent to the 50^{th} percentile of observations (113 stations). The median summer rainfall was highest (455 mm) in 2007, while the years including 2001, 2006, 2011 and 2012 had relatively low median rainfall. For example, 50 percent of the observations were below 111 mm of summer rainfall in 2011, indicating dry conditions at more than half of the Mesonet stations and was consistent with significant drought during the period (Hoerling et al. 2013; Tadesse et al. 2015).

The analysis of summer drought for each year (2000 - 2013) was computed by calculating the average summer rainfall from the14-year average. Precipitation values representing 50% and 25% of the long-term average rainfall were calculated for each station. These values were then deducted from the long-term average at every station to obtain values of 25% and 50% precipitation. If the annual rainfall was between 25% and 50% deficiency then it was classified as moderate drought. If the annual rainfall was less than the value of 50% deficiency then it was classified as severe drought. For example, at the Acme Mesonet station:

Average summer rainfall (1981-2010) = 260 mm

50 % of average summer rainfall = 50% of 260 = 130 mm

25 % of average summer rainfall = 25 % of 260 = 65 mm

50 % deficiency = 260 -130 = 130 mm

25 % deficiency= 260 – 65 = 195 mm

Summer rainfall during 2011 = 83 mm

Thus, the summer rainfall at Acme in 2011 was less than the calculated 50% deficiency and was subsequently classified as severe drought.

Based on annual rainfall deficiency, the majority of the stations received less than normal amounts of rainfall in 2001, 2006, 2011, and 2012, whereas stations received normal to above normal rainfall in 2004, 2007, 2008, and 2013 (Fig. 3.3b). For example, in 2011, drought occurred at nearly all stations whereby 70% of stations included at least the moderate drought classification with 29% of those classified as severe.

A frequency distribution was completed for drought periods when compared with the total period by computing total summer rainfall (Jun-Aug) for 1582 site-years (14 years × 113 sites) of total data. The results displayed in Fig. 3.3c demonstrate that drought site years have a significant right skew in distribution whereby the summer rainfall ranged from 50 to 350 mm with the greatest number falling within 150 mm bin. Conversely, the frequency distribution for all years (drought plus normal) ranged from 50 to 500 mm with the highest number falling within the 250 mm bin.

Figure 3.3d shows the anomalies in summer rainfall calculated from a 30-year rainfall data (climatological normal) from COOP sites compared with the rainfall anomalies computed from a 14-year data from Mesonet stations, two from each climate divisions of Oklahoma. The correlation analysis showed a strong relationship ($r^2 = 0.91$) between the anomalies of rainfall obtained from two data sources, suggesting drought

years (2001, 2006, 2011 and 2012) identified in our analysis can represent the climatic extremes of Oklahoma in the last decade based on climatological normal perspective.

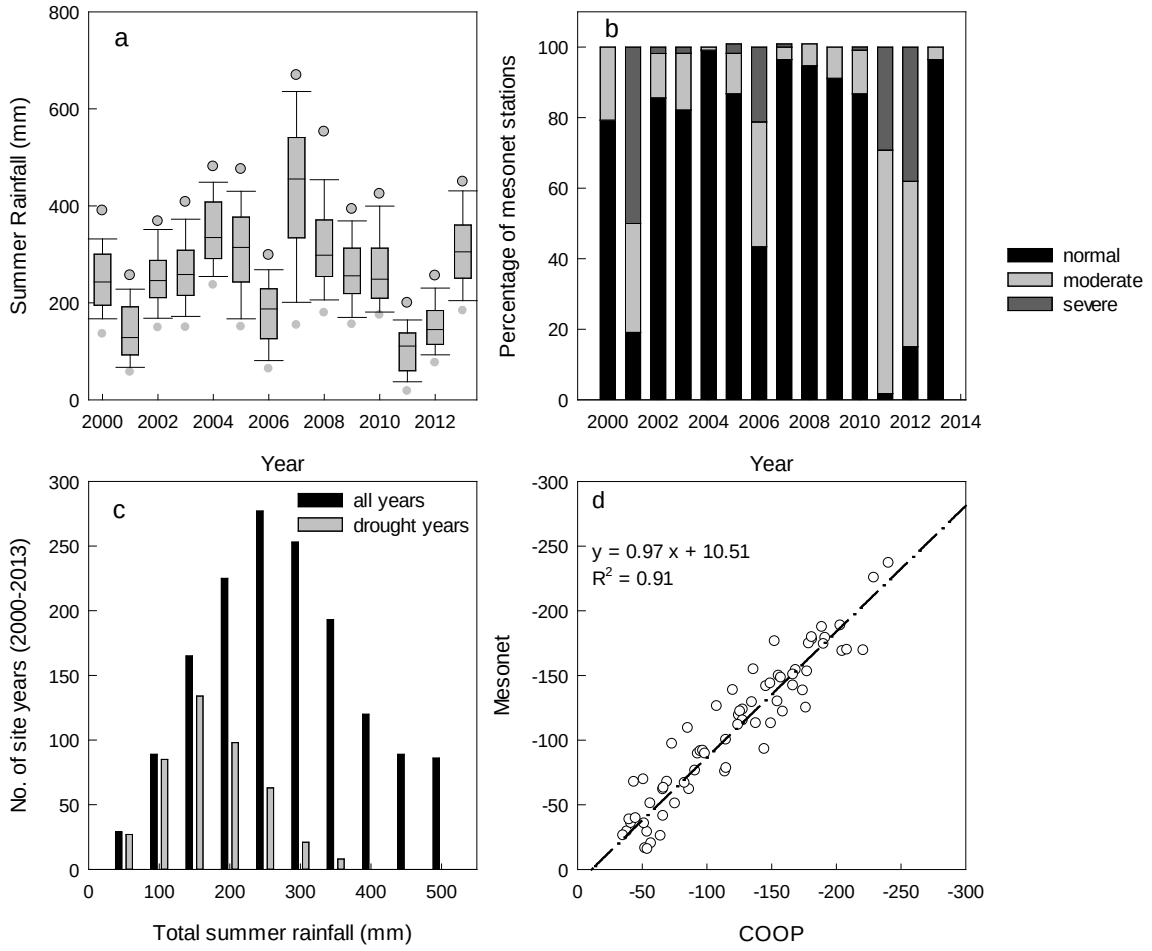

Figure 3.3. Summer rainfall across 113 Mesonet sites during 2000-2013 (a). The solid lines in the box represent the median and the dots above and below the box represent the 95 and 5 percentiles, respectively. Yearly summer drought analysis by rainfall deficiency: percentage of the Mesonet stations under three drought categories (severe, moderate and normal) for 2000 - 2013 (b). The frequency distribution of site-year grouped under different summer rainfall regimes (c) for whole study period (2000 - 2013) and for drought years (2001, 2006, 2011, and 2012). Correlation of rainfall anomalies calculated from 30-year rainfall data from COOP (Cooperative Observer Program) and 15-year rainfall data from Mesonet stations (d).

3.3.2 The relationship between rainfall anomaly and LSWI anomaly

Once the drought years were selected, the relationship between summer rainfall anomalies and LSWI anomalies was investigated. Figure 3.4 displays the LSWI anomalies and summer rainfall anomalies for individual pixels over the 113 Mesonet stations during drought years (2001, 2006, 2011, and 2012). Overall, the anomalous summer rainfall results in anomalous LSWI at most Mesonet stations during drought years. As such, the anomalies in summer rainfall and LSWI revealed a strong relationship between rainfall and vegetation water content. For example, pixel-based correlation analyses between summer rainfall anomalies and LSWI anomalies are presented in Fig. 3.4 (inset graphs). For all identified drought years, strong relationships (r^2= 0.61 – 0.67) between anomalies of summer rainfall and anomalies of LSWI were identified. Although the magnitudes of the anomalies of summer rainfall and LSWI varied from year to year, the relationship between two parameters was consistently strong.

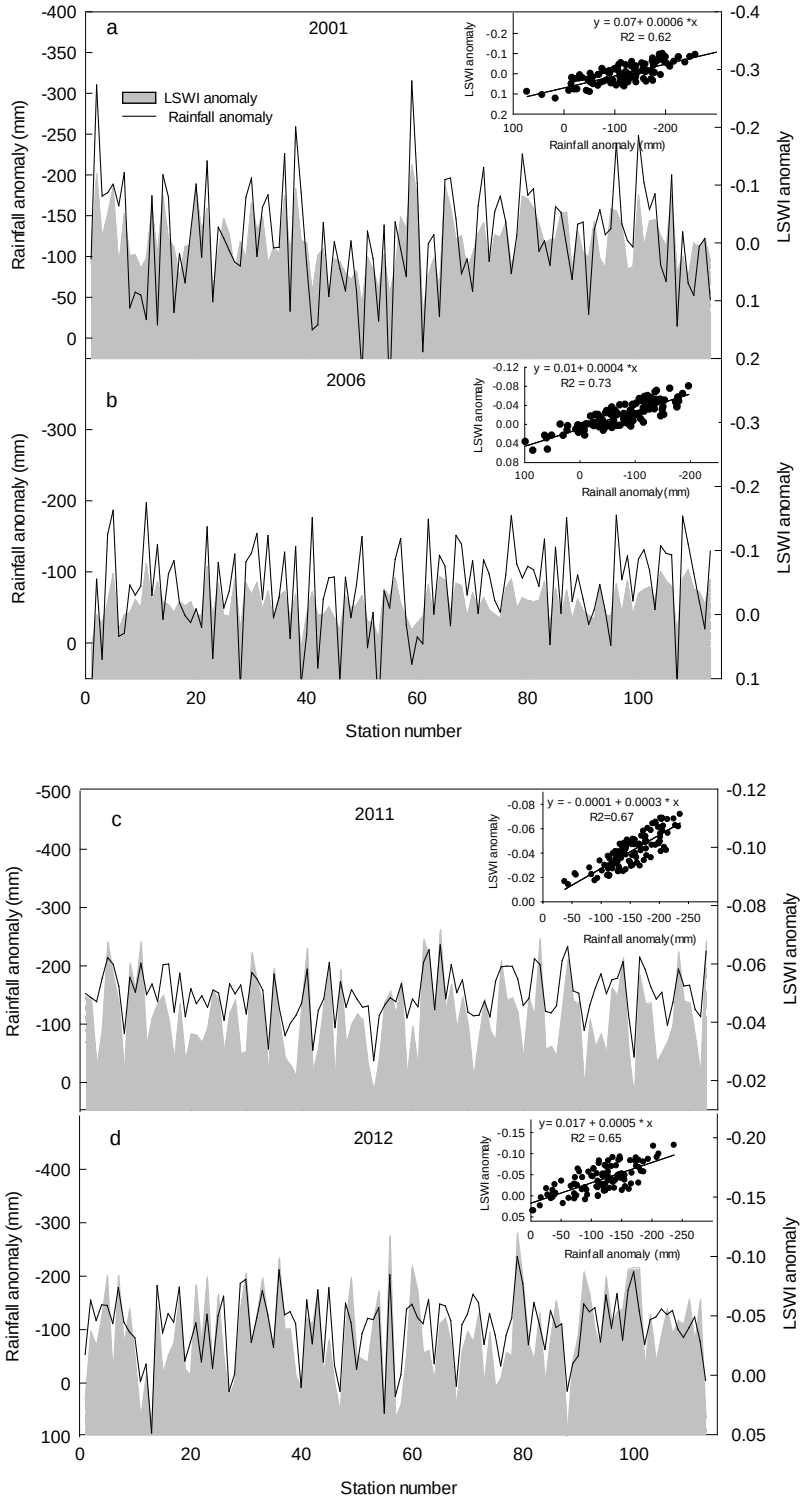

Figure 3.4. Dynamics of summer rainfall and LSWI anomalies in drought years: (a) 2001, (b) 2006, (c) 2011 and (d) 2012 at 113 Mesonet stations. The inset graphs are the regression analyses between summer rainfall and LSWI anomalies (n=113).

3.3.3 The relationship between soil water content (SWC) anomaly and vegetation indices anomaly

Figure 3.5 presents the Pearson correlation coefficients (r) between soil water content anomalies (SWCanomalies) and three vegetation anomalies (NDVI, EVI, and LSWI). As expected, a better relationship (r_{LSWI}=0.52) of SWC-anomalies was observed with LSWI-anomalies than NDVI anomalies (r_{NDVI}=0.40) and EVI-anomalies (r_{EVI}=0.44). We examined the correlation coefficients (r_{LSWI}, r_{EVI} and r_{NDVI}) for all 113 Mesonet stations. Figure 3.6 compares the r values derived for NDVI, EVI, and LSWI anomalies with SWC anomalies. The analysis showed the significant difference between r_{LSWI} & r_{NDVI}, and r_{LSWI} & r_{EVI} with p-values less than 0.0001. As a whole, there are significant r values that fall above the 1:1 line towards the r_{LSWI}. The r_{LSWI} was 25% and 20% higher than r_{NDVI} and r_{EVI}, respectively, suggesting LSWI as a better indicator of soil water content as compared to NDVI and EVI.

3.3.4 The relationship between LSWI-based drought duration and summer rainfall

Figure 3.7 shows the scatter plot of DNLSWI versus total summer rainfall across 113 Mesonet stations binned into 50 mm classes. The result highlights that LSWI was highly sensitive to summer rainfall and the DNLSWI rapidly decreased as the amount of rainfall increased. Specifically, the DNLSWI was more than 50 days when summer rainfall was less than 150 mm indicating water stress (LSWI < 0) during active growing period of the vegetation. Conversely, the DNLSWI was less than two weeks when summer rainfall was greater than 400 mm.

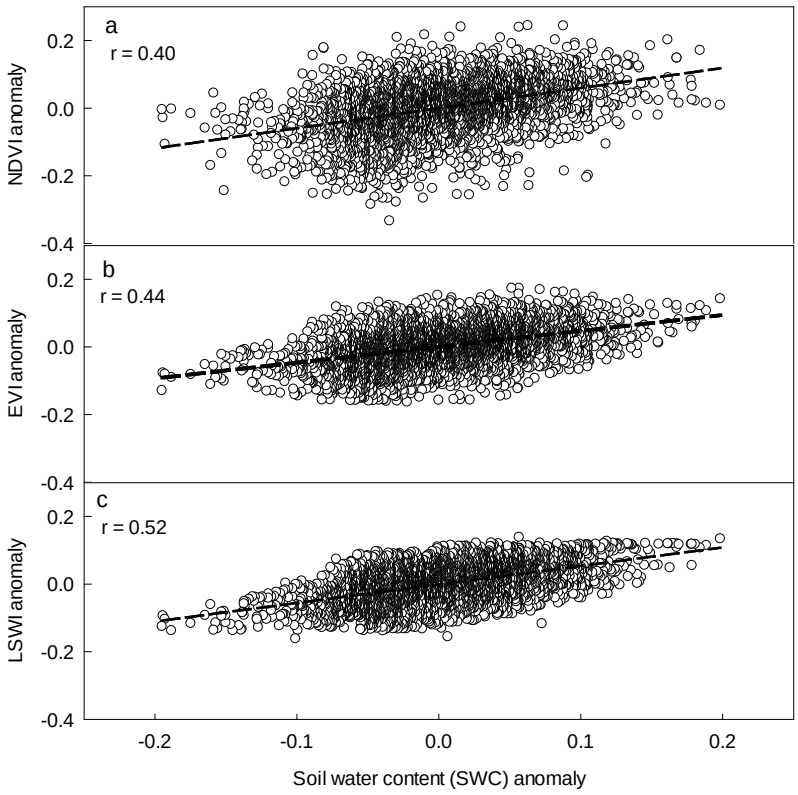

Figure 3.5. Correlation analysis between soil water content (SWC) anomaly and vegetation indices (VIs) anomaly a) NDVI, b) EVI and c) LSWI. Each point represents the VIs anomaly and SWC anomaly value for each month of the summer from 2000-2013.

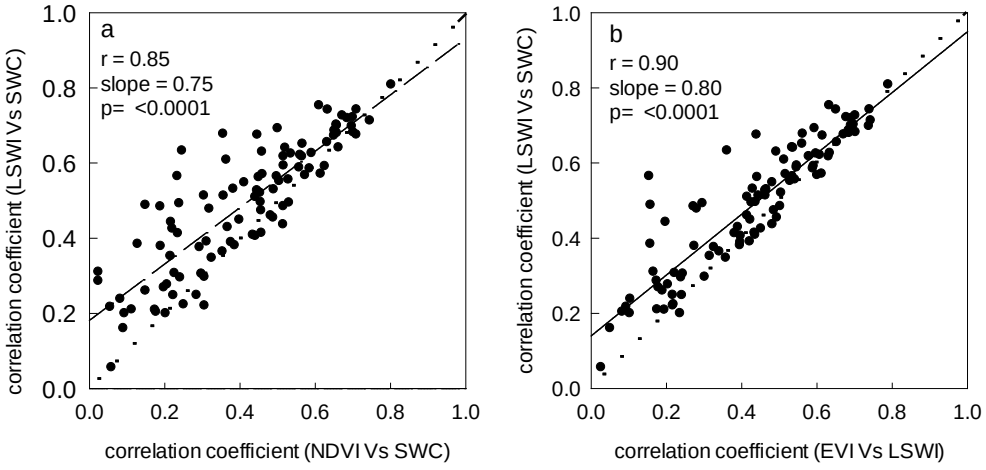

Figure 3.6. Relationship between the values of correlation coefficients of VIs anomaly and SWC anomaly. Each point represents the correlation coefficient obtained by plotting monthly anomaly values for each station.

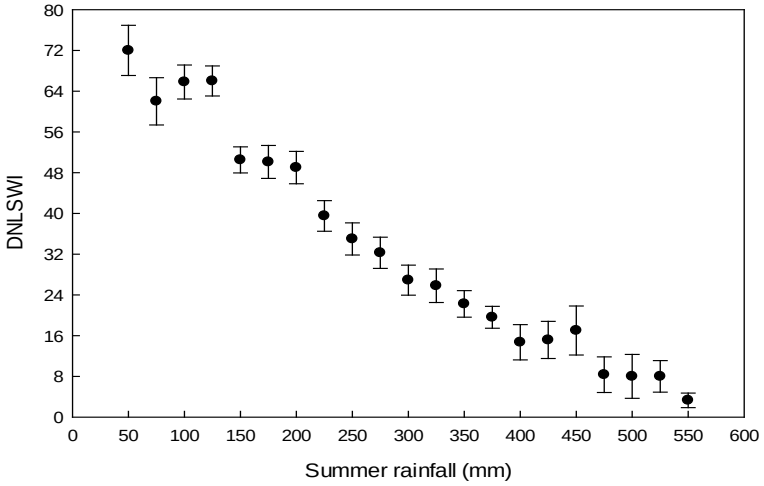

Figure 3.7. Relationship between summer rainfall and duration of LSWI < 0. Each point is an average for all Mesonet stations binned by 50 mm of summer rainfall.

The longitudinal gradient of summer rainfall is a widely recognized pattern in Oklahoma where the amount of rainfall decreases from East (mean summer rainfall ~ 300mm) to West (mean summer rainfall ~ 150 mm; Fig. 3.8a). To understand the occurrence of drought across the rainfall gradient of Oklahoma, we counted total DNLSWI during summer months (Jun-Aug) from 2000 to 2013 for all Oklahoma Mesonet stations. As expected, a distinct increasing pattern of total number of DNLSWI was observed across East-West gradient of Oklahoma (Fig. 3.8b), which was opposite to the rainfall pattern. The sites towards the east with greater amount of average summer rainfall had the least DNLSWI whereas a general increment of DNLSWI was observed with lesser precipitation as we moved from East to West.

3.3.5 Characteristics of DNLSWI and USDM drought history (2000-2013)

The pattern associated with DNLSWI for 113 Mesonet stations during the study period (2000-2013) is presented as box plots in Fig. 3.9a. These plots revealed the distribution of DNLSWI among the Mesonet sites within a year and among years. The median DNLSWI was relatively greater during the drought years (2000 = 32 days, 2006 =48 days, 2011 =56 days and 2012 = 56 days) than non-drought years.

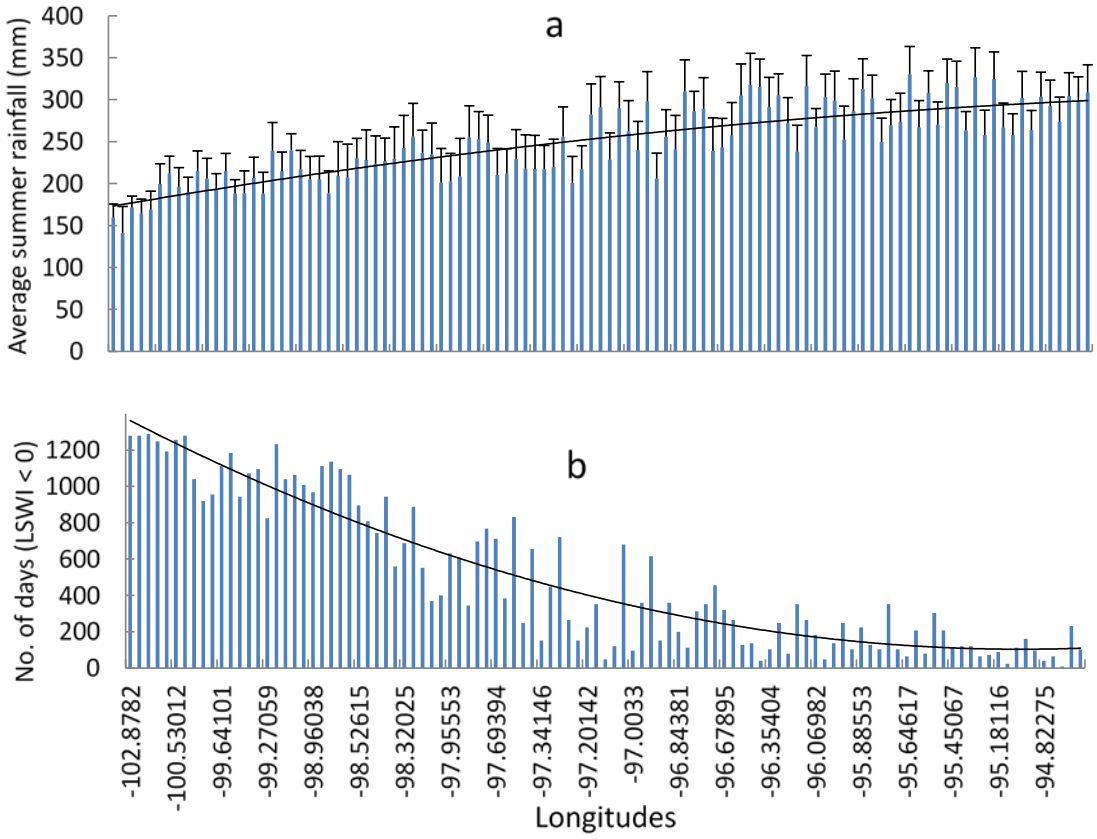

Figure 3.8. The performance of LSWI to track East-West rainfall gradient of Oklahoma: (a) average summer rainfall gradient from East to West and (b) DNLSWI (total number of days with LSWI < 0 during summer months) from 2000-2013 for 113 Mesonet stations arranged by East-West geographical locations.

The distribution as well as the median DNLSWI was the lowest in 2007 which was a pluvial year and the wettest summer on record in central Oklahoma (Arndt et al. 2009;

Christian et al. 2015b; Dong et al. 2011). Figure 3.9b shows the frequency distribution of the Mesonet stations (113 stations over 14 years) with associated DNLSWI (113 stations over 3 months) for the total study period and drought years separately. The count was highest for DNLSWI equal to 8 days because it is very common that majority of the stations could have LSWI below zero for 8 days over limited period during seasonal drying. However, the ratio of drought years to all years increased as the DNLSWI increased, suggesting that drought years contributed larger counts for the higher DNLSWI (Fig 3.9c). For example, ratio of 0.13 for DNLSWI equal to 8 days means only 13 % of the total counts was contributed by the drought years, while for DNLSWI equal to 64 days, drought years contributed 63% of the total counts, suggesting higher DNLSWI during the drought years.

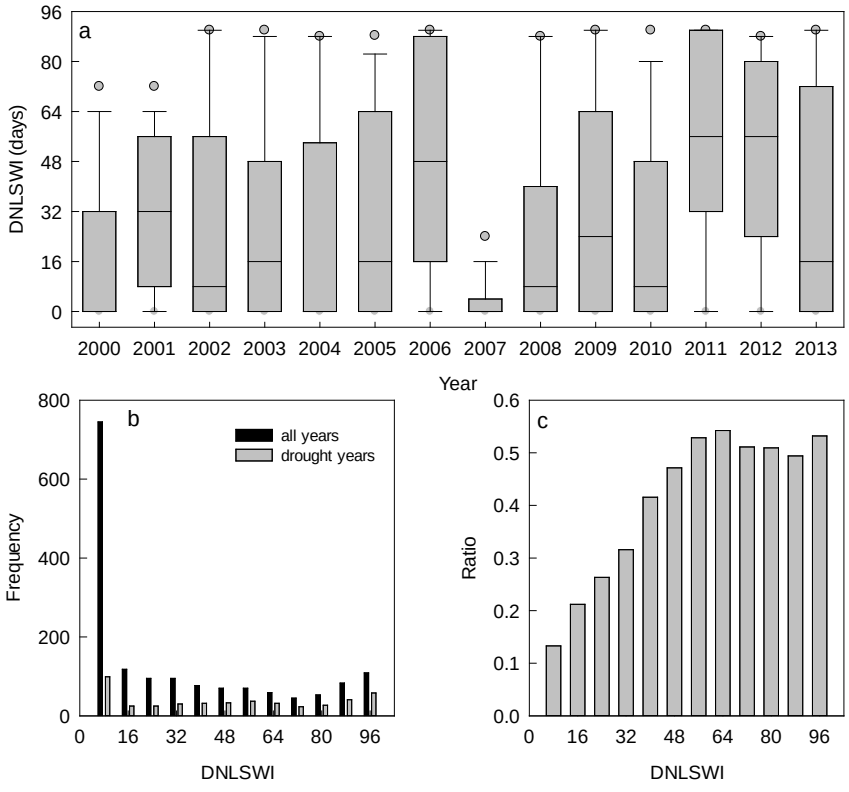

Figure 3.9. Duration of LSWI < 0 (DNLSWI) across 113 Mesonet sites during 2000-2013(a). The solid lines in the box represent the median and the dots above and below the box represent the 95 and 5 percentiles, respectively. The frequency distribution of the Mesonet stations (113 stations times 14 years) with associated DNLSWI for 2000 -2013 (b) and the ratio of number of stations with drought years to total years (drought and normal) for respective DNLSWI bins (c).

Figure 3.10 shows the weekly percentage of Oklahoma Mesonet sites affected by D0 to D4 drought from 2000 to 2013. The drought periods spanning 2006, 2011, and 2012 were evident and reached D4 status for extended periods. The plot also depicts the pluvial condition during 2007 when D0 drought occurred in a very limited temporal window. However, significant areas, especially sites in western Oklahoma where drought conditions persisted even though majority of the state yielded above normal precipitation, showed higher intensity summer drought in 2013, which was also considered as an overall pluvial year based on total year rainfall.

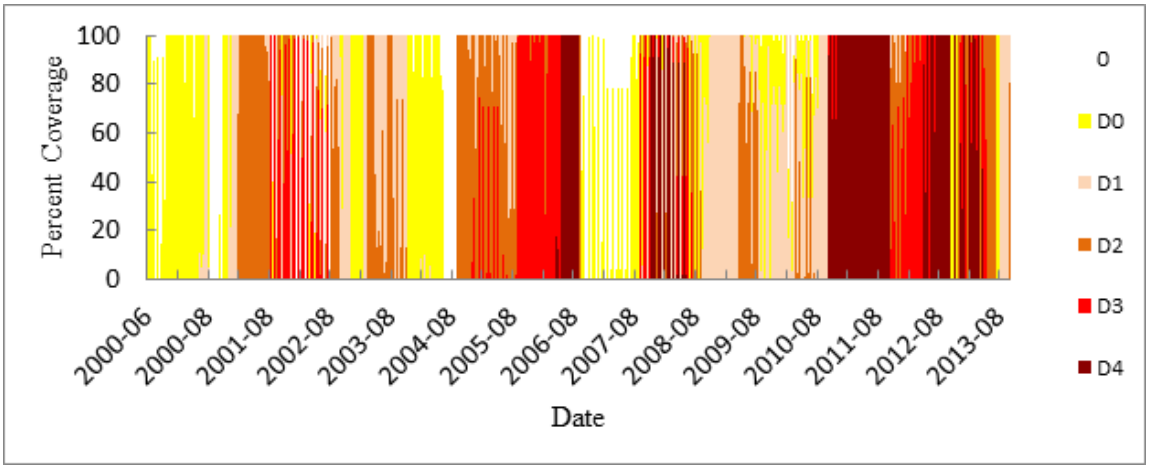

Figure 3.10. Percent of Oklahoma area covered by a USDM drought designation from 2000-2013. The designations 0 (no drought), D0 (Abnormally dry), D1 (Drought-Moderate), D2 (Drought-Severe), D3 (Drought-Extreme), and D4 (Drought-Exceptional) are the drought intensity classes defined by USDM (Data Source: U.S. Drought Monitor).

3.3.6 The Relationship between LSWI-based drought severity and USDM drought intensity categories

The LSWI values corresponding to its NDVI values for each week based on USDM weekly map is plotted in Fig. 3.11. Results showed that larger negative values of LSWI corresponded to higher drought intensity categories identified by USDM classes (i.e, D3 and D4 - extreme and exceptional), while no drought and abnormally dry categories (0 and D0) corresponded to the larger positive LSWI values. Further, moderate to severe drought categories (D1 and D2) corresponded to intermediate LSWI values. Based on this LSWI-NDVI two-dimensional scatter plot, we identified the range of LSWI values for each drought categories used by USDM in Bajgain et al. 2015. Due to the large number of site years and mixture of land cover types, the groupings of drought intensity could not be visualized effectively within the range formulated on observations at two tallgrass prairie sites. However, the general pattern that higher drought intensity tends to have lower LSWI values and vice-versa was observed for all land cover types as well as grasslands and croplands. Compared to all land cover types and croplands, grasslands showed better relationships to the drought intensity categories. To determine the agreement between LSWI-based drought intensity classification based on the LSWI value range and USDM drought categories (Table 1), we computed the percentage of pixels that fall within the defined LSWI value range for the particular drought class. The assessment was performed for different land cover types (all land covers, grasslands and croplands) (Fig. 3.12a).

Table 3.1. A summary of the USDM Drought Intensity Classes and the LSWI-based classes (see Bajgain et al., 2015)

USDM Drought Intensity Class	Description	LSWI-D values
0	non-drought	
D0	abnormally dry	LSWI > 0.1
D1	drought-moderate	0 < LSWI ≤ 0.1
D2	drought-severe	-0.1 < LSWI ≤ 0
D3	drought-extreme	
D4	drought-exceptional	LSWI ≤ -0.1

Overall, the agreement was higher (>60%) for low intensity (0 and D0) and high intensity (D3 and D4) droughts (the two ends of drought class), but the intermediate drought intensity (D1 and D2) had relatively low agreement. However, the relationship was slightly improved when computed for individual land cover types with grasslands showing the best agreement.

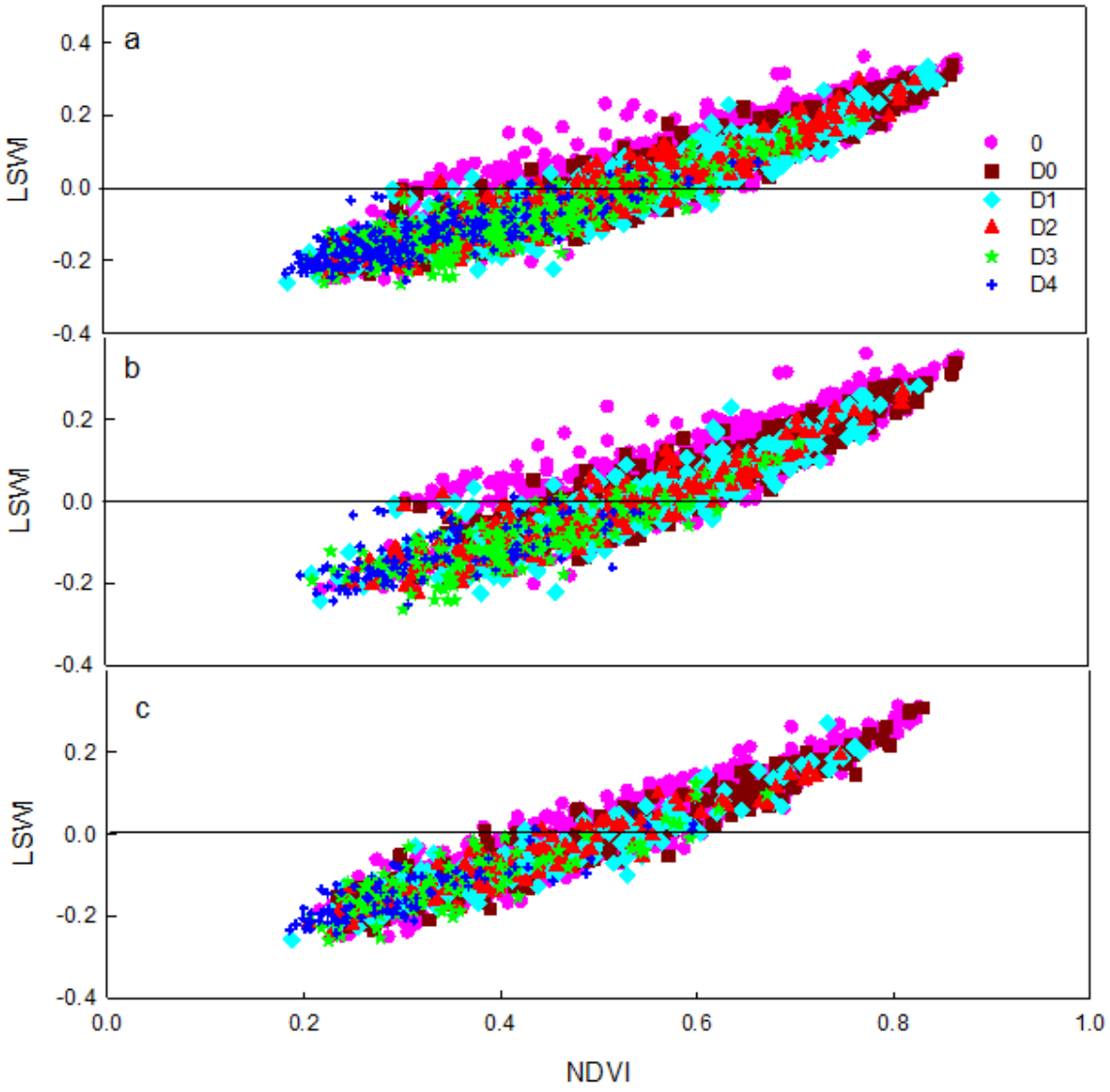

Figure 3.11. Relationship between: NDVI and LSWI for individual pixels of the all types (a), grasslands (b), and croplands (c) land cover sites for Jun – Aug over a 14-year study period (2000-2013). Each point in the plot represents the weekly observation of drought intensity designation for the study area as determined from U.S. drought monitor (USDM) drought maps.
(http://droughtmonitor.unl.edu/MapsAndData/**).**

Furthermore, we analyzed the agreement of the LSWI-based drought classification for nine climate divisions of Oklahoma to further analyze the spatial variability of drought tracking by the LSWI-based algorithm (Fig. 3.12b). The LSWI-

identification showed better agreement (>80 %) with USDM 0 and D0 (no dry & abnormally dry) classes in the eastern humid areas whereas the agreement was low (<30%) for the same drought classes in the western arid areas (panhandle). However, the western region identified as severe to exceptional drought (D3 &D4) by USDM matched very well with the new LSWI-based classification. For example, 91% of the pixels were classified as severe and exceptional droughts in the panhandle region whereas USDM also identified the same drought intensity. However, only 19 % of the low intensity drought pixels matched well with the lower intensity drought classification of USDM.

The relationship between USDM drought intensity, DNLSWI and average LSWI value is presented in Fig. 3.13. The general observation was that drought intensity increased as DNLSWI became longer. For short DNLSWI periods (0-24 days) the drought impact was sharp and then plateaued between 24-48 days. As DNLSWI became larger (> 48 days), the addition of each new day resulted into larger drought impacts identified as a higher drought intensity class by the USDM (Fig 3.13). This relationship was further supported by the average LSWI values which declined as DNLSWI increased. The decreasing pattern of average LSWI was also persistent for the shorter DNLSWI but declined sharply as the DNLSWI was longer than 50-60 days.

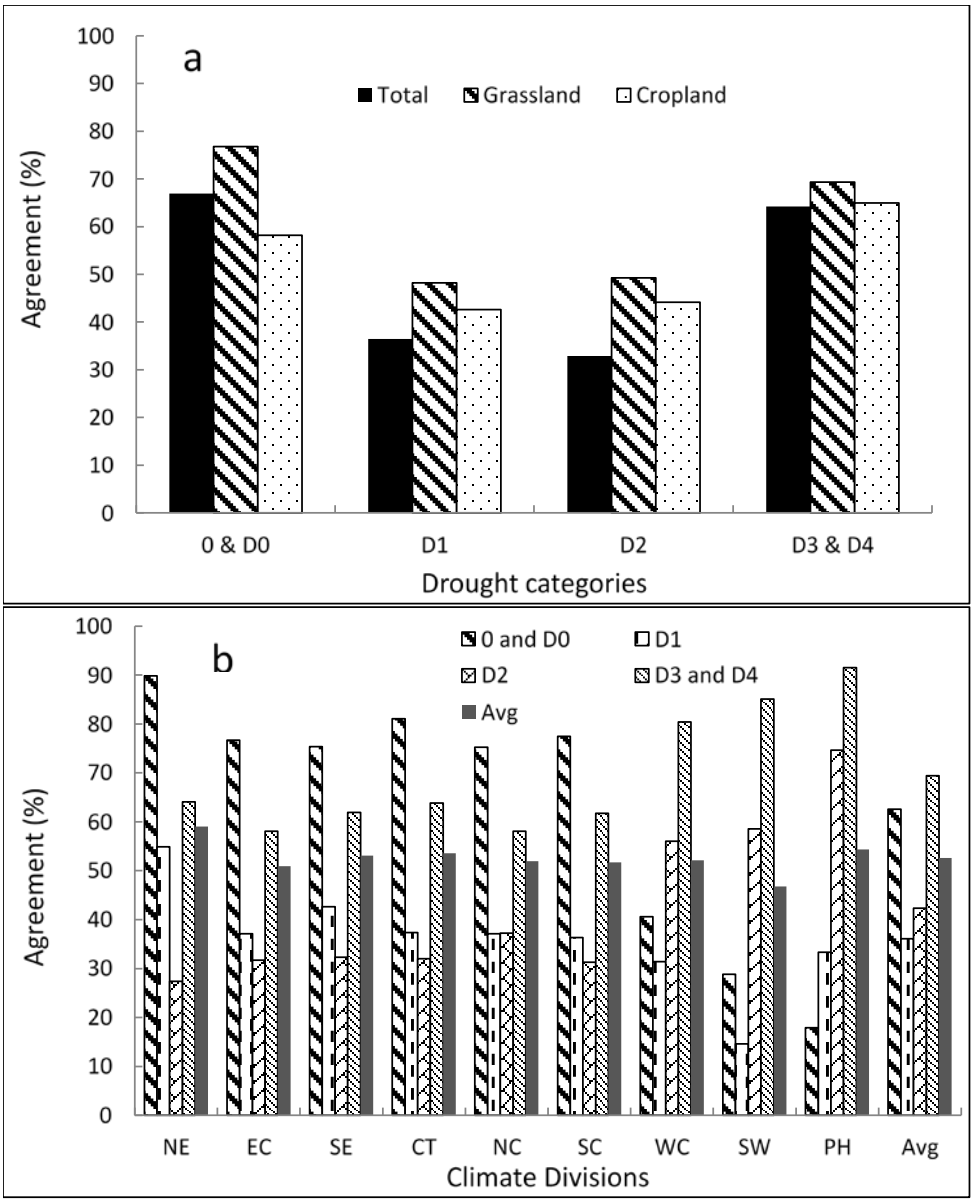

Figure 3.12. Agreement of the drought intensity class to the LSWI-based classification adapted from Bajgain et al. 2015 for different a) land cover and b) climate divisions of Oklahoma (NE: North Eastern; EC: East Central; SE: South Eastern; CT: Central; NC: North Central; SC: South Central; WC: West Central; SW: South Western and PH: Panhandle)

3.4 Discussion

The correlation analyses between summer rainfall anomalies and LSWI anomalies in drought years revealed sensitivity of LSWI to summer rainfall variability in Oklahoma.

Higher negative anomalies in summer rainfall resulted in larger decline in LSWI values, an indication of drought-impacted vegetation (Bajgain et al. 2015; Wagle et al. 2014). Regardless of different land cover and soil types across 113 Oklahoma Mesonet sites LSWI tracked droughts in majority of the study sites. However, it over classified the low intensity droughts in arid western regions of Oklahoma. Given the anticipated future increase in precipitation variability (Liu et al. 2012; Zhang and Nearing 2005), ecosystems in this region are expected to be particularly susceptible to droughts resulting large losses for food and livestock industries. Our results suggested that the ability of LSWI to track the summer rainfall anomalies could be one of the important features to assess and track agricultural droughts. Our finding on the performance of LSWI to track water content of the ecosystem was consistent with the results by Chandrasekara et al. 2011 that demonstrated LSWI as a potential indicator of increasing water content in the ecosystem following the onset of monsoon in India. Since commonly used NDVI and EVI are not always good indicators of vegetation conditions especially during adverse climatic conditions for vegetation growth (Gamon et al. 1995; Gamon et al. 1993), LSWI can better track the drought-impacted vegetation because of its higher sensitivity to drought (Bajgain et al. 2015; Chandrasekara et al. 2011; Tian et al. 2013; Wagle et al. 2014) . The opposite longitudinal patterns of DNLSWI and summer rainfall suggested that counting the DNLSWI (in days) has the ability in tracking the drought across various mesonet sites of Oklahoma. The results illustrate that LSWI can be used as an effective tool to monitor dryness persisted in the diverse (land cover and soil types) ecosystems in semi-arid and semi-humid regions in eastern and central Oklahoma. However, the spatial variability of drought tracking ability was observed based on drought intensity. In Eastern

humid regions of Oklahoma both USDM-D and LSWI-D showed no drought (0 drought class) when average summer rainfall was above 250-300 mm (Table 2). However, in western dry region of Oklahoma, USDM and LSWI based drought categories were different. For example, above 150 mm of summer rainfall was considered as no drought categories by USDM, but LSWI showed severe drought category (D3) with 150-300 mm of summer rainfall. The less agreement between our LSWI-based and USDM drought categories for the low drought intensity categories is because of the fact that dry areas like panhandle region of Oklahoma has higher negative LSWI values, and consequently, the LSWI-based algorithm showed higher drought severity. LSWI values are considered proxy of vegetation water content and are the physical values whereas USDM considered several factors including local reports of drought conditions (such as reports from water managers and residents) (Svoboda et al. 2002). This made USDM assessment more locally adjusted despite of coarse spatial resolution.

Table 3.2. USDM and LSWI based drought classes in Eastern and western Oklahoma binned by average summer rainfall of the Mesonet stations located in the areas.

	Eastern OK		Western OK	
Summer Rain (mm)	USDM-D class	LSWI-D class	USDM-D class	LSWI-D class
50-100	3	2	5	5
100-150	2	2	4	5
150-200	2	3	1	3
200-250	0.5	0.5	0	3.5
250-300	0	0	0.2	3
300-350	0	0	0	1.5
350-400	0	0	0	0
400-450	0	0		
450-above	0	0		

One of the main reasons behind attempting to establish the relationship between summer rainfall and LSWI was to determine the hydrological status of the ecosystem. The total amount of summer rainfall received by a particular ecosystem in a particular year could be related to DNLSWI which in turn can be inferred in terms of drought intensity. Though, our results showed a smooth decreasing trend of DNLSWI with increasing summer rainfall, site specific relationship could not be established (Bajgain et al. 2015) because averaging multiple data points produced a smoother overall trend. Thus, additional experiments are needed to identify the threshold values for each site with different soil and crop types in the future. Rainfall expressed as a percentage departure from the long-term average for a given period is widely used index for drought monitoring where monitoring other parameters such as soil moisture or evapotranspiration are costly and difficult (Nicholson 1989, 2000). With this approach,

where total summer rainfall is inferred in terms of DNLSWI for assessing drought is extremely valuable since LSWI is derived from satellite sensors. Therefore, it is very important to apply this information rendered from LSWI and summer rainfall relationship while developing drought monitoring network for this region.

Knowledge of LSWI-based drought intensity could be critical for assessing drought with different parameters like DNLSWI. Quantifying drought intensity in terms of LSWI and defining a threshold for each USDM drought class will be an important implication for a future drought-monitoring program. For example, secretarial disaster area determination and notification process depends on the USDM drought intensity classification for designating any geographical unit as a disaster area (USDA, 2012). The criteria used are the area should be under either D3 or D2 (at least 8 consecutive weeks) drought class. USDM drought classification involves a series of information for finding a threshold, comprised of complex procedures as well as could have a limited spatial precision because it relies on spatially interpolated climate data input (Tadesse et al. 2015). Our results suggested that this USDM drought intensity class can be linked with DNLSWI. The intersection of intensity curve and $LSWI_{avg}$ curves in Fig. 3.13 established a threshold point at which drought impacts increased sharply as $LSWI_{avg}$ declined. This threshold value is between the D2 and D3 drought intensity classes and can be inferred in terms of DNLSWI, which is approximately 60-62 days. Many agencies have used USDM drought intensity class thresholds to guide measures in a variety of assistance programs such as Livestock Forage Disaster Program (LFP), Emergency Haying and Grazing, Livestock Indemnity Program, Noninsured Crop Disaster Assistance program (NAP) and Crop Insurance Basics (Mallya et al. 2013; Mizzell and Lakshmi 2003; Otkin et al. 2015).

Such assistance programs can alternatively input DNLSWI thresholds for simple and easy operations as well as for a better precision in terms of spatial resolution (500m). However, validation of this approach of LSWI-based thresholds for such kind of applications remains a further research topic.

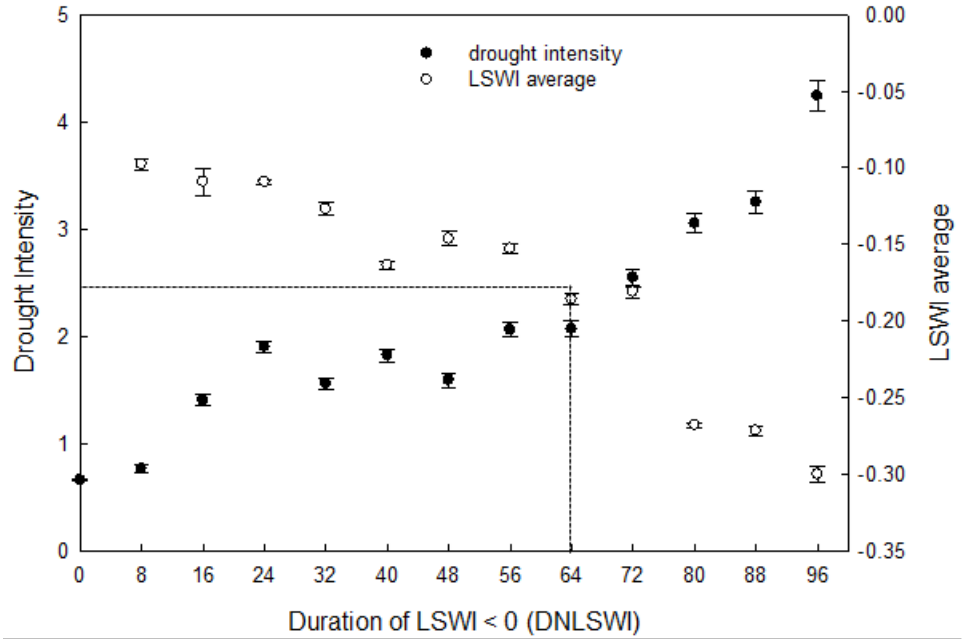

Figure 3.13. Relationship between USDM based drought intensity classes, DNLSWI (duration of LSWI < 0) and average LSWI. The USDM drought intensity classes 0, D0, D1, D2, D3, and D4 are set to 0, 1, 2, 3, 4, and 5 respectively.

The MODIS derived LSWI-based drought assessment algorithm, is simple and has a higher spatial resolution (~500). However, the LSWI-based drought algorithm can have a limitation when the reflectance from land surface is impacted by cloud cover (Jensen 2009). An appropriate gap-filling algorithm can create a continuous dataset, thereby reducing the effect of unreliable observations, which is needed for making the drought monitoring algorithm robust. Another limitation is the threshold values used in the algorithm. We used LSWI < 0 during the growing season as the indicator of

agricultural drought in tallgrass prairie based on calibration made on two study sites (Bajgain et al. 2015) .Although, the algorithm showed good agreement in most of the Mesonet sites, the DNLSWI clearly over-classified D0 and D1 drought conditions in the arid regions of Oklahoma .This is because these regions receive less rainfall than the semi-arid to semi-humid regions of eastern Oklahoma, where the algorithm was originally calibrated. This result suggests that it is necessary to further refine the LSWI-based algorithm to better represent drought severity in arid western regions of Oklahoma. One of the possible adjustments could be the LSWI threshold values for the arid region considering more negative magnitudes of the LSWI values in arid regions. This adjustment could reduce the discrepancies observed between the LSWI and USDM drought classification especially for lower drought intensity resulted from the larger negative values of LSWI, a common feature of arid region.

5. Conclusions

Results of LSWI analysis for the period of 2000-2013 for 113 Mesonet stations across Oklahoma revealed valuable information within the context of drought tracking. A strong correlation and dynamics between LSWI-anomalies and summer rainfall anomalies comprises a fact that LSWI is sensitive to rainfall variations and can be used as an indicator of drought occurrence in an ecosystem. It is then deduced that DNLSWI had the close association with the vegetation condition under rainfall variations. Pixel based drought intensity classification has been tested to validate the LSWI-based drought class for different land cover and soil types. Despite a relatively lower degree of agreement for the intermediate drought classes, the LSWI-based drought intensity class was reliable for

low and high intensity classes defined by USDM. There was a longitudinal sensitivity for low intensity droughts between eastern and western Oklahoma as shown by lower agreement of D0 and D1 drought with USDM in panhandle region (western Oklahoma). The drought assessment at larger scale could be made more effective by incorporating information and features of LSWI such as DNLSWI from a site level to a regional scale with further improvement for arid regions where larger negative LSWI values are common. The analogy of DNLSWI to USDM drought intensity class could be made complement in current drought monitoring program and algorithms. Results also demonstrated that by counting the number of DNLSWI, drought intensity thresholds can be established and used as a simple complementary tool in several applications.

3.6 Supplementary materials

Table S1. The location and biophysical features of the 113 Oklahoma Mesonet sites

SN	Name	ID	County	Latitude	Longitude	Land cover	Soil
1	Acme	ACME	Grady	34.80833	-98.02325	Grassland	Sandy loam
2	Ada	ADAX	Pontotoc	34.79851	-96.66909	Grassland	Sandy loam
3	Altus	ALTU	Jackson	34.58722	-99.33808	Cropland	Clay loam
4	Alva	ALVA	Woods	36.70823	-98.70974	Cropland	Clay loam
5	Antlers	ANTL	Pushmataha	34.24967	-95.66844	Cropland	N/A
6	Apache	APAC	Caddo	34.91418	-98.29216	Cropland	Loamy sand
7	Ardmore	ARDM	Carter	34.19258	-97.08568	Cropland	Loam
8	Arnett	ARNE	Ellis	36.07204	-99.90308	Shrubs	Sandy loam
9	Beaver	BEAV	Beaver	36.80253	-100.53012	Grassland	Loam
10	Bessie	BESS	Washita	35.40185	-99.05847	Grassland	Silt loam
11	Bixby	BIXB	Tulsa	35.96305	-95.86621	Cropland	Sandy loam
12	Blackwell	BLAC	Kay	36.75443	-97.25452	Cropland	Silt loam
13	Boise City	BOIS	Cimarron	36.69256	-102.49713	Cropland	Clay loam
14	Bowlegs	BOWL	Seminole	35.17156	-96.63121	Grassland	Sandy loam
15	Breckinridge	BREC	Garfield	36.41201	-97.69394	Cropland	Silt loam
16	Bristow	BRIS	Creek	35.7805	-96.35404	Grassland	Sandy loam
17	Broken Bow	BROK	McCurtain	34.0433	-94.6244	Grassland	N/A
18	Buffalo	BUFF	Harper	36.83129	-99.64101	Cropland	Loam
19	Burbank	BURB	Osage	36.63459	-96.81046	Cropland	N/A
20	Bourneville	BURN	Love	33.89376	-97.26918	Cropland	Loamy sand
21	Butler	BUTL	Custer	35.5915	-99.27059	Cropland	Silt loam
22	Byars	BYAR	Garvin	34.8497	-97.0033	Grassland	Loamy sand
23	Camargo	CAMA	Dewey	36.02866	-99.34652	Cropland	Loam
24	Centrahoma	CENT	Coal	34.60896	-96.33309	Grassland	Sandy loam

25	Chandler	CHAN	Lincoln	35.65282	-96.80407	Grassland	Sandy clay loam
26	Cherokee	CHER	Alfalfa	36.74813	-98.36274	Cropland	Loam
27	Cheyenne	CHEY	Roger Mills	35.54615	-99.7279	Shrubs	Sandy loam
28	Chikashaw	CHIC	Grady	35.03236	-97.91446	Cropland	N/A
29	Clayton	CLAY	Pushmataha	34.65657	-95.32596	Grassland	N/A
30	Cloudy	CLOU	Pushmataha	34.22321	-95.2487	Grassland	Silt loam
31	Cookson	COOK	Cherokee	35.68001	-94.84896	Grassland	Silt loam
32	Copan	COPA	Washington	36.90987	-95.88553	Cropland	Loam
33	Durant	DURA	Bryan	33.92075	-96.32027	Grassland	Sandy loam
34	El Reno	ELRE	Canadian	35.54848	-98.03654	Grassland	Silt loam
35	Erick	ERIC	Beckham	35.20494	-99.80344	Grassland	Loamy sand
36	Eufaula	EUFA	McIntosh	35.30324	-95.65707	Grassland	Loam
37	fairview	FAIR	Major	36.26353	-98.49766	Cropland	Silt loam
38	fittstown	FITT	Pontotoc	34.55205	-96.71779	Grassland	Sandy loam
39	Foraker	FORA	Osage	36.84053	-96.42777	Cropland	Sandy loam
40	freedom	FREE	Woodward	36.72562	-99.14234	Grassland	Silt loam
41	Fort Cobb	FTCB	Caddo	35.14887	-98.46607	Cropland	Loamy sand
42	Goodwell	GOOD	Texas	36.60183	-101.6013	Grassland	Loam
43	Grandfield	GRAN	Tillman	34.2392	-98.7397	Cropland	Clay loam
44	Guthrie	GUTH	Logan	35.84891	-97.47978	Grassland	Sandy loam
45	Haskell	HASK	Muskogee	35.74798	-95.64047	Cropland	Silt loam
46	Hectroville	HECT	Okmulgee	35.84162	-96.0024	Grassland	Loam
47	Hinton	HINT	Caddo	35.48439	-98.48151	Cropland	Sandy loam
48	Hobart	HOBA	Kiowa	34.98971	-99.05283	Cropland	Silty clay loam
49	Hollis	HOLL	Harmon	34.6855	-99.83331	Cropland	N/A
50	Hooker	HOOK	Texas	36.85518	-101.22547	Cropland	loam
51	Hugo	HUGO	Choctaw	34.03084	-95.54011	Grassland	Loam
52	Idabel	IDAB	McCurtain	33.83013	-94.8803	Grassland	Silt loam
53	Inola	INOL	Rogers	36.14246	-95.45067	Cropland	Loam

54	Jay	JAYX	Delaware	36.4821	-94.78287	Grassland	Silt loam
55	Kenton	KENT	Cimarron	36.82937	-102.8782	Grassland	Loam
56	Ketchum Ranch	KETC	Stephens	34.52887	-97.76484	Grassland	Loam
57	Kingfisher	KING	Kingfisher	35.8805	-97.91121	Cropland	Sandy Loam
58	Lahoma	LAHO	Major	36.38435	-98.11139	Cropland	Silt loam
59	Lane	LANE	Atoka	34.30876	-95.99716	Cropland	Sandy loam
60	Madill	MADI	Marshall	34.03579	-96.94394	Grassland	N/A
61	Mangum	MANG	Greer	34.83592	-99.42398	Grassland	Sand
62	Marena	MARE	Payne	36.06434	-97.21271	Grassland	Sandy clay loam
63	May ranch	MAYR	Woods	36.98707	-99.01109	Cropland	Sandy loam
64	McAlester	MCAL	Pittsburg	34.88231	-95.78096	Grassland	Loamy sand
65	Medford	MEDF	Grant	36.79242	-97.74577	Grassland	N/A
66	Medicine Park	MEDI	Comanche	34.72921	-98.56936	Grassland	Sandy loam
67	Miami	MIAM	Ottawa	36.88832	-94.84437	Grassland	Silt loam
68	Minco	MINC	Grady	35.27225	-97.95553	Grassland	Silt loam
69	Marshall	MRSH	Logan	36.11685	-97.60685	Cropland	Silt loam
70	Mt Herman	MTHE	McCurtain	34.31072	-94.82275		N/A
71	Newkirk	NEWK	Kay	36.8981	-96.91035	Grassland	Silt loam
72	Newport	NEWP	Carter	34.2281	-97.20142	Grassland	N/A
73	Ninnekah	NINN	Grady	34.96774	-97.95202	Cropland	N/A
74	Norman	NORM	Cleveland	35.2556	-97.4836	Grassland	Silt loam
75	Nowata	NOWA	Nowata	36.74374	-95.60795	Grassland	Silt loam
76	Oilton	OILT	Creek	36.03126	-96.49749	Grassland	Sandy loam
77	Okemah	OKEM	Okfuskee	35.43172	-96.26265	Grassland	Silt loam

78	Okmulgee	OKMU	Okmulgee	35.58211	-95.91473	Grassland	Loam
79	Pauls Valley	PAUL	Garvin	34.7155	-97.22924	Grassland	Silt loam
80	Pawnee	PAWN	Pawnee	36.36114	-96.76986	Cropland	Silty clay loam
81	Perkins	PERK	Payne	35.99865	-97.04831	Cropland	Loam
82	porter	PORT	Wagoner	35.8257	-95.55976	Grassland	Sandy loam
83	Pryor	PRYO	Mayes	36.36914	-95.27138	Grassland	Silt loam
84	Putnam	PUTN	Dewey	35.89904	-98.96038	Cropland	Loam
85	Red rock	REDR	Noble	36.3559	-97.15306	Grassland	Loam
86	Ringling	RING	Jefferson	34.19365	-97.58812	Grassland	Sandy loam
87	Sallisaw	SALL	Sequoyah	35.43815	-94.79805	Grassland	Silt loam
88	Seiling	SEIL	Woodward	36.19033	-99.0403	Grassland	Loam
89	Shawnee	SHAW	Pottawatomie	35.36492	-96.94822	Grassland	Silt loam
90	Skiatook	SKIA	Osage	36.4153	-96.03706	Grassland	Sandy loam
91	Slapout	SLAP	Beaver	36.59749	-100.26192	Grassland	Sand
92	Spencer	SPEN	Oklahoma	35.54208	-97.34146	Grassland	Sandy loam
93	Stigler	STIG	Haskell	35.26527	-95.18116	Grassland	Silt loam
94	Stillwater	STIL	Payne	36.12093	-97.09527	Grassland	Silty clay loam
95	Stuart	STUA	Pittsburg	34.87642	-96.06982	Grassland	Loamy sand
96	Sulphur	SULP	Murray	34.5661	-96.95048	Grassland	N/A
97	Tahlequah	TAHL	Cherokee	35.97235	-94.98671	Cropland	Silt loam
98	Talihina	TALA	Rogers	36.57431	-95.74515	Grassland	N/A
99	Tipton	TIPT	Tillman	34.43972	-99.13755	Cropland	Sandy loam
100	Tishomingo	TISH	Johnston	34.33262	-96.67895	Grassland	Silt loam
101	Vanoss	VANO	Pontotoc	34.79146	-96.84381	Grassland	N/A
102	Vinita	VINI	Craig	36.77536	-95.22094	Grassland	Silt loam
103	Walters	WALT	Cotton	34.3647	-98.32025	Grassland	N/A
104	Washington	WASH	McClain	34.98224	-97.52109	Grassland	Loam
105	Watonga	WATO	Blaine	35.84185	-98.52615	Cropland	Loam
106	Waurika	WAUR	Jefferson	34.16775	-97.98815	Grassland	Sandy loam
107	Weatherford	WEAT	Custer	35.5083	-98.77509	Cropland	Silt loam
108	Webber falls	WEBB	Muskogee	35.47298	-95.13209	Cropland	Silt Loam
109	Westville	WEST	Muskogee	35.489	-95.1233	Grassland	Silt loam
110	Wilburton	WILB	Latimer	34.90092	-95.34805	Grassland	Silt loam
111	Wister	WIST	Le Flore	34.98426	-94.68778	Grassland	Silt loam
112	Woodward	WOOD	Woodward	36.42329	-99.41682	Grassland	Sandy loam
113	Wyona	WYNO	Osage	36.51806	-96.34222	Grassland	Silt loam

Chapter 4: Contrasting carbon dioxide and water vapor fluxes between winter wheat and tallgrass prairie in central Oklahoma

Abstract

Winter wheat (*Triticum aestivum* L.) and tallgrass prairie are common land cover types in the southern plains of the United States. During the last century, agricultural expansion into native grasslands was extensive, particularly managed pasture or dryland crops such as winter wheat. In this study, we measured carbon dioxide (CO_2) and water vapor (H_2O) fluxes from winter wheat and tallgrass prairie sites at El Reno in Central Oklahoma using the eddy covariance technique in 2015 and 2016. The objective of this study was to contrast CO_2 and H_2O fluxes between these two ecosystems to provide insights on the impacts of conversion of tallgrass prairie to winter wheat on regional carbon and water budgets. Daily net ecosystem CO_2 exchange (NEE) reached seasonal peaks of - 9.4 and -8.8 g C m^{-2} in 2015 and - 6.2 and -7.5 g C m^{-2} in 2016 at winter wheat and tall grass prairie sites, respectively. The winter wheat site was a net sink of carbon for four months (February-May), whereas the tallgrass prairie site was a net sink of carbon for seven months (March-September). At the annual scale, the winter wheat site was a net source of carbon (56 ± 13 and 33 ± 9 g C m^{-2} yr^{-1} in 2015 and 2016, respectively). In contrast, the tallgrass prairie site was a net sink of carbon (-128 ± 69 and -119 ± 53 g C m^{-2} yr^{-1} in 2015 and 2016, respectively). The daily ET reached seasonal maximum of 6.0 and 5.3 mm in 2015 and 7.2 and 8.2 mm day^{-1} in 2016 at the winter wheat and tallgrass prairie sites, respectively. Although ecosystem water use efficiency (EWUE) was higher in winter wheat (11 - 13 g CO_2 mm^{-1} ET) than in tallgrass prairie (7 – 8.5 g CO_2 mm^{-1}

ET) at the seasonal scale, summer fallow contributed higher water loss from the wheat site resulting into lower EWUE at the annual scale. Considering the large scale of land use conversion from prairie to winter wheat, our results indicate that the differences in magnitudes and patterns of CO_2 and H_2O fluxes between the two ecosystems can influence carbon and water budgets at the regional scale.

4.1 Introduction

Land use has changed rapidly across much of North America during the last century, mainly due to intensification and expansion of agricultural cultivation in many central and western states (Turner and Meyer 1994; Wright and Wimberly 2013). In the Great Plains region, agricultural expansion into native grasslands has been extensive, as particularly either managed pasture or dryland crops such as wheat (winter and spring, *Triticum aestivum* L.) and sorghum (Sorghum bicolor L.) (Lark et al. 2015; Riebsame 1990). The savannas and tallgrass prairie have been replaced by cultivated crops and only about 4 % of tall grass prairie which once covered a large portion of the central US remains today (Claassen et al. 2011; Fischer et al. 2007).

Grasslands contributed about 77% (2.3 million hectares) of new croplands in the US from 2008-2012 (Lark et al. 2015). Out of the converted land, 26% was planted to corn (*Zea mays L.*), followed by wheat (25%). The expansion of wheat was more common across the central plains, with spring wheat in the north and winter wheat in the south (Lark et al. 2015). Land cover remote sensing datasets from the Cropland Data Layer (CDL) produced by United States Department of Agriculture (USDA) National Agricultural Statistics Service (NASS) also showed about 1.1 million hectares of

grassland converted to winter wheat from 2008 to 2015, in the southern plains (Oklahoma, Texas) (Fig. 4.1a). The area converted from tallgrass prairie to winter wheat was highest in 2008 and lowest in 2013 (Fig. 4.1a inset bar graph). To understand the border implications of such land use change in the region, a comparative analysis of carbon dioxide (CO_2) and water vapor (H_2O) fluxes of cultivated systems (e.g., winter wheat) and their native counterparts (tallgrass prairie) can provide insights into the changes in carbon and water budgets.

Major sections of the Southern Great Plains are dominated by winter wheat, a C3 species, generally planted in September/October and harvested in June/July of the following year. Traditionally, a 3-4 months fallow period from harvest to planting is considered an important component of the farming system to accumulate soil moisture for the next wheat crop cycle (Dhuyvetter et al. 1996; Lyon et al. 2007). In contrast, the growing season of tallgrass prairie (mixture of C3 and C4 species, dominantly warm season) starts between March and May depending on spring temperature and remains active until September/October (Cooley et al. 2005; Fischer et al. 2007). The dynamics of the land surface processes resulting from the combined interactions of climate, vegetation cover, and management practices are closely coupled with the dynamics of the lower atmosphere and are very significant in the mid-continental regions such as the southern plains. Thus, the change from prairie to winter wheat shifts the magnitude and seasonal timing of energy, momentum, CO_2, and H_2O fluxes between the atmosphere and ecosystem in this region (McPherson and Stensrud 2005). Further, the change in vegetation over an extended region may induce changes in the circulation patterns resulting into changes in weather conditions over much larger regions (Cooley et al.

2005; Fischer et al. 2007; Song et al. 1997). Observational analysis using Oklahoma Mesonet data (McPherson et al. 2007) demonstrated that the winter wheat belt in Oklahoma significantly altered the mesoscale atmospheric environment (Haugland and Crawford 2005; McPherson et al. 2004). Numerical modeling simulations, conducted by replacing native grassland vegetation with winter wheat in Oklahoma showed weakened winds within the planetary boundary layer due to insufficient sensible heat which impacted the mesoscale circulation (McPherson and Stensrud 2005). Similarly, spatial heterogeneity caused by intermixing of winter wheat in Oklahoma into grasslands induced the vertical velocities of 1-2 ms^{-1}, which is linked to convective cloud formation (Weaver and Avissar 2001). Various studies in the past have quantified within season and inter-annual variations in CO_2, H_2O, and energy fluxes in tallgrass prairies and crop fields of the southern plains (Fischer et al. 2012; Meyers 2001; Suyker and Verma 2001; Suyker et al. 2003). However, this study focuses on contrasting CO_2 and H_2O fluxes of winter wheat and tallgrass prairie ecosystems within the context of land use change, a significant human intervention in the native prairies of southern plains over the past century and continuing today. Specifically, the following questions were addressed in this study: a) What were the magnitudes and seasonal patterns of CO_2 and ET fluxes in tallgrass prairie and winter wheat? b) What is the impact of management activities (fallow on winter wheat site and grazing on tallgrass prairie site) on the total annual carbon and water budgets of the two sites? and c) what are the differences in seasonal and annual dynamics of ecosystem water use efficiency (EWUE) between winter wheat and tallgrass prairie sites? This study has a great significance to understand the impacts of land conversion from grassland to winter wheat on carbon and water budgets since the

southern plains of the United States has seen the dramatic land use change in the last decades.

4.2 Materials and methods

4.2.1 Study sites

The measurements were conducted in two sites: a) native tallgrass pastureland (64 ha) and b) winter wheat cropland (11 ha) spaced about 2.7 km at the US Department of Agriculture- Agricultural Research Service (USDA- ARS), Grazinglands Research Laboratory (GRL, 35.561319, -98.035742, 428m), in El Reno, Oklahoma (Fig. 4.1b). El Reno has a temperate continental climate with an average air temperature of 14.9 °C and an average annual rainfall of 860 mm for the 1091-2000 period (Fischer et al. 2012).

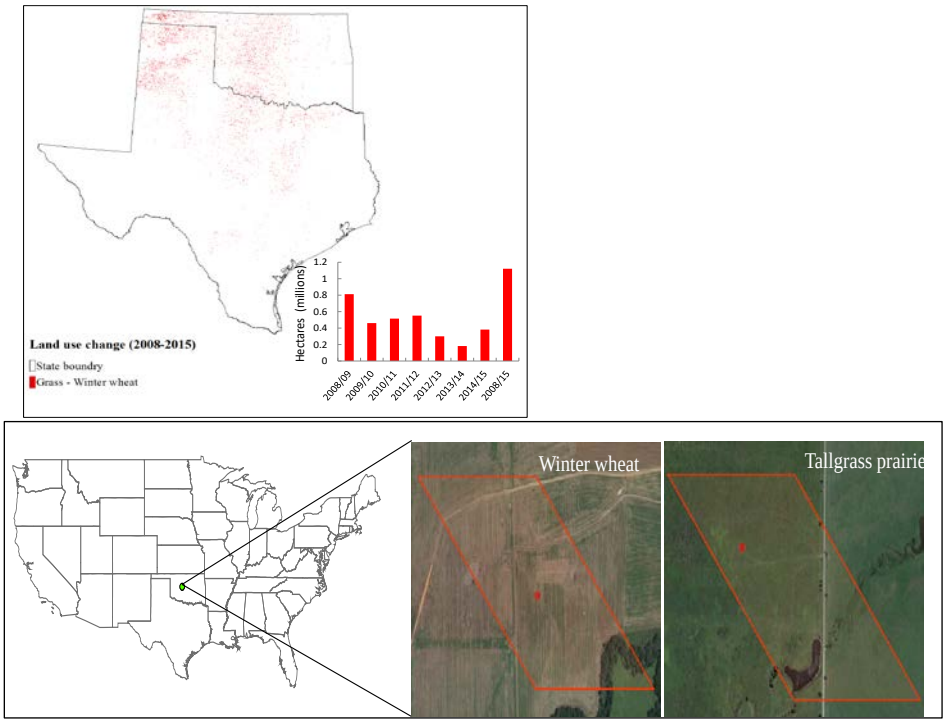

Figure 4.1. (a) Map represents the grassland conversion to winter wheat (2008-2015) in the southern plains (Oklahoma, Texas). Inset bar graph represents the yearly change in land area from grassland to winter wheat. (b) Location and landscape features of study sites. The red dots represent the location of the flux tower and the red rectangles represent the size of one Moderate Resolution Imaging Spectroradiometer pixel (~500m spatial resolution).

Winter wheat is a cool season crop representing the dominant cultivated ecosystem (converted from tallgrass prairie) of central Oklahoma. The first season of winter wheat was planted on 29th September 2014, on a tilled and fertilized field dominated by silt loam soil. and was harvested on 10th June, 2015 and the land was kept fallow during the summer months with weed control by tillage and herbicide application. The second season of winter wheat was planted on 9th September, 2015 and harvested on 10th June, 2016. The other details on management practices are presented on Table 1. Tallgrass prairie is predominantly warm season vegetation representing the native, mixed species grassland of Oklahoma. The site has silt loam soil with big bluestem (*Andropogon gerardi* Vitman) and little bluestem (*Schizachyrium halapense* (Michx.) Nash.) as dominant species. The study site was grazed for nine months (Jan-Feb, Jun-Dec) in 2015 and for six months in 2016 (Jan, May-Jun, Aug-Oct) at different grazing intensities. More information on the management activities at study sites and climatic features of the study years are presented in Table 1 and Fig. 4.2.

Table 4.1 Major management activities at the winter wheat and tallgrass prairie sites during the observation period.

Date	Management
Winter Wheat site	
Sep, 2014	Chisel plow tillage
Sep, 2014	Pre-plant fertilizer (32-23-0 @ 168 kg/ha)
Sep-29,2014	Planting (Gallagher variety with seeding rate 89.6 kg/ha)
Oct -29,2014	Starter fertilizer (32-23-0 @ 56 kg/ha)
Jun-10,2015	Harvest
Jun-30,2015	Tillage (tandem disc harrow)
Jul-29,2015	Herbicide RT 3 glyphosate, Weedmaster (dicamba and 2,4 D)
Aug-18, 2015	Tillage
Sep-06, 2015	Pre-plant fertilizer (32-23-0 @ 112 kg/ha)
Sep-09, 2015	Planting (Gallagher variety with seeding rate 89.6 kg/ha)
Sep-12, 2015	Starter fertilizer (32-23-0 @ 81.8 kg/ha)
Jun-10, 2016	Harvest
Jun-24, 2016	Herbicide RT3 glyphosate, Weedmaster (dicamba and 2,4 D)
Jul-19, 2016	Tillage (tandem disc harrow)
Aug-18, 2016	Tillage (tandem disc harrow)
Tallgrass Prairie site	
01-Jan, 2015 to 15-Feb, 2015	Grazing (Cows average weight of 520 kg with stocking rate @ 0.40 hd/ha)
01-Jun, 2015 to 31-Jul, 2015	Grazing (Cows average weight of 480 kg with stocking rate @ 0.40 hd/ha)
01-Aug, 2015 to 31-Dec, 2015	Grazing (Cows average weight of 576 kg with stocking rate @ 0.96 hd/ha)
01-Jan, 2016 to 31-Jan, 2016	Grazing (Cows average weight of 576 kg with stocking rate @ 0.73 hd/ha)
30-May, 2016 to 10-Jun, 2016	Grazing (Cows average weight of 576 kg with stocking rate @ 0.72 hd/ha)
31-Aug, 2016 to 18-Oct, 2016	Grazing (Cows average weight of 576 kg with stocking rate @ 0.72 hd/ha)

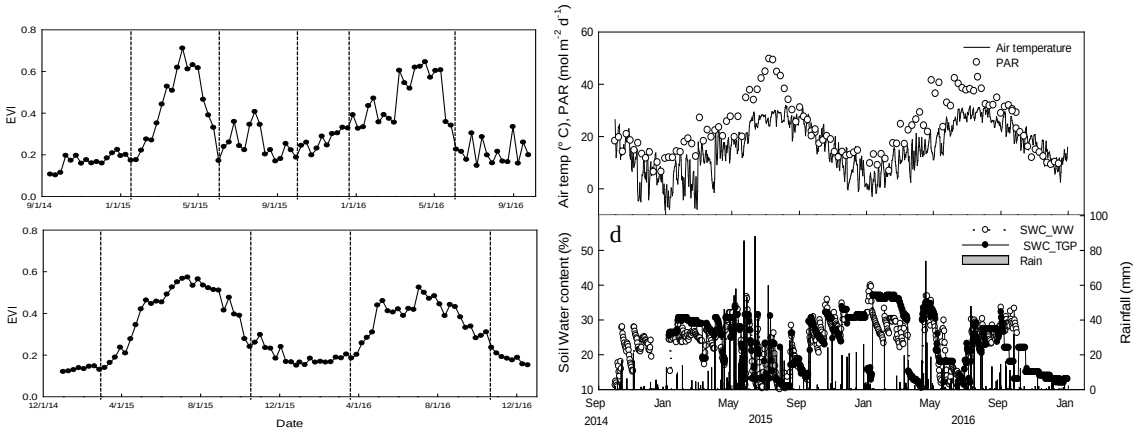

Figure 4.2 Seasonal dynamics of enhanced vegetation index (EVI) of winter wheat (a) and tallgrass prairie (b); photosynthetically active radiation (PAR) and mean air temperature (c); and soil water content (SWC) and rainfall at winter wheat and tallgrass prairie sites (d). Each data point for PAR and EVI represents 8-day mean.

4.2.2 Eddy covariance and other supplementary measurements

Eddy covariance (EC) towers were deployed to measure CO_2, H_2O and energy fluxes from the winter wheat (35.5685, -98.0558) and tallgrass prairie (35.54865°, -98.03759°) ecosystems. Continuous measurements of CO_2 and H_2O fluxes from October 2014 to September 2016 for winter wheat and from January 2015 to December 2016 for tallgrass prairie respectively are presented in this study.

The measurement system at each site consisted of a three-dimensional sonic anemometer (CSAT3, Campbell Scientific Inc., Logan, UT, USA) and an open path infrared gas analyzer (LI-7500, LI-COR Inc., Lincoln, NE, USA). The sensors were mounted at a 2.5 m height from the ground and the system was set up at the center of each site facing south, towards the prevalent wind direction. The fetch area was about 300 m in all directions. The *EddyPro* processing software (LI-COR Inc., Lincoln, NE, USA), was used to process the raw data, collected at 10 Hz frequency (10 samples sec^{-1}), to get 30-min fluxes. The software employed correction factors for coordinate alignment,

temperature due to humidity influence, and compensation of density fluctuations in infrared gas analyzer using the Webb-Pearman-Leuning (WPL) theory to make necessary corrections in the high frequency data. Negative sign convention is used to denote CO_2 uptake by the ecosystem whereas positive sign denotes the CO_2 release by the ecosystem to atmosphere.

Auxiliary sensors measured other metrological and soil variables. Quantum sensors (LI-190, LI-COR Inc. Lincoln, NE, USA) were used to measure photosynthetic photon flux density (PPFD). Net radiometers (CNR1, Kipp and Zonen, Delft, The Netherlands) were used to measure net radiation (Rn) over plant canopy. Temperature and relative humidity were measured by using temperature and relative humidity probes (HMP45C, Vaisala, Helsinki, Finland). Similarly, self-calibrating heat flux sensors (HFT3.1, Radiation& Energy Balance Systems, Inc, Seattle, WA, USA) at 5-cm depth were used to measure soil heat fluxes (G). Soil moisture content was measured at about 5-cm depth using Hydra probe (Delta-T, Lexington, MA, USA).

4.2.3 Vegetation measurements and phenology

Leaf area index (LAI) was measured at biweekly intervals during the active growing season using the LAI-2200 (LI-COR Biosciences, Lincoln, NE, USA). Six measurements were made within the eddy covariance footprint area at each site. Aboveground biomass (AGB) was measured by destructive sampling from 0.5 m^2 quadrats with three replicates at each site. The fresh samples were oven dried at 70 °C for 72 hours and total aboveground dry weight was measured by weighing the oven dried

samples. The 8-day Enhanced Vegetation Index (EVI) (Huete et al. 2002) was computed from the land surface reflectance data from MOD9A1 data product downloaded from the University of Oklahoma data portal (http://eomf.ou.edu/modis/visualization/gmap/).

Winter wheat in this region is often a dual-purpose crop in which cattle grazing is allowed over the winter (generally November-February) and the crop is allowed to grow for grain harvest after removal of the cattle. However, the winter wheat site was not grazed during this study. The tallgrass prairie is generally used for grazing. Based on EVI time series data, we divided the one year cycle of winter wheat into two categories: growing season and non-growing season. The growing season for winter wheat comprises the period from planting to harvesting which is referred to as I-A (November-January) and I-B (February-June) whereas the non-growing season (summer fallow) is the period between harvesting (June) and the next planting (September), denoted as II. For the tallgrass prairie, the calendar year is divided into growing season (March to mid-October) and non-growing season (January, February and mid-October to December) based on phenology represented by the EVI time series data (Fig. 4.2a, b).

4.2.4 Data Screening and Gap filling for eddy flux tower data

Quality flags were applied for screening erroneous data. Data outside a ± 3.5 standard deviation range from a 14-day running mean window were identified as outliers and were removed (Wagle et al. 2015a). This allowed us to filter out the data outside of the accepted range of $-50 < CO2\ flux < 60\ \mu mol\ m^{-2}\ s^{-1}$, $-20 < LE < 600\ W\ m^{-2}$, and $-100 < H < 400 W\ m^{-2}$ (Joo et al. 2016; Ní Choncubhair et al. 2016; Zeri et al. 2011). We used the online R package "REddyProc" tool developed at the Max Planck Institute for

Biogeochemistry, Jena, Germany (Moffat et al. 2007; Reichstein et al. 2005) for gap filling of flux data and partitioning of NEE into ecosystem respiration (ER) and gross primary production (GPP). The gaps in the datasets (18 and 22% at the winter wheat site and 24 and 32% at the tallgrass prairie site in 2015 and 2016, respectively) were due to filtering of bad quality and unreliable values and malfunctioning of the sensors were gap filled. Average value of measurements immediate before and after the gap was used to fill half hourly gaps. Gaps of two hours or fewer hours were filled by linear interpolation. Mean diurnal variation, look up tables, and regressions techniques were used to fill the larger gaps either in isolation or in combination based on the requirements described in previous studies (Amiro et al. 2006; Falge et al. 2001; Hui et al. 2004; Moffat et al. 2007; Wilson and Baldocchi 2001). The NEE was partitioned into ER and GPP using the regression model constructed by plotting ER versus either soil or air temperature. This model defines the temperature sensitivity of ER by estimating the other parameters to separate ER and GPP from NEE (Lloyd and Taylor 1994; Reichstein et al. 2005).The gap filled NEE and partitioned GPP and ER data were used to compute the daily, seasonal and annual carbon budgets.

4.2.5 Energy Balance Closure

The plausibility of fluxes from the EC system was assessed based on energy balance closure (EBC). According to the first law of thermodynamics, the sum of turbulent fluxes (latent, LE and sensible heat, H) should be equivalent to the available energy, (i.e., R_n-G). The imbalance between available energy and turbulent fluxes indicates inaccurate estimates of scalar fluxes. Many research studies reported EBC as a

standard test of eddy covariance data (Foken 2008; Twine et al. 2000; Wilson et al. 2002). Turbulent fluxes (LE +H) are commonly underestimated by about 10-30% relative to the estimates of available energy (Rn-G) (Aubinet et al. 1999; Barr et al. 1994; Foken 2008; Wilson et al. 2002).The EBC, based on half-hourly data, was 83% and 85% in winter wheat and tallgrass prairie, respectively in 2015 and 77% for both sites in 2016 (Fig. 4.3).

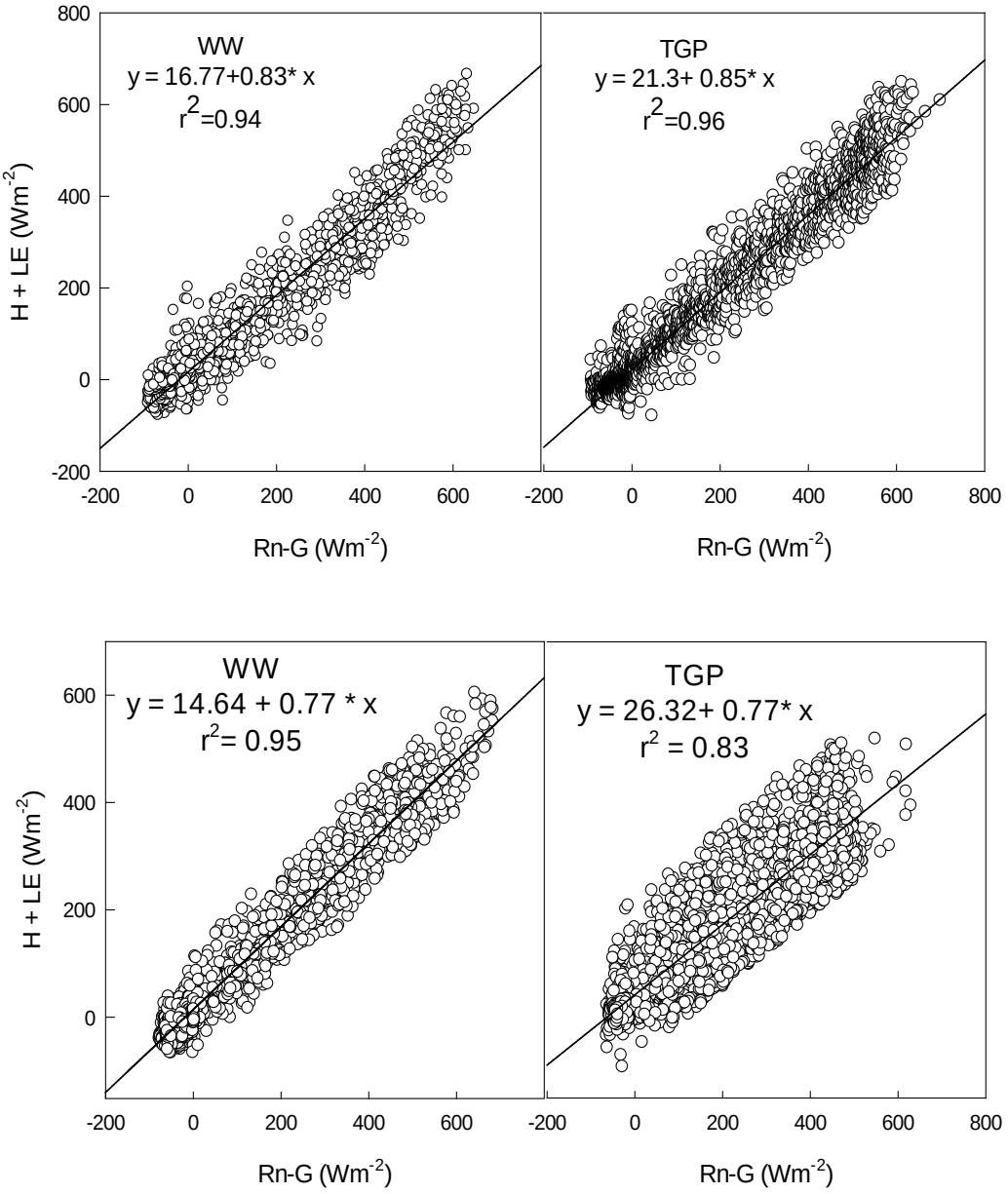

Figure 4.3 Relationship between the available energy [net radiation (Rn) – soil heat flux (G)] and the sum of turbulent fluxes [(latent heat (LE) + sensible heat (H)] at winter wheat (WW) and tall grass prairie (TGP) sites in 2015 (top) and 2016 (bottom).

4.2.6 Estimates of evapotranspiration (ET) and ecosystem water use efficiency (EWUE)

ET (mm 30 min^{-1}) was calculated from the H_2O fluxes (mmol m^{-2} s^{-1}) measured by the eddy covariance system using the following equation:

$$ET = (H_2O \text{ flux} \times 18.01528 \times 1800)/10^6 \quad (1)$$

The computed half hourly ET values after gap-filling were used to generate daily, monthly, and seasonal ET values. We estimated ecosystem water use efficiency (EWUE) at monthly and seasonal scales: a) monthly EWUE as the ratio of monthly GPP to monthly ET and b) seasonal EWUE as the ratio of seasonal GPP to seasonal ET over the growing season (Tubiello et al. 1999; Wagle and Kakani 2014). Only the daytime ET was considered in the calculation because the carbon sequestration by the vegetation occurs during daytime only.

4.3 Results

4.3.1 Seasonal dynamics of weather, soil moisture, and plant growth

Patterns of air temperature, rainfall, soil water content (SWC), and photosynthetically active radiation (PAR) for the two sites during the study period are shown in Fig. 4.2c, d. The highest daily mean air temperature reached approximately 32 °C in August, 2015 (15-year average maximum air temperature of 28 °C). The study sites received above normal rainfall (1273 mm) in 2015, with the 30-year average (1981-2010)

annual precipitation of 925 mm. Notably, the sites received record high rainfall of 393 mm in May 2015 (30-year average May rainfall= 124 mm). Both sites showed similar trends in SWC fluctuations corresponding with rainfall events. Distinct seasonality in LAI and AGB were observed for winter wheat and tallgrass prairie in both years (Fig. 4.4). The maximum recorded LAI was 5.0 and 4.7 m^2m^{-2} for winter wheat and 5.4 and 4.3 m^2m^{-2} for tallgrass prairie in 2015 and 2016, respectively. The maximum recorded AGB was 881 and 865 g m^{-2} for winter wheat and 1048 and 1306 gm^{-2} for tallgrass prairie in 2015 and 2016, respectively.

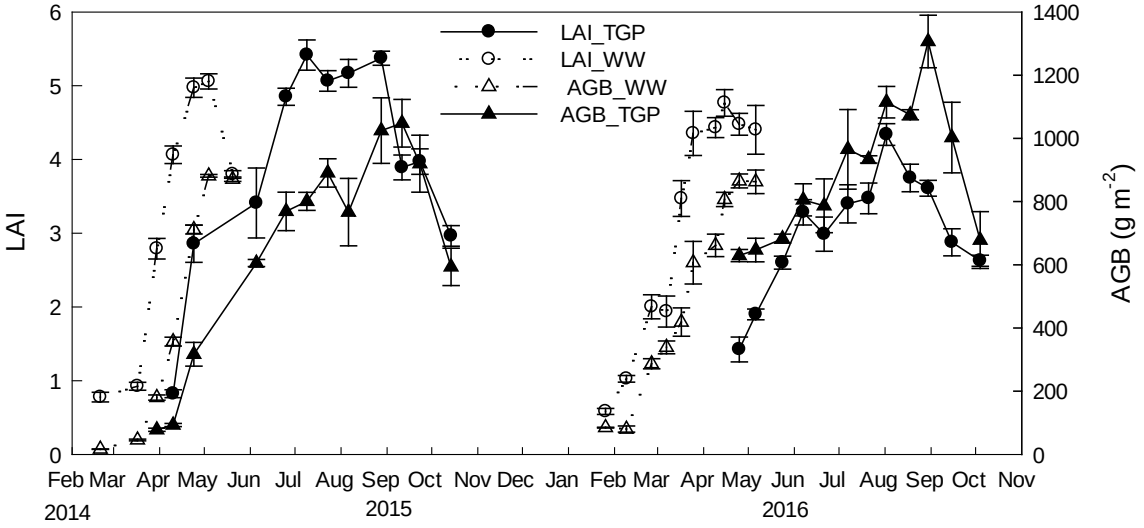

Figure 4.4 Patterns of leaf area index (LAI) and aboveground total dry weight (TDW) of winter wheat (WW) and tallgrass prairie (TGP) during the study period.

4.3.2 Diurnal dynamics of carbon dioxide and water vapor fluxes

The diurnal trends of NEE for winter wheat and tallgrass prairie for different months during the active growing season are compared in Fig. 4.5. Considerable variations in NEE rates were observed between sites as well as among months during the growing season. The rates of NEE were higher in 2015 than in 2016 at both sites. As expected,

NEE rates increased with the plant development, reaching a maximum during peak growth, and declined during the late growing season due to vegetation senescence. The NEE rates reached maximum for winter wheat in April (-24.22 ± 0.97 and, -24.79 ± 0.53 µmol m^{-2} s^{-1} in 2015 and 2016, respectively) and for tallgrass prairie in July (-20.55 ± 0.74 and, -14.40 ± 0.83 µmol m^{-2} s^{-1} in 2015 and 2016, respectively). Solar radiation was one of the primary drivers for determining diurnal rates of the fluxes within the growing season. With increasing maximum PAR from 40 $molm^{-2}day^{-1}$ in February to 48 $molm^{-2}day^{-1}$ in April (Fig. 4.2c), winter wheat achieved its maximum carbon uptake. Similarly, the maximum PAR in July (70 $molm^{-2}day^{-1}$) corresponded with the highest NEE rate in tallgrass prairie.

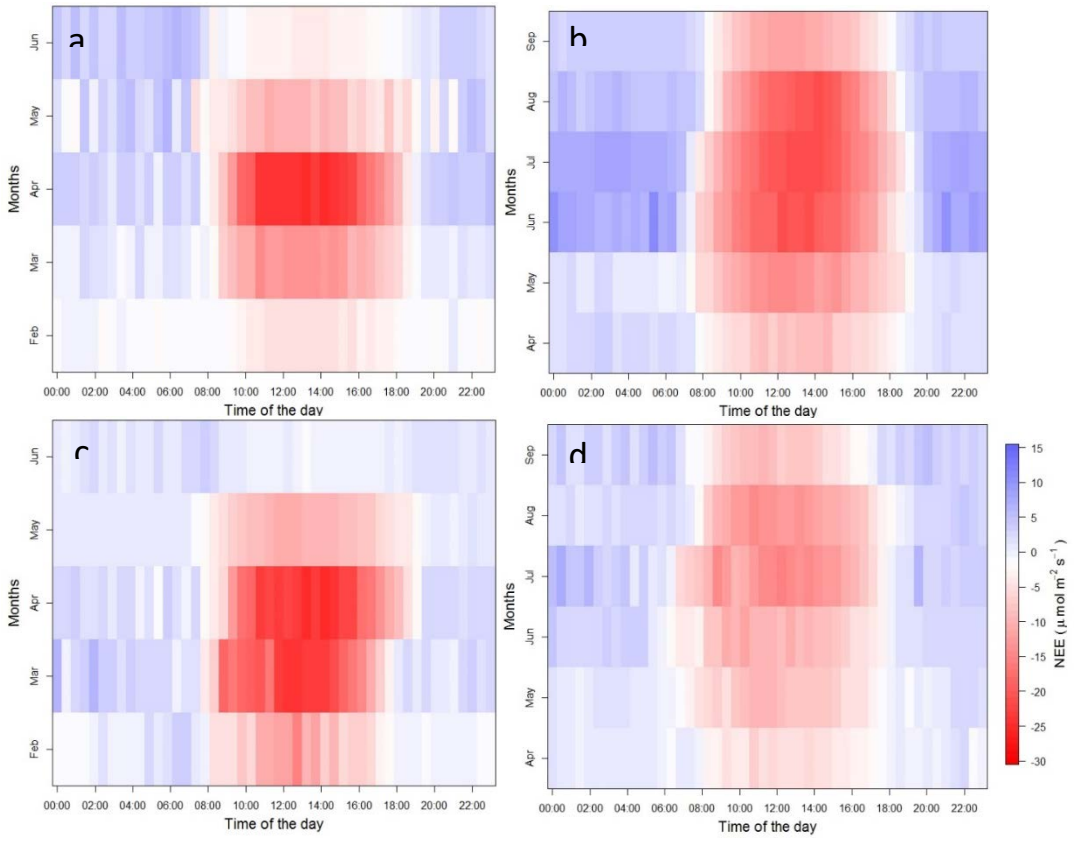

Figure 4.5. Half-hourly binned diurnal courses of net ecosystem CO_2 exchange (NEE) in winter wheat (WW) (left) and tall grass prairie (TGP) (right) for the entire months across the growing season (top – 2015 and bottom - 2016).

Diurnal ET trends at tallgrass prairie and winter wheat sites across the growing season are compared in Fig. 4.6. Like NEE rates, ET rates were higher in 2015 than in 2016 at both ecosystems. The ET rates reached a maximum in April for winter wheat and in June for tallgrass prairie. Peak hourly ET was 0.86 ± 0.06 (2015) and 0.44 ± 0.06 (2016) in winter wheat and 0.62± 0.02 (2015) and 0.65 ± 0. 03 (2016) mm hr^{-1} in tallgrass prairie. The role of PAR was also evident in determining the rate of ET in both ecosystems. The average SWC at both ecosystems was above 15 % by volume (Fig. 4.2d) during the most of the growing season, suggesting that the ecosystems did not experience severe drought during the study period. However, the rates of fluxes were impacted by grazing in the tallgrass prairie (the site was grazed from May to December in 2015 and January, May-June, and August- October in 2016).

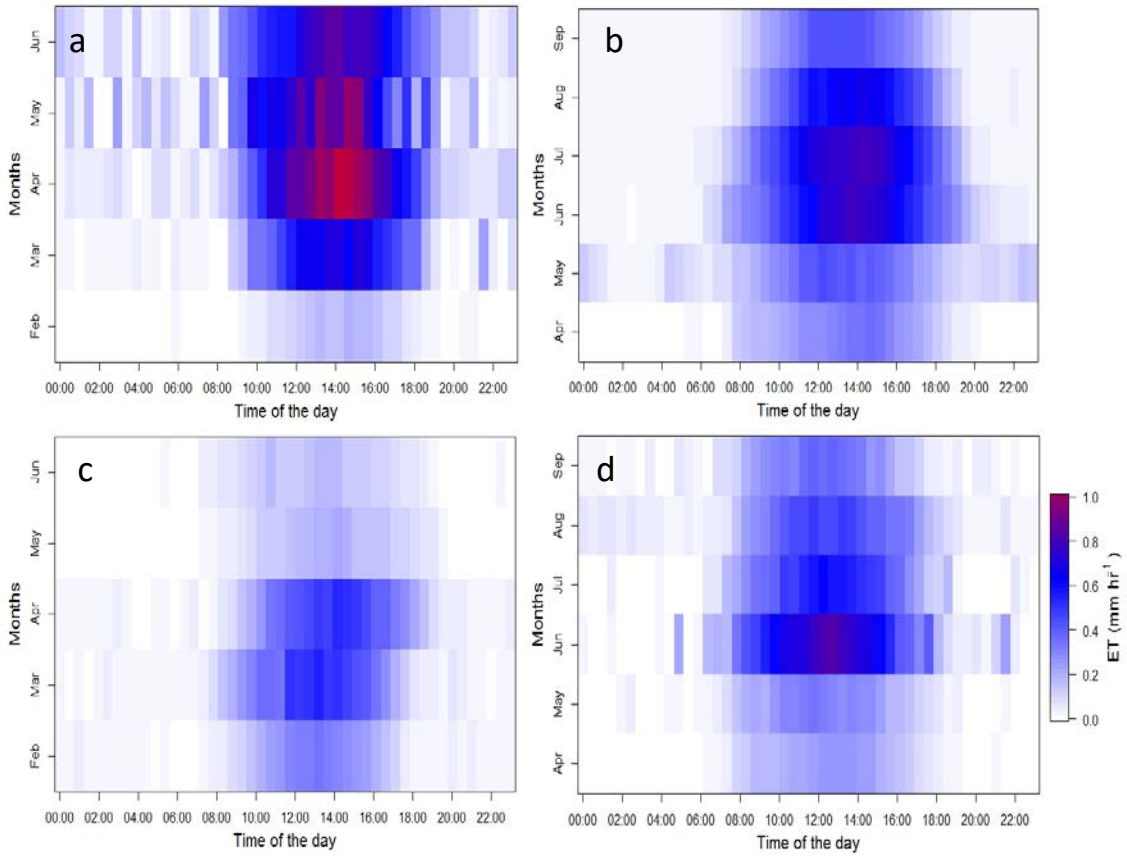

Figure 4.6. Half-hourly binned diurnal courses of evapotranspiration (ET) in winter wheat (WW) (left) and tall grass prairie (TGP) (right) for the entire months across the growing season (top – 2015 and bottom - 2016).

4.3.3 Seasonal dynamics of carbon dioxide and water vapor fluxes

Figure 4.7 shows the seasonal dynamics of daily NEE, ER, GPP, and ET from the winter wheat and tallgrass prairie sites. Winter wheat was a sink of carbon (negative NEE) for ~100 days between DOY 32 (February 1) and 132 (May 12), while tallgrass prairie was a sink of carbon for 144 days between DOY 105 (April 15) and 248 (September 5). The carbon uptake rate by winter wheat began to increase from early February and reached a maximum in April with the active growth of the crop followed by a rapid decrease towards crop senescence (mid- May). For tallgrass prairie, CO_2 uptake

rate began to increase in mid-March and reached a maximum in July before a rapid decrease towards senescence (early October) when release of CO_2 (ER) dominated over CO_2 assimilation (GPP). Substantial rates of carbon uptake were observed during the active growing season by both ecosystems (Fig. 4.7) because of rates of carbon assimilation (GPP) exceeded carbon release (ER). However, the magnitude of carbon uptake (NEE) was greater in winter wheat (-9.24 g C m^{-2} d^{-1} in 2015 and - 8.69 g C m^{-2} d^{-1} in 2016) than in tallgrass prairie (-6.23 g C m^{-2} d^{-1} in 2015 and -7.52 g C m^{-2} d^{-1} in 2016). The higher NEE in winter wheat resulted from lower ER (4.84 g C m^{-2} d^{-1} in 2015 and 5.57 g C m^{-2} d^{-1} in 2016) and higher GPP (14.08 g C m^{-2} d^{-1} in 2015 and 14.27 g C m^{-2} d^{-1} in 2016) in winter wheat as compared to tallgrass prairie (ER= 5.87 and 5.62 g C m^{-2} d^{-1} and GPP= 12.11 and 10.19 g C m^{-2} d^{-1} in 2015 and 2016, respectively). However, the relatively higher rates of NEE occurred for a short period (only during April) in winter wheat, while NEE rates were consistently higher for three months (June-August) in tallgrass prairie.

Large variation in ET was observed between two ecosystems and the ET rates showed a clear seasonal pattern corresponding to the seasonality of the respective crops (Fig. 4.7d). At the winter wheat site, the magnitude of daily ET was the highest (6.0 and 5.4 mm day^{-1}) on 10th and 23rd May in 2015 and 2016, respectively, while in tallgrass prairie, the highest daily ET (7.2 and 8.2 mm day^{-1}) was observed on 10th and 31st June in 2015 and 2016, respectively. Higher ET was observed during the period of higher LAI values, which is earlier in the year for winter wheat than tallgrass prairie. However, two significant peaks (~29th June and ~29th July) of ET can be seen for winter wheat in 2015

during the summer even after winter wheat was harvested due to the contribution from the growth of weeds.

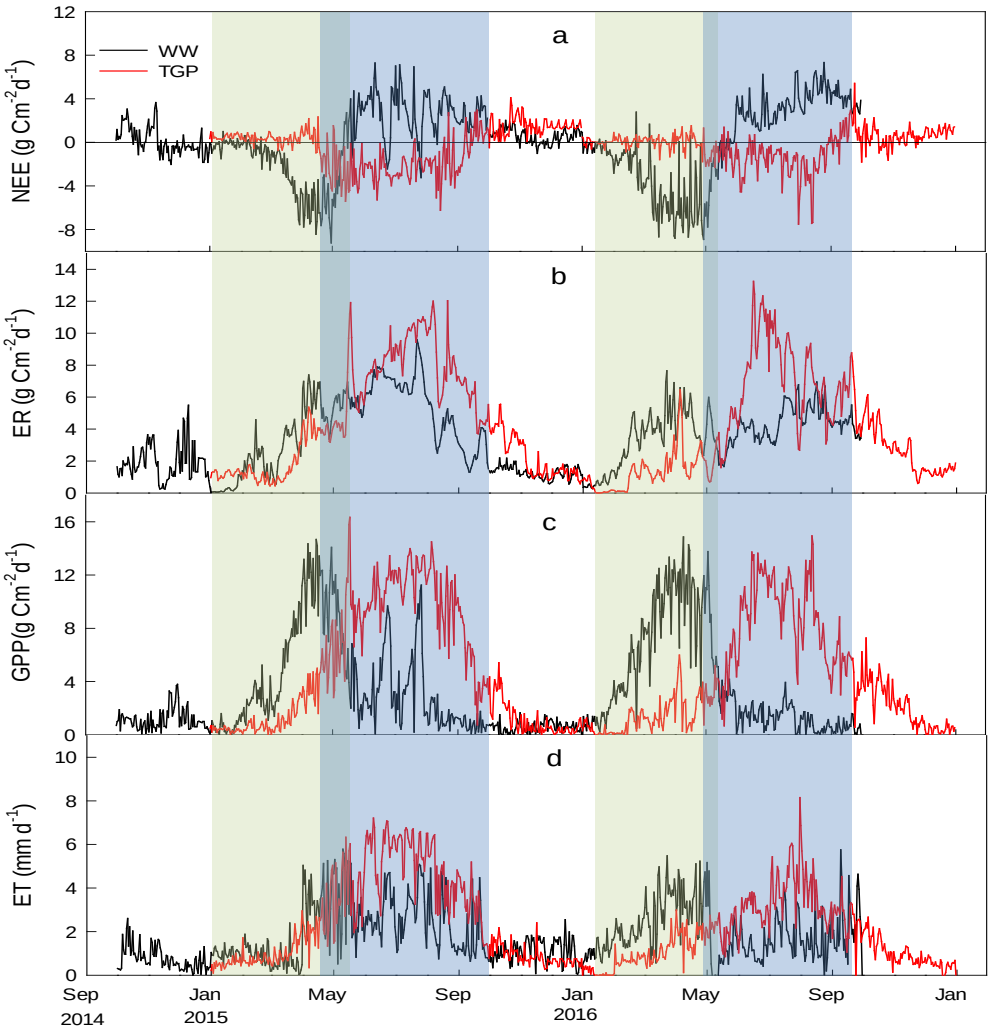

Figure 4.7. Growing season patterns of: (a) net ecosystem CO_2 exchange (NEE), (b) ecosystem respiration (ER), (c) gross primary productivity (GPP), (d) evapotranspiration (ET) in winter wheat (WW) and tall grass prairie (TGP) sites. Data lines represent daily values of CO_2 and water fluxes. The growing seasons are represented by shaded regions.

4.3.4 Seasonal and annual (calendar year) sums of carbon dioxide and water vapor fluxes

The growing season, non-growing season, and annual (based on Fig. 4.2a) values of GPP, ER, and NEE for both ecosystems are shown in Table 2. Cattle grazing is generally allowed in first half of the growing season (GS I-A) of winter wheat. This period had low plant activity indicated by lower cumulative GPP (150 ± 23 and, 93 ± 14 g C $m^{-2)}$, ER (176 ± 32 and, 176 ± 32 g C m^{-2}), and NEE (26 ± 6 and, 46 ± 12 g C m^{-2}) in 2015 and 2016, respectively. Cumulative growing seasonal values (GS) of GPP and ER fluxes from the tallgrass prairie were larger than those from the winter wheat in both years. The NEE during the 2015 growing season for tallgrass prairie (-276 ± 43 g C m^{-2}) was similar to winter wheat (-251 ± 43 g C m^{-2}). However, it was more than double in winter wheat (-403 ± 73 g C m^{-2}) than in tallgrass prairie (-159 ± 61 g C m^{-2}) during the 2016 growing season. The growing season GPP total was 921 ± 169 and 996 ± 137 g C m^{-2} in winter wheat as compared to 1663 ± 233 and 1346 ± 103 g C m^{-2} in tallgrass prairie in 2015 and 2016, respectively. Similarly, the growing season ER total in winter wheat was 672 ± 154 and 603 ± 102 g C m^{-2} compared to 1386 ± 221 and 1186 ± 145 g C m^{-2} in tallgrass prairie in 2015 and 2016, respectively. These results show that both ecosystems were carbon sinks on a seasonal scale. However, the winter wheat site was a carbon source on an annual scale when the carbon fluxes of the fallow period were considered. The non-growing season (NGS II) of winter wheat, which is comprised of mostly summer fallow, had larger positive NEE values attributed to higher ER and lower GPP. On the other hand, the growing season was longer and ER rates were lower in tallgrass prairie during the non-growing season (NGS II). Thus, the winter wheat

ecosystem released about 56 ± 13 and, 33 ± 9 g C m^{-2} (positive NEE), while tallgrass prairie ecosystem gained about -128 ± 69 and, -119 ± 53 g C m^{-2} (negative NEE) on an annual scale in 2015 and 2016, respectively.

Table 4.2. Sums of net ecosystem CO2 exchange (NEE), gross primary production (GPP), ecosystem respiration (ER), and evapotranspiration (ET) (± uncertainty), and average ecosystem water use efficiency (EWUE= GPP/ET) from Winter Wheat (WW) and Tallgrass prairie (TGP) fields during their respective growing seasons. Growing season (GS) refers to Oct - May (WW) and March - mid-Oct (TGP). Non-growing season refers to Jun-Sep (WW) and Jan-Feb & mid-Oct- Dec (TGP) and whole year is an integrated flux for 12 months (Oct-Sep and Jan-Dec, respectively for WW and TGP).

		Winter Wheat					Tallgrass Prairie		
		Growing season (GS)			Non-growing	Annual	Growing	Non-growing	Annual
	Year	I-A (Fall)	I-B (Spring)	Total (I-A + I-B)	season (NGS)		Season (GS)	season (NGS)	
GPP (g C m^{-2})	2015	150 ± 23	771 ± 146	921 ± 169	312 ± 81	1233 ±168	1663 ± 233	41 ± 19	1704 ± 252
	2016	93 ± 14	903 ± 123	996 ± 137	129 ± 48	1125 ± 185	1346 ± 103	152 ± 80	1498 ± 183
ER (g C m^{-2})	2015	176 ± 32	496 ± 122	672 ± 154	638 ± 143	1311 ± 153	1386 ± 221	203 ± 29	1589 ± 250
	2016	139 ± 19	464 ± 93	603 ± 102	555 ± 97	1158 ± 209	1186 ± 145	192 ± 23	1378 ± 168
NEE (g C m^{-2})	2015	26 ± 6	-277 ± 37	-251 ± 43	325 ±96	56 ± 13	-276 ± 43	148 ± 26	-128± 69
	2016	46 ± 12	-439 ± 61	-403 ± 73	357 ± 101	33 ± 9	-159 ± 61	40 ± 8	-119 ± 53
ET (mm m^{-2})	2015	94 ± 15	256 ± 81	350 ± 96	301 ± 102	651 ± 69	826 ± 72	93 ± 17	919 ± 89
	2016	135 ±74	294 ± 40	429 ± 114	214 ± 56	644 ± 111	588 ± 102	81 ± 15	669 ± 117
EWUE	2015	1.2	11.3	6.2	3.9	5.5	7.2	1.6	5.4
(g CO_2 mm^{-1}ET)*	2016	3.2	12.7	7.9	4.4	6.0	8.5	1.6	8.1

**g CO2 mm^{-1} ET= g Cmm^{-1}ET (44.01/12.01)*

Annual ET was greater in tallgrass prairie (919 ± 89 mm) than in winter wheat site (651± 69 mm) in 2015, but was similar in 2016 at both sites (winter wheat = 644 ± 111 mm and, tallgrass prairie = 669 ± 117 mm). Monthly ET was also generally higher for tallgrass prairie except in March and April (Fig. 4.8 b,e). Winter wheat had the

highest GPP (334 g C m^{-2}) during the peak growth (AGB= 400 g m^{-2}) in April when the total ET reached the maximum (101 mm). The highest ET in the tallgrass prairie was observed in April (71 and 53 mm $month^{-1}$ in 2015 and 2016, respectively) when the tallgrass prairie was in the initial phase of the growing season (AGB=300 g m^{-2}) with a cumulative GPP of 127 and 71 g C m^{-2}. For tallgrass prairie, ET reached its maximum (2015= 180 mm and 2016= 127 mm) in the month of July, with the corresponding AGB of 900 and 875 g m^{-2} and a cumulative GPP of 379 and 314 g C m^{-2} in 2015 and 2016, respectively.

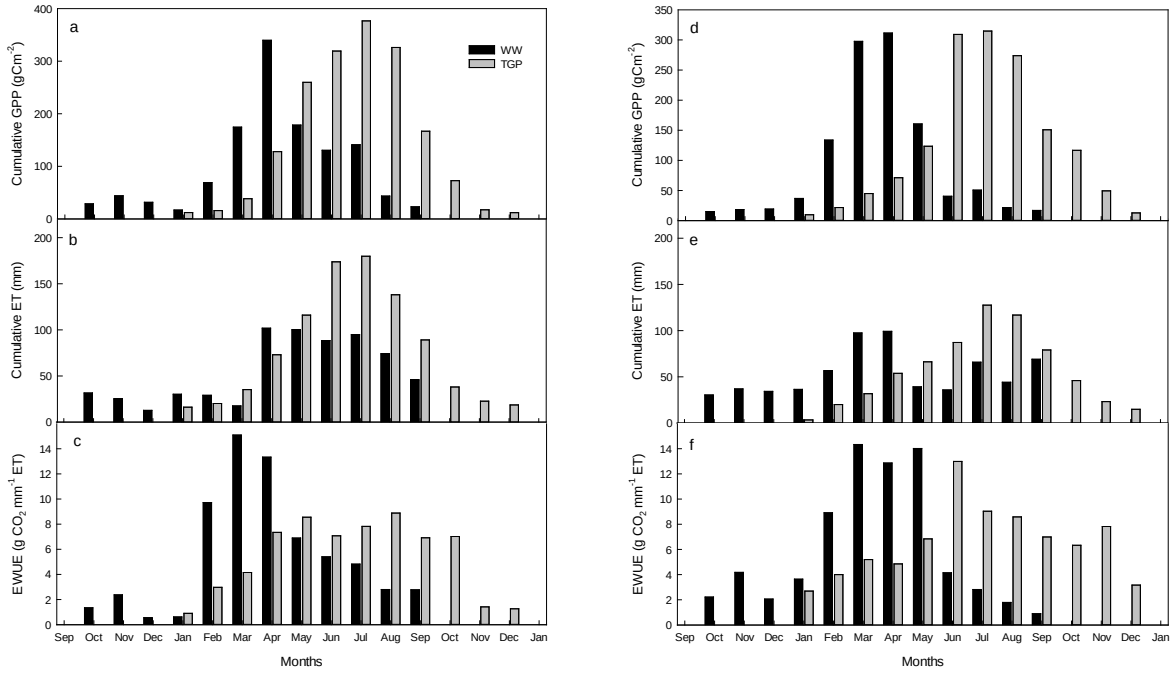

Figure 4.8. Monthly cumulative gross primary productivity (GPP), evapotranspiration (ET), and average ecosystem water use efficiency (EWUE) in Winter Wheat (WW) and Tallgrass Prairie (TGP) sites in 2015 (a-c) and 2016 (d-f).

The GPP to ER ratio for the study period at the two sites are presented in Fig. 4.9. Generally, the ratio was greater than one (net carbon uptake) from February to June in

winter wheat and from April to October in tallgrass prairie. In winter wheat, the ratio decreased after June when the crop was harvested, while in tallgrass prairie the ratio decreased after October with the onset of senescence.

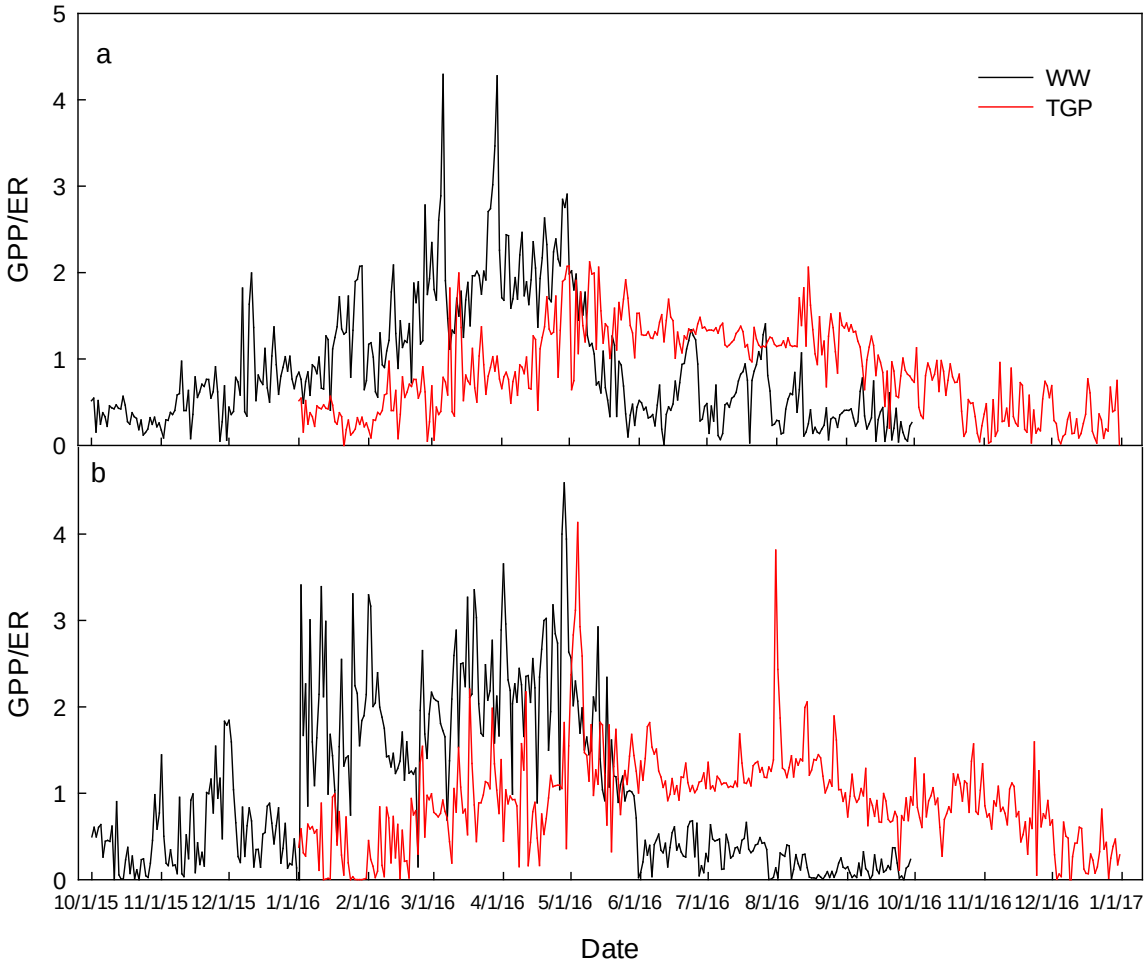

Figure 4.9. The daily dynamics of ratio of gross primary productivity (GPP) to ecosystem respiration (ER) at Winter Wheat (WW) and Tallgrass Prairie (TGP) sites.

4.3.5 Seasonal dynamics of ecosystem-level water use efficiency (EWUE)

EWUE was lower in the early and late growing season and higher during the peak growth of the vegetation at both sites (Fig.4.8 c, f). In winter wheat, the EWUE reached a

maximum of 15 and 14.3 g CO_2 mm^{-1} ET (March) in 2015 and 2016, respectively, while the highest EWUE in tallgrass prairie was 8.8 and 13.9 g CO_2 mm^{-1} ET in August 2015 and June 2016, respectively. The peak growing season EWUE was substantially higher for winter wheat (11.3 and, 12.7 g CO_2 mm^{-1} ET in 2015 and 2016, respectively) than for tallgrass prairie (7.2 and, 8.5 g CO_2 mm^{-1} ET in 2015 and 2016, respectively) (Fig.4.8, Table 2).

4.3.6 Rainfall, management activities, and carbon flux rates

We demonstrated four specific cases from the two study sites to illustrate the impact of climate and management activities on carbon fluxes (Fig. 4.10.). Case I: Before a week of rain pulse event on July 26, carbon fluxes (NEE, GPP and ER) in tallgrass prairie site started declining. It took few days after rain to increase the carbon fluxes. Case II: In the 1st week of June 2016, at the tallgrass prairie site, NEE decreased by about 3 µmolm^{-2} s^{-1} during the first week of grazing. After about one week of grazing, the carbon uptake rate increased again. Case III: In winter wheat site, herbicide RT 3 glyphosate, Weedmaster (dicamba and 2,4 D) was applied on June 29, 2015 to kill the weeds. This caused the reduction in GPP at a higher rate than that of ER resulting into positive NEE, which was negative a week before herbicide was applied. Case IV: The winter wheat site was tilled using a tandem disc harrow on June 30, 2015 to inhibit the growth of weeds for maintaining fallow. This management activity also caused changes in the carbon fluxes particularly GPP and NEE. GPP was reduced at a higher rate, while ER remained unchanged making NEE of the site positive.

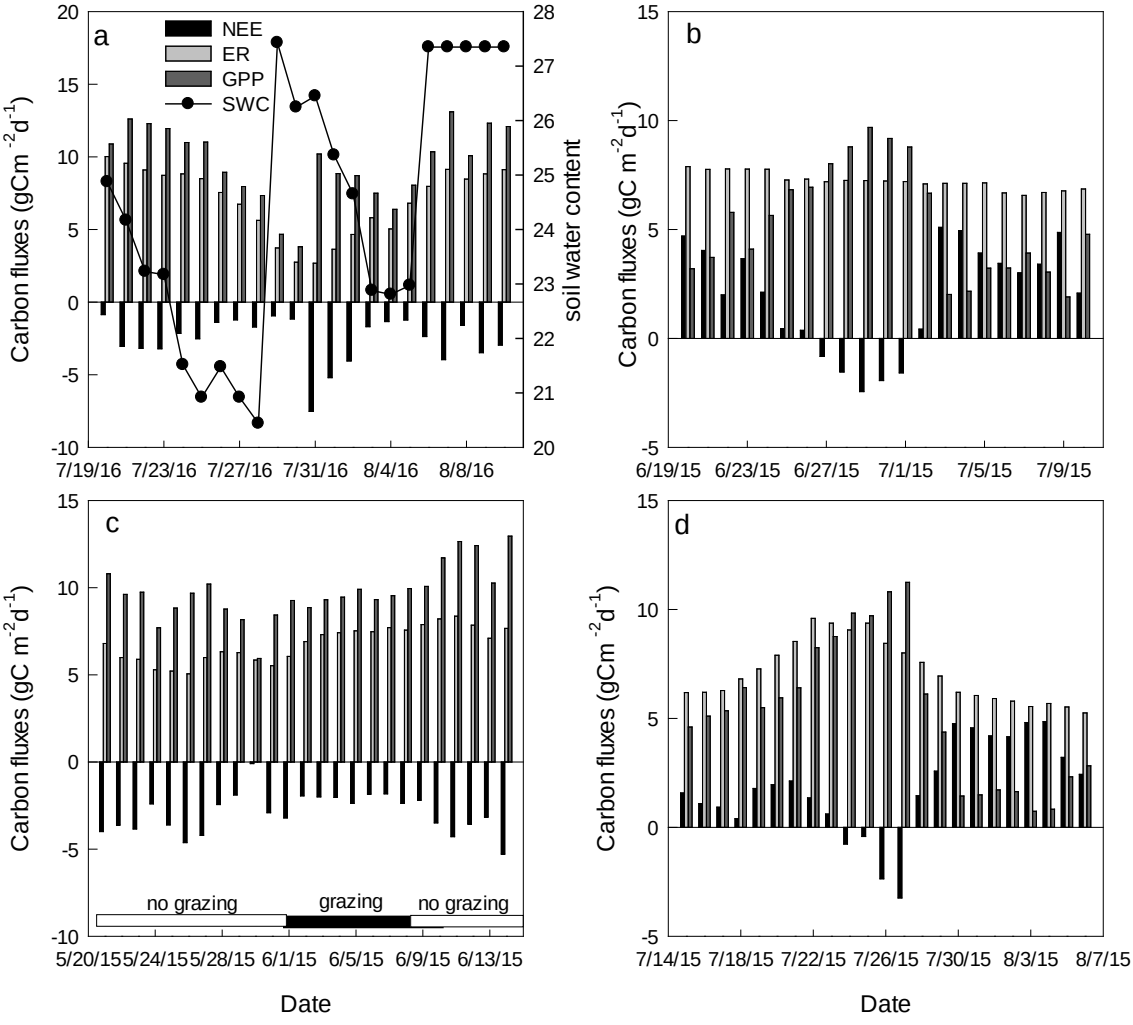

Figure 4.10. Changes in carbon fluxes in winter wheat (WW) and tallgrass prairie(TGP) sites due to climate and management activities: (a) rainfall events (TGP), (b) tillage (WW), (c) grazing (TGP) and (d) herbicide application (WW). The arrows represent the occurrence of the events.

4.4 Discussion

4.4.1 Comparison of CO_2 and H_2O fluxes of winter wheat and tallgrass prairie

Management activities, weather conditions, and soil types at the study sites influenced the magnitudes of the CO_2 and H_2O fluxes. The year 2015 was wetter and hotter whereas 2016 was close to the average of 30-year weather records of the study

sites. Similarly, the grazing events at the tallgrass prairie sites impacted the rates of fluxes recorded in this study. The maximum diurnal peak rate of -24 (2015) and – 25 (2016) µmol m^{-2} s^{-1} measured in the winter wheat ecosystem was close to the maximum NEE of -25 to -30 µmol m^{-2} s^{-1} measured for winter wheat ecosystem of Ponca City, Oklahoma (Fischer et al. 2007; Gilmanov et al. 2003)**.** Additionally, the daily peak NEE value (2015= -9.24 and 2016= -8.8 g C m^{-2} d^{-1}) of winter wheat measured in our study was similar to the daily peak NEE value of -9.3 g C m^{-2} d^{-1} at Billings, Oklahoma (Fischer et al. 2007) and -8.18 g C m^{-2} d^{-1} at Ponca City, Oklahoma (Gilmanov et al. 2003). The daily peak NEE values of about -12 to -13 g C m^{-2} d^{-1} from the European winter wheat ecosystems (Belgium and Germany) were higher than that those -8 to -9.3 g C m^{-2} d^{-1} from winter wheat ecosystems in Oklahoma (Table 3).

Table 4.3 The maximum rates of net ecosystem exchange (NEE, g C m-2 d-1) and evapotranspiration (ET, mm d-1) of winter wheat and tallgrass prairie at different study sites.

Sites	Year	Vegetation	NEE_{max}	ET_{max}	References
Ponca City, OK	1997-1998	Winter Wheat	-8.2	7.0	(Gilmanov et al. 2003)
Billings, OK	2001-2003	Winter Wheat	-9.3	5.2	(Fischer et al. 2007)
Selhausen, Belgium	2007-2009	Winter Wheat	-12.0	-	(Schmidt et al. 2012)
Thuringia, Germany	2001	Winter Wheat	-13.3	5.7	(Anthoni et al. 2004)
El Reno, OK	2015	Winter Wheat	-9.2	6.0	This study
El Reno (Burned), OK	2005-2006	Tallgrass Prairie	-6.9	5.5	(Wagle et al. 2015b)
El Reno (Unburned), OK	2005-2006	Tallgrass Prairie	-5.2	5.7	(Wagle et al. 2015b)
Fermi, IL	2005-2007	Tallgrass Prairie	-9.5	5.6	(Wagle et al. 2015b)
Konza Prairie, KS	2007-2012	Tallgrass Prairie	-9.1	7.6	(Wagle et al. 2015b)
Shilder, OK	1997	Tallgrass Prairie	-8.1	-	(Suyker and Verma 2001)
El Reno, OK	2015	Tallgrass Prairie	-6.3	7.0	This study

The peak diurnal NEE rates of -20 μmol m^{-2} s^{-1} (2015) and -15μmol m^{-2} s^{-1} (2016) in tallgrass prairie in our study were slightly lower than the values of -28 μmol m^{-2} s^{-1} and -22 μmol m^{-2} s^{-1} in 2005 and 2006 reported for a tallgrass prairie ecosystem at El Reno, Oklahoma (Fischer et al. 2012). The maximum NEE daily values of tallgrass prairie varied from -5.2 to -8.1 g C m^{-2} d^{-1} at various sites in southern plains (Suyker and Verma 2001; Wagle et al. 2015b) (Table. 3), which are in agreement with the maximal NEE daily value of –6.3 g C m^{-2} d^{-1} (2015) and -7.5 g C m^{-2} d^{-1} (2016) measured in our study.

In the winter wheat ecosystem, the maximum daily ET of 6 mm d^{-1} (2015) and 5.3 mm d^{-1} (2016) measured in our study was similar with the maximal daily ET values of 7 mm day^{-1} measured in winter wheat at Ponca City, Oklahoma, but the maximum daily ET of 7.2 mm d^{-1} (2015) and 8.2 mm d^{-1} (2016) in tallgrass prairie ecosystem was slightly higher than 5 mm d^{-1} reported for tallgrass prairie at Ponca city, Oklahoma (Burba and Verma 2005). Similarly, the annual ET of 651 and 644 mm measured at our winter wheat site in 2015 and 2016, respectively, was slightly lower than that of 750, 714, and 742 mm of ET at the winter wheat site of Oklahoma in 1997, 1998, and 1999, respectively (Burba and Verma 2005). On the other hand, the annual ET from tallgrass prairie site in our study was relatively higher (919 mm) in 2015 and was similar (679 mm) in 2016 compared to the range (485 to 716 mm) of ET values reported for six different tallgrass prairie sites by Wagle et al. (2017). The higher values of ET was most likely due to the high amount of rainfall received in 2015 which is in agreement with the higher ET values (807 mm yr^{-1}) reported for tallgrass prairie when Oklahoma received higher rainfall in 1997 (Burba and Verma 2005). Although the weather condition and management activities (e.g., grazing) are site specific and impact on the rate of atmospheric exchanges, the CO_2 and H_2O fluxes reported in our study are comparable to the values reported in the literature.

4.4.2 Impacts of management activities on carbon fluxes

Application of herbicide and tillage for keeping the land fallow at winter wheat site during summer months impacted the carbon fluxes. These activities contributed to the change in annual carbon budgets. For example, the weekly average of NEE was

changed from -0.39 g C m^{-2} to 3.79 g C m^{-2} after herbicide was applied to kill the weeds. Similar switch in NEE was observed when the site was tilled for maintaining the fallow (Fig. 4.10). Summer fallow contributed only about 25% and 11% GPP to the annual budget whereas the carbon loss due to ER was about 48% and 47% in 2015 and 2016, respectively, resulting into the positive annual NEE (carbon source) from the winter wheat site. This loss of carbon from the fallow in winter wheat-fallow system was in consistent with the study conducted in Montana, USA. About 135 g C m^{-2} was lost between April to September from the fallow field of Montana in 2013/2014 (Vick et al. 2016). Livestock grazing in prairie pasture is a common feature of the southern plains (Gillen et al. 1998; Hickman et al. 2004; Luo et al. 2012; Zhou et al. 2017a). Grazing plays an important role in modifying the vegetation phenology, canopy structure, and productivity of grasslands which, in turn, alters the magnitude and temporal patterns of CO_2 and H_2O fluxes of the ecosystem (Luo et al. 2012; Owensby et al. 2006; Wayne Polley et al. 2008). For example, in the 1st week of June 2016, the tallgrass prairie NEE decreased by about 3 $\mu molm^{-2}s^{-1}$ during the first week of grazing (Fig. 4.10). After about one week of grazing, the ecosystem again increased the carbon uptake rate. Although the effects of grazing are not quantified completely in this study, it can be argued that the tallgrass prairie ecosystem in our study would be larger sink (more negative NEE) with less or no grazing since in both years the pasture was grazed intensively. However, low productivity has been reported for prairie that was ungrazed for long periods due to senescent vegetation that shades out new green leaves (Belsky 1986; Dalgleish and Hartnett 2009).

4.4.3 Change in seasonal patterns and magnitudes of water vapor fluxes

Some researchers have reported that the cropping sequence that utilize summer cover crops in place of fallow increased the ecosystem productivity and resulted to less evaporative water loss (Farahani et al. 1998a; Farahani et al. 1998b; McGee et al. 1997).While the objective of summer fallow is to accumulate water for the subsequent crop, the wheat-fallow system has been found to be inefficient in storing soil water due to greater loss by soil evaporation, transpiration from weeds, deep percolation, and runoff (Black et al. 1981; Farahani et al. 1998b). When land use is converted from grassland to winter wheat with bare summer fallow, the resulting ecosystem is less water efficient due to the resulting amount of moisture loss to evaporation when no or minimal amounts of carbon are fixed. In our study, the EWUE in winter wheat declined to about 5.5 - 6 g CO_2 mm^{-1} ET at the annual scale from about 11 - 13 g CO_2 mm^{-1} ET at the seasonal scale due to loss of water during the fallow period with more release of carbon than the uptake. Although more amount of water was lost as ET from tallgrass prairie than from the winter wheat, results showed that tallgrass prairie was more water efficient (EWUE= 6.8 g CO_2 mm^{-1} ET in 2015 and 8.2 g CO_2 mm^{-1} ET in 2016 than winter wheat (EWUE= 6.19 g CO_2 mm^{-1} ET in 2015 and 6.4 g CO_2 mm^{-1} ET in 2016 g CO_2) at the annual scale. Throughout the southern plains, the dominant agricultural crop is winter wheat, which is planted in early fall and harvested in June. This pattern contrasts sharply with the seasonal cycle of tallgrass prairie, which is most active from May to August. The change from prairie to winter wheat shifts the magnitude and seasonal timing of energy, momentum, H_2O, and CO_2 fluxes between the atmosphere and ecosystem. Many studies in the past have examined the role of variation of ET in relation to the atmospheric

processes determining the change in the regional climate (Clark et al. 2001; Katul et al. 2012; Shukla and Mintz 1982; Wang and Eltahir 2000). The soil-plant system is embedded within the atmospheric boundary layer where change in ET due to change in land surface influences the precipitation patterns and frequency at the regional scale (Katul et al. 2012). Currently, there exist known impacts of the winter wheat in the southern plains on surface-layer and boundary layer processes (Haugland and Crawford 2005; McPherson and Stensrud 2005; McPherson et al. 2004). Further, the southern plains region is located in a region with strong feedbacks between the land surface and the atmosphere across various spatial and temporal scales during the growing season (Basara and Christian 2017; Basara and Crawford 2002b; Ferguson and Wood 2011; Ford et al. 2015a; Ford et al. 2015b; Guo and Dirmeyer 2013; Guo et al. 2006; Koster et al. 2004; Ruiz-Barradas and Nigam 2013; Santanello Jr et al. 2013; Santanello Jr et al. 2009; Santanello Jr et al. 2015). Thus, the shift in the ET (latent heat flux) resulting from land use change (tallgrass to winter wheat) could impact the overall water balance of terrestrial ecosystems, atmospheric circulations, and the regional climate of the southern plains, especially given expansion of the winter wheat within the region. Such impacts could also influence the timing and severity of convective storms in the region. Considering recent research findings that the overall variability of precipitation in the region is increasing (Christian et al. 2015b; Flanagan et al. 2017; Weaver et al. 2016) which could additionally yield downstream impacts related to excessive precipitation (McCorkle et al. 2016) and rapid development of drought (Bajgain et al. 2017; Otkin et al. 2013; Zhou et al. 2017b).

4.4.4 Land use change, winter wheat-summer fallow, and carbon sink potential

Despite large differences in carbon uptake (NEE) in 2015 and 2016 at both ecosystems, winter wheat and tallgrass prairie ecosystems were carbon sinks in both years during their respective growing seasons (Table. 2). The higher carbon uptake during the growing season in 2016 in winter wheat than 2015was due to the good crop growth resulted from higher amount of fall rainfall (Fig. 4.2d). Similarly, the higher amount of rainfall during May in 2015 contributed to the higher carbon uptake during the 2015 growing season by tallgrass prairie than in 2016. The carbon fluxes showed large differences (winter wheat released 56 and 33 g C m^{-2} in 2015 and 2016, respectively and tallgrass prairie accumulated -128 and -119 g C m^{-2} in 2015 and 2016, respectively) when accounted for at the annual scale. This difference in carbon fluxes between the two sites suggests that although the tallgrass prairie had a longer growing season than winter wheat, the carbon sink potential was similar during the growing season in 2015 and the carbon sink of tallgrass prairie was smaller in 2016 than that of winter wheat. This is due to less loss of carbon via ER displayed by the higher ratio of GPP over ER in winter wheat ecosystem (Fig. 4.9 and Table 4.2). The average GPP to ER ratios for winter wheat during the growing season were 1.6 (2015) and 1.7 (2016), while the same ratios during the growing season were 1.2 (2015) and 1.1 (2016) for tallgrass prairie. Until harvest of winter wheat, the ecosystem was a carbon sink due to higher GPP than ER. The transition of sink to source of carbon resulted from lower GPP and higher ER (low GPP:ER ratio) after harvesting during the summer month with increased temperature and decomposition of winter wheat residue. Consequently, the winter wheat ecosystem was a potential carbon source offsetting the growing season carbon sink magnitude when accounted for

the annual time scale. On the other hand, the annual GPP in the tallgrass prairie ecosystem was sufficient to cover the carbon expense caused by ER with a GPP:ER ratio of about 1.07 (both years) and resulting in a net cumulative carbon balance (NEE) of -128 and –119 g C m^{-2} in 2015 and 2016, respectively. This differential capacity in carbon uptake potential between these two ecosystems have a broader interpretation when accounting the tallgrass prairie converted land determined using the remote sensing land use dataset as in Fig. 4.1. Overall, about 3.6 million tallgrass prairie pixels were converted to winter wheat pixels between 2008 to 2015 which is equivalent to about 1.1 million hectares of land area. The area of the pixels was multiplied by the difference in carbon fluxes between winter wheat and tallgrass prairie to estimate the total carbon contributed by the converted pixels (tallgrass to winter wheat) in the southern plains. This estimation suggested that the southern plains could contribute a substantial amount of carbon to atmosphere which otherwise would have been a potential carbon sink (2015= -128 and 2016= -119 g C m^{-2} y^{-1}). Conversion from a sink (tallgrass) to a source (winter wheat) during 2008 to 2015, the total additional carbon release from the converted winter wheat fields would be about 0.6 million tons (616 kg per ha) in 2015 and about 0.36 million tons (363 kg per ha) in 2016 which otherwise would have been a sink of about 1.4 and 1.3 million tons (1,408 and 1,309 kg per ha) of carbon in 2015 and 2016, respectively, had the fields remained as a tallgrass prairie. These results, indicate that the land use change from grassland to winter wheat has significant effect on the carbon cycle of the southern plains. The prevailing practice of keeping land fallow after harvesting the winter wheat for capturing moisture from summer rainfall for the following winter wheat crop caused the ecosystem to release more carbon to the atmosphere. Although the main

goal of fallow is to ensure soil moisture for the subsequent winter wheat, it has been found that summer fallow rotation system is not effective with respect to productivity, economic risk, organic matter storage and even soil water storage (Kolberg et al. 1996; McGee et al. 1997; Peterson et al. 1996). Only 25% precipitation efficiency was achieved from the summer fallow in terms of soil water storage (McGee et al. 1997; Peterson et al. 1996). The use of cover crops after winter wheat during summer could be a better practice to compensate for carbon loss via ER by fixing more carbon into the ecosystem via photosynthesis from cover crops. However, any changes in the summer fallow system must consider the effect on the soil moisture availability required to stabilize production for the next crop cycle.

It is important to mention the uncertainties associated with the rates of land use change and the spatial heterogeneity of land management, soil properties, and weather variables across the region. However, the ecosystems chosen are the representative of the practices of the southern plains. While the size of the potential carbon sink/source at the regional level can`t be estimated with greater confidence from this study, it can be inferred that the change of grassland to winter wheat with a summer fallow reduced the carbon sink potential and made the ecosystem less water efficient (more water loss for less carbon fixed). Also, the winter wheat fields in our study had been in wheat for many years and had depleted soil carbon relative to tallgrass prairie. For the first few years after conversion there would be an even greater loss of carbon, and then at some new semi-equilibrium, the estimated carbon loss become more relevant. Therefore, it appears that

fallow land after harvesting of winter wheat is a factor that needs to be considered for managing the ecosystem sustainably.

4.5 Conclusions

Carbon dioxide and water vapor fluxes were measured using the eddy covariance system from two major ecosystems of the southern plains (winter wheat and tall grass prairie) in 2015 and 2016. Both ecosystems were carbon sinks during their active growing seasons. Despite having the greater carbon sink potential demonstrated by higher hourly rate and daily integrated values of NEE in winter wheat than in tall grass prairie, winter wheat ecosystems were a source of carbon when the carbon budgets for the summer fallow period were included. Similarly, the significant water loss due to evaporation from the fallow land (winter wheat-fallow rotation) when little carbon was fixed caused the winter wheat ecosystem to be less water efficient than the tallgrass prairie ecosystem despite higher growing season EWUE. Results suggest that the differences in magnitudes and patterns of carbon dioxide and water vapor fluxes between winter wheat and tallgrass prairie can exert influence on the carbon and water budgets of the whole region under land use change scenarios.

Chapter 5: Modeling of carbon sequestration and greenhouse gas dynamics in managed and native pasture

Abstract

Pasture grasslands used to graze livestock make up about 45% of land use in Southern Great Plains are also one of the most sensitive and important ecosystems of North America. Better grassland management practices thus have the potential to mitigate climate change by shaping carbon sequestration and methane production. The hypothesis tested was that the application of fertilizers in the managed pasture would increase the primary productivity of the ecosystem for few years but this increase in carbon sink would be counteracted by the increasing rate of greenhouse gas emissions in the long run. We used DeNitrification- DeComposition, a process-based model and simulated the carbon sequestration and greenhouse gas emissions from 1999 -2016 at managed and native pastures located at El Reno, Oklahoma. The increased in productivity was measured in terms of GPP in managed pasture to that of native pasture particularly in years with good rainfall, resulting into higher soil organic carbon (SOC) sequestration rate. Similarly, the stronger signal of N_2O flux was observed in the managed pasture than that in the native pasture. Therefore, the advantage from increased SOC due to the fertilizer application, measured in terms of global warming potential (GWP) was outweighed by the GWP calculated from the increased magnitude of N_2O fluxes in wet years thereby giving the positive net global warming potential. A more fundamental understanding of how pasture management practices contribute to the local and global N_2O emissions allowed us to take step towards the development of land use and management policies to mitigate the climate change impacts.

5.1 Introduction

A steady increase in the concentration of the greenhouse gases in the atmosphere has been observed throughout the past decades (Change 2007; Mitchell et al. 1995; Solomon et al. 2009; Stocker 2014) and this is speculated to be a major causative factor in increasing the earth`s surface temperature and human induced global climate change (Crowley 2000; Keohane and Olmstead 2016; Pielke et al. 2002). Agriculture and livestock have been considered significant contributors of the greenhouse gas (GHGs) emissions (Garnett 2009; Searchinger et al. 2008; Steinfeld et al. 2006). Nitrous oxide (N_2O) one of the major GHGs from agriculture accounted for about 58% of the total global emissions, with about 16-33% of this total attributed to the direct emissions from grazing land (De Klein et al. 2008; Delgado et al. 2013). Both the croplands and grasslands of Southern Plains contribute significantly to the total GHGs emissions of the region. Approximately 43 tetragrams carbon dioxide equivalent (Tg CO_2 eq.) of net GHGs emissions has been reported from the agricultural sector (including crop, animal and forest) of US Southern Plains (Steiner et al. 2015). Out of the 32.9 Tg CO_2 eq. of total N_2O emissions in 2008 from Southern Plains, approximately more than half (17.3 Tg CO_2 eq.) was contributed from the grasslands (USDA, 2011). A grazing agro-ecosystem is complex, considering too many factors that are inter-related and influenced by local climate, soil environment and management decisions. Therefore, it is very unlikely that the experimental comparison of greenhouse gas emissions under different pasture management is feasible. Modeling simulation offers the only feasible method for systematically comparing two pasture management systems for a longer time period.

Beef cattle production is the main economic activity in Southern Plains of US. Grasslands that are primarily used as grazing pastures constitute the significant land-use area in the Southern Plains (Coppedge et al. 2001; Ji and Peters 2003) are also one of the most sensitive and important ecosystems of North America. With the US population expected to increase from 319 million to 417 million between 2014 and 2060 (US Census, 2014), the demand for beef is also expected to grow annually. Thus, the beef production will imply pressure on the grassland to produce more beef by grazing more or achieved more by converting native grassland into improved pasture. Intensive grazing or overgrazing in some parts of the continents has already resulted into land degradation (Oldeman 1994) thereby leading to the depletion of soil carbon stocks (Conant and Paustian 2002). However, studies showed that better pasture management can potentially sequester substantial quantities of C in the soil. Grassland is one of the largest carbon (C) sequestration pools of the atmospheric CO2 (Jones and Donnelly 2004; Lal 2004; Schuman et al. 2002). Globally more than 3.5 billion ha of grassland contained about 20% of the world`s soil carbon stocks (Ramankutty et al. 2008). More of the C in the grassland can be sequestered by improving the pasture by applying fertilizers, irrigation and other management inputs. Incorporation of legumes, application of irrigation and fertilizers, and planting of more productive forage species are considered improved management practices (IPCC, 2004) (Conant et al. 2001). About 14% and 17 % increase in SOC have been reported in the temperate and tropical grassland respectively with one of the improved management practices implied for 20 years (Ogle et al. 2004).

Native grasslands are improved with the aim of enhancing plant production potential. Managed pastures undergo various changes in quick succession compared to natural pasture caused by human management intervention. Activities like fertilizer application, deposition of manure by livestock, burning, tillage practices can have substantial influence on the fundamental biophysical processes such as mineralization and decomposition because addition of such managements inputs changes the soil Carbon (C) and Nitrogen (N) pool. This can alter the soil environmental conditions such as moisture, temperature, pH and Eh (redox potential) thereby increasing the magnitude of the greenhouse gas (GHG) emission. Due to the fact that there is a strong coupling between soil C and N dynamics, the changes in soil C driven by management factors could bring concomitant changes in soil N. While majority of the studies found improved pasture management as a potential mechanism to mitigate global warming by C sequestration (Ellis and Ramankutty 2008; Smith 2008; Smith et al. 2000), few studies have examined the associated impacts on N emissions from the soil (Conant et al. 2005). In one hand fertilization adds the biomass incorporation into the soil providing opportunity to sequester higher amounts of atmospheric CO_2. On the other hand, fertilization increases soil mineral N concentrations, causing more fluxes of N_2O from the ecosystem. N2O is a powerful biogenic GHG, which has 300 times global warming potential than CO_2 (Carlsson-Kanyama and González 2009; Lashof and Ahuja 1990). Therefore, the hypothesis to be tested is that the application of fertilizers in the improved pasture would increase the primary productivity of the ecosystem for few years but this increase in C sink would be counteracted by the increasing rate of GHGs emissions in the long run. We will be testing this hypothesis using the DeNitrification- DeComposition

(DNDC) model simulations. DNDC is a process-based model that simulates the emissions and consumption of gases within the ecosystem based on the interactive functions among local climate, local soils and on-site management practices (Giltrap et al. 2010; Li 2007). The combination of field measurements and modeling simulations help to examine the effects of grassland management practices on C sequestration and GHGs emissions. Specifically, the study will assess the effects of management practices on the net C balance and GHGs emissions in the managed pasture amended with fertilizers.

5.2. Materials and Methods

5.2.1 Basic description of DNDC model

DNDC is a process based biogeochemical model that simulates soil carbon, nitrogen dynamics, plant growth and biogenic GHGs via different sub models i.e. soil-climate/thermal hydraulic flux, decomposition and denitrification, plant growth, nitrification and fermentation (Li et al. 1992a). Conceptual model of DNDC consists of three layers. The outer layer of the model consists of ecological drivers or primary drivers which are the basic inputs such as climate, topography, soil, vegetation and human activities that turns on the model. The second layer is the biogeochemical field which is an assembly of soil environmental factors such as soil temperature, soil moisture, soil redox potential (Eh), soil pH, and substrate concentration. All these factors form the multi dimension field which determines the transfer and transformation of chemical elements within the field. The central part of the model consists of the core processes where biogeochemical reactions take place producing GHGs. GHGs are the products of redox reactions through electron exchange between electron donors and acceptors mediated by

microbes during the process of energy harnessing by breaking down the soil organic matter. Occurrence of the electron exchange is determined by the Eh of the soil as described by the Nerst equation:

$$Eh = E0 + RT/nF * \ln([B]/[C]) \quad (1)$$

Where, Eh= redox potential, volts

E0= standard redox potentials, volts

R= gas constants

T= temperature, Kelvins

F= Faraday constants,

B= Concentration of oxidant, mol

C= Concentration of reductant, mol

When the suitable Eh is established, the functional group of bacteria builds up their full capacity by rapid generation and horizontal gene transfer with in short period of time. After the microbes built up their capacity, the reactions rate is then controlled by the concentrations of the relevant nutrient substrates based on Michaelis-Menten equation:

$$R = Rmax * A / (Ka + A) * B / (Kb + B) \quad (2)$$

R= reaction rate

Rmax= maximum reaction rate

A, B = concentrations of substrate A and B (electron donors and acceptors)

Ka, Kb = half saturation constants for substrate A and B

Since both the reactions share a common factor i.e B (electron acceptors, the coupling of (1) and (2) are used for modeling the redox reactions.

Brief description of employed submodels:

1. Thermal Hydaulic flux (Soil-Climate)- simulation of soil temperature and soil moisture

The biogeochemistry of soil environment are mainly controlled by soil temperature and soil moisture. DNDC utilizes a cascade of equations in calculating average temperature and soil moisture profiles at daily time scale. The equations involved in calculation of temperature and moisture are gradient-driven equations. The difference in mean daily air temperature and the temperature of a soil at certain layer determine the heat flux between the soil surface and the atmosphere and is calculated using following equation series:

$$q_s = \frac{(T1 - Tair)}{(z1 - 0)} * -k_1 \quad (3)$$

$$q_{i,\,i-1} = \frac{(Ti - Ti-1)}{(zi - zi-1)} * -k_{\,i,\,i-1} \quad (4)$$

$$q_b = \frac{(T_{b1} - T_{mean})}{(z_{b1} - z_{deep})} * K_{bl} \quad (5)$$

where q is the heat flux (Js^{-1}), k is the soil thermal conductivity (J cm g-1 °C-1), T is the temperature (°C), Tair is the air temperature (°C), Tmean is the mean annual air temperature (°C), zbl is the depth at the bottom of the profile (cm) and zdeep is the depth where temperature variation is assumed to be negligible (5m). The subscripts 1, i and b represent the soil surface layer, ith layer and the bottom of soil profile respectively.

The model simulates soil moisture in terms of evapotranspiration as an output using precipitation and irrigation data as input data. At the beginning of each time step the model assumes water input saturates the soil layer by layer, where the surplus from one layer fills the next deep layer and the surface runoff and water intercepted by vegetation is not considered (Li et al. 1992). Evapotranspiration is calculated using the Thornthwaite equations:

$$PET = DAY * \left(\frac{1.6}{NM}\right) * \left(10 * \frac{T_m}{I}\right)^a \quad (6)$$

$$a = 0.49 + 0.07 * I - 7.71 * e^{-5} * I^2 + 6.75 * e^{-7} * I^3 \quad (7)$$

$$I = \sum_{n=1}^{12} \left(\frac{T_m}{5}\right)^{1.5} \quad (8)$$

where, *PET* is the potential evapotranspiration (cmd^{-1}), a is coefficient of *PET*, *DAY* is the $1/12^{th}$ fraction of the hours of a day (daylight hours), *NM* is the number of days in a month, and T_m is the mean monthly temperature (° C). The model consider PET is zero when the mean air temperature is below zero and the evapotranspiration is regulated by the volumetric soil water content (θ) as described by the following equations:

$E = PET$; if $\theta > \theta_{fc}$ (9)

$E = \left(\frac{(\theta - \theta_{wp}}{(\theta_{fc} - \theta_{wp})}\right) * PET$; if $\theta_{fc} > \theta > \theta_{wp}$ (10)

$PET = 0$; if $\theta < \theta_{wp}$ (11)

where E is the actual evapotranspiration (cmd^{-1}), θ is the actual soil water content (% water filled pore space), θ_{fc} is soil water content at field capacity and θ_{wp} is soil water content at plant wilting point.

2. The decomposition submodel

Depending on the simulated oxygen content of the soil, soil decomposition submodel alternates with the denitrification submodel. Three soil organic pools: plant decomposable residues, microbial biomass and humads are determined first and then the first order kinetics as in equations 9-11 are used to calculate the decomposition of labile and resistant components of each organic pools. The soil is either source or sink of C depending on the C/N ratio which also determines the speed of the decomposition process (Gilmour et al. 1985).

$$dC/_{dt} = \mu_{CLAY} * \mu_{CN} * \mu_{tn} * (S * k_1 + (1 - S) * k_r \quad (12)$$

$$\mu_{CLAY} = \log\left(\frac{0.14}{CLAY}\right) + 1 \quad (13)$$

$$\mu_{CN} = \frac{0.2+7.2}{(CP/_{NP})} \quad (14)$$

where, μ_{CLAY}, μ_{CN}, $and\ \mu_{tn}$ are the reduction factor for nitrification for clay content, *C/N* ratio and temperature respectively, *CLAY* is the fraction of clay in the soil, *S* is the labile organic *C* fraction in the pool, k_1 and k_r is the specific decomposition rate of labile and resistant fraction (d^{-1}), *CP* and *NP* are the carbon (kg C ha^{-1} d^{-1}) and nitrogen (kg N $ha^{-1}d^{-1}$) produced by the potential residue decomposition.

3. The denitrification submodel

The denitrification submodel is switched on under anaerobic condition, i.e. the rainfall events trigger the activity of denitrifiers and their potential growth rate (*(dB/dt)g)* and death rate (*(dB/dt)d)* are given by equations (12) and (13), respectively.

$$\left(dB/_{dt}\right)g = u_{DN} * B\ (t) \quad (15)$$

$$\left(dB/_{dt}\right)d = M_c * Y_c * B\ (t) \quad (16)$$

where, u_{DN} is the relative growth rate of denitrifiers and is calculated by equation (14) given by the relative growth rate of NO_3^-, NO_2^-, or N_2O denitrifiers (μ_{NXOY}), B(t) is the total biomass of denitrifiers (kg C ha^{-1}), M_c is the maintenance coefficient of carbon, and Y_c is the maximum growth yield on soluble carbon.

$$u_{DN} = \mu_{t,dm} * (\mu_{NO3} * \mu_{PHNO3} + \mu_{NO3} * \mu_{PHNO2} + \mu_{NO2} * \mu_{PHNO2} + \mu_{N2O} * \mu_{PHN2O} \quad (17)$$

Bacteria consumes the soluble carbon for cell synthesis and finally the CO2 production is the result from the excess of available carbon than that is required for the bacterial cell synthesis and is calculated by equations (15) and (16)

$$dC_{con}/_{dt} = \left(\mu_{DN}/_{Y_c} + M_c\right) * B(t) \quad (18)$$

$$dCO2/_{dt} = {}^{dC_{con,t}}/_{dt} - ({}^{dB}/_{dt})_g \quad (19)$$

where, ${}^{dC_{con}}/_{dt}$ is the change in the total consumption of soluble carbon over time, $dCO2/_{dt}$ is the change in CO_2 production over time.

3.1 Emissions of N_2 and N_2O and CH_4

N_2 and N_2O emissions from soil are calculated as a function of adsorption coefficient (AD) and air-filled porosity (PA) and is given by equations (17) and (18) respectively

$$P\ (N2) = 0.017 + ((0.025 - 0.0013 * AD) * PA \quad (20)$$

$$P\ (N2O) = (0.0006 + 0.0013 * AD) + (0.013 - 0.005 * AD) * PA \quad (21)$$

where, $P\ (N2)$ and $P\ (N2O)$ are the emitted fraction of the total N_2 and N_2O evolved in a day.

In DNDC, CH4 uptake in dry land is positively correlated with soil organic carbon, soil temperature, and negatively correlated with soil moisture. Specifically, it is calculated by using the following two equations:

$$CH_4uptake * = \frac{0.001 * soil\ temperature * (36.26 * \log(wrcvl + wrcl + wrcr + wcrb + wcrhl + wcrhr + whumus + 0.000001)}{28} \quad (22)$$

$$CH_4uptake = CH_4uptake * (0.5 * (1 - WFPS) \quad (23)$$

where soil temperature and WFPS are the soil temperature and moisture (in water filled porosity) of the first soil layer; wrcvl, wrcl, wrcr, wcrb, wcrhl, wcrhr, and whumus are content (in kg C ha^{-1}) of different soil organic carbon pools.

4. Crop growth submodel

This submodel helps DNDC to simulate the carbon turnover in soils using the daily crop growth curve (Giltrap et al. 2010). The climate-soil system and the crop growth are linked by the Nitrogen cycling (decomposition to plant growth). The plant biomass is computed from total N uptake, which is calculated from the crop potential maximum yield (derived from literature for each crop), and C/N ratio specific to that crop and is partitioned into different plant parts. Some or whole plants residues are again returned to the soil depending upon the harvest, tillage and grazing. A potential maximum biomass is calculated using the potential maximum yield and biomass partitioning ratios. The potential maximum Nitrogen uptake is calculated as a ratio between potential maximum biomass and estimated C/N ratio. The crop fractional growth obtained from the crop growth curved

is multiplied by the potential maximum Nitrogen uptake resulting into potential cumulative crop Nitrogen content. The crop Nitrogen demand is then simulated based on the availability of dissolved inorganic nitrogen in soil, determined from their concentration in the soil water solution and the current soil moisture(Li et al. 1994).

5.2.2 Development of the conceptual model

The management practices like fertilizers application and grazing in improve pasture will have impact on carbon dynamics, and greenhouse gas emissions mainly by three ways: a) Loss or gain of soil organic carbon (SOC) primarily depending on addition or decomposition of plants litter into the soil pool, b) changing the concentration of the substrates like NO_3^-, and c) by directly influencing the soil environment by changing soil pH and Eh (Fig. 1). The amount of SOC available for the microbes determines the amount of the gas emissions from the soil. Once the suitable environment is developed in the soil, particular group of microbes gets activated and their biomass is determined by the growth rate in the model. Fertilizer application will increase the plant production and generally that leads to the increment of SOC pool whereas grazing decreases the SOC of the soil pool. Farm management practices alter the soil moisture, temperature, redox potential, and SOC and available N content. The change in these factors will determine the rate and direction of nitrification, denitrification and decomposition either collectively or simultaneously.

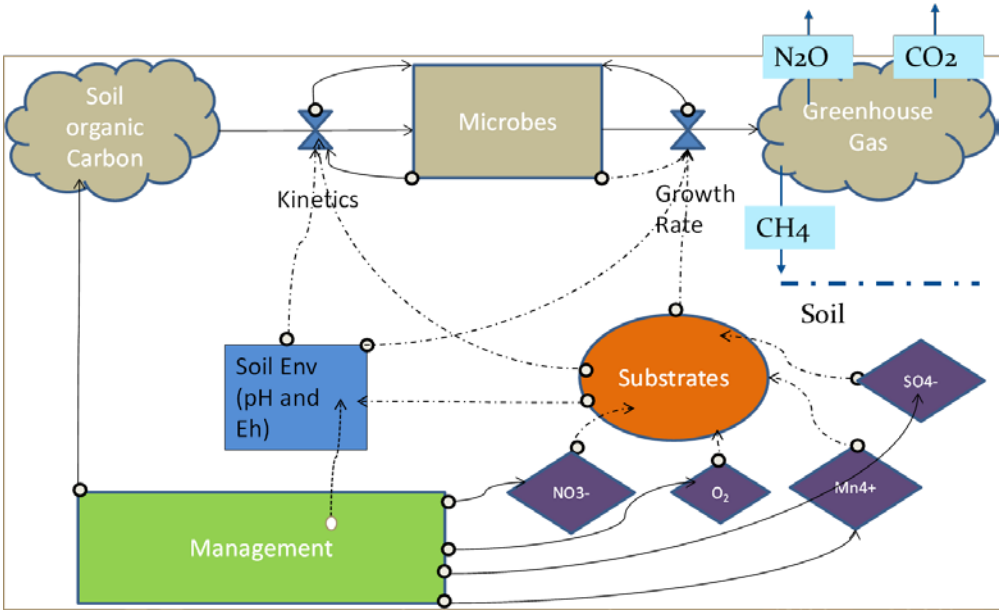

Figure 5.1. The sequential model framework representing management, soil environment and gas emissions dynamics.

5.2.3 Study sites and parameterization

The study sites i) native (98.03759°W, 35.5486565° N) and improved (98.04529 °W, 35.54679° N) pastures are located near El Reno, OK at the United States Department of Agriculture-Agriculture Research Service (USDA-ARS) Grazing Research laboratory (GRL). Both native and improved pasture sites are open terrain, slightly sloped from east to west and is covered by natural tallgrass prairie in silty clay loam soil with the annual average temperature 15 C and average annual preciptation is 794 mm.

Some of the parameters were selected from historical field and laboratory measurements. The climate, soil and crop parameters used for calibration of the model based on sensitivity analysis of Arango et. al, 2013 are presented in Table 1. The sensitive parameters identified were tested for a specified range by running the model in several interations which allowed the best calibration of the model under study site conditions.

Table 5.1 Climate, soil and crop parameters used on calibration of the model based on sensitivity analysis of Arango et. al, 2013 (Dissertation)

Serial Number	Parameters
	Climate
1	NH_3 and NH_4 in the rainfall
2	Temperature
3	Precipitation
	Soil
4	Bulk Density
5	pH
6	SOC at surface
7	Clay fraction
8	Field Capacity
9	Soil Microbial Index
	Crop
10	Maximum Yield
11	Total Degree Days

5.2.4 Model validation

Nine site years of data from three eddy covariance (EC) sites were used to validate the gross primary productivity (GPP) simulated from the model. The simulated GPP obtained by running DNDC for both native and managed pasture in 2005, 2006, 2014-2016 were used to compare the measured values. Model Efficiency (ME, equation (24) and the coefficient of determination (R^2) will be used to evaluate the performance of the model. The values of ME ranges from - ∞ to 1, where 1 corresponds an ideal fit of the observations. R^2 examines the relationship between model simulated values and field measurements.

$$ME = 1 - \frac{\sum_{j=1}^{n}(M_j - O_j)}{\sum_{j=1}^{n}(O_j - \overline{O})^2} \quad (24)$$

where, O, $\overline{O}$, M and n are measured, mean, modeled and total number of observation values, respectively.

5.2.5 Calculation of Global Warming Potential (GWP)

The GWP resulting from fertilizer applications in managed pasture was calculated for better understanding the influence of fertilizers in global warming. Net Global Warming Potential (NGWP) represents the net balance of GWP reulting from increaased N_2O flux and increased carbon uptake. The following equations were used to calculate the GWP and NGWP.

$$N_2O_{GWP} = (N_2O \text{ (kg } N_2O\text{-N ha}^{-1}) /28) * 44 * 298 \quad (25)$$

where 28 is the molecular weight of N in N_2O and 44 is the molecular weight of N2O and 298 is the global warming potential equivalent of 1 kg N_2O relative to reference gas (CO_2) in 100 years (IPCC, 2007).

$$SOC_{GWP} = (SOC_{SR} \text{ (kgCha}^{-1})/12) *44 \quad (26)$$

where SOC_{SR} is the sequestration rate of soil organic carbon obtained by change in SOC per year and 12 and 44 represents the molecular weight og C and CO_2 respectively.

$$CH_{4GWP} = CH_4 \text{ (kgCH}_4\text{-Cha}^{-1})/12 * 16 *25 \quad (27)$$

where 12 is the molecular weight of C in CH4 and 16 is the molecular weight of CH_4.The global warming potential of 1 kg CH4 is equivalent to 25 kg CO_2 (IPCC,2007)

$$NGWP = N_2O_{GWP} - SOC_{GWP} - CH_{4GWP} \quad (28)$$

5.3 Results

5.3.1 Comparison of modelled carbon fluxes with Eddy covariance (EC) measurements

The modeled results of Gross Primary Productivity (GPP) are plotted together with the EC measuremetns and are presented in Fig. 5.2. Despite the greater discrepancies between simulated GPP and observed GPP in natve pasture particularly in 2006 and 2016 , the model showed good performance in the peak growing season in other years at both pastures. In 2006 and 2016, GPP was over estimated towards the end of the growing season in native pasture (Fig. 5.1 e, g) but showed very consistent trends with the observed GPP for the rest of the growing season. Regardless of the year and sites, we observed consistenent over estimation of simulated GPP during the dry summer months of Oklahoma (June-August) except 2015. The year 2015 received above average rainfall at both sites and the simulated results showed consistently correspondance with the observed GPP values throughtout the year (Fig. 5.2 b,f).

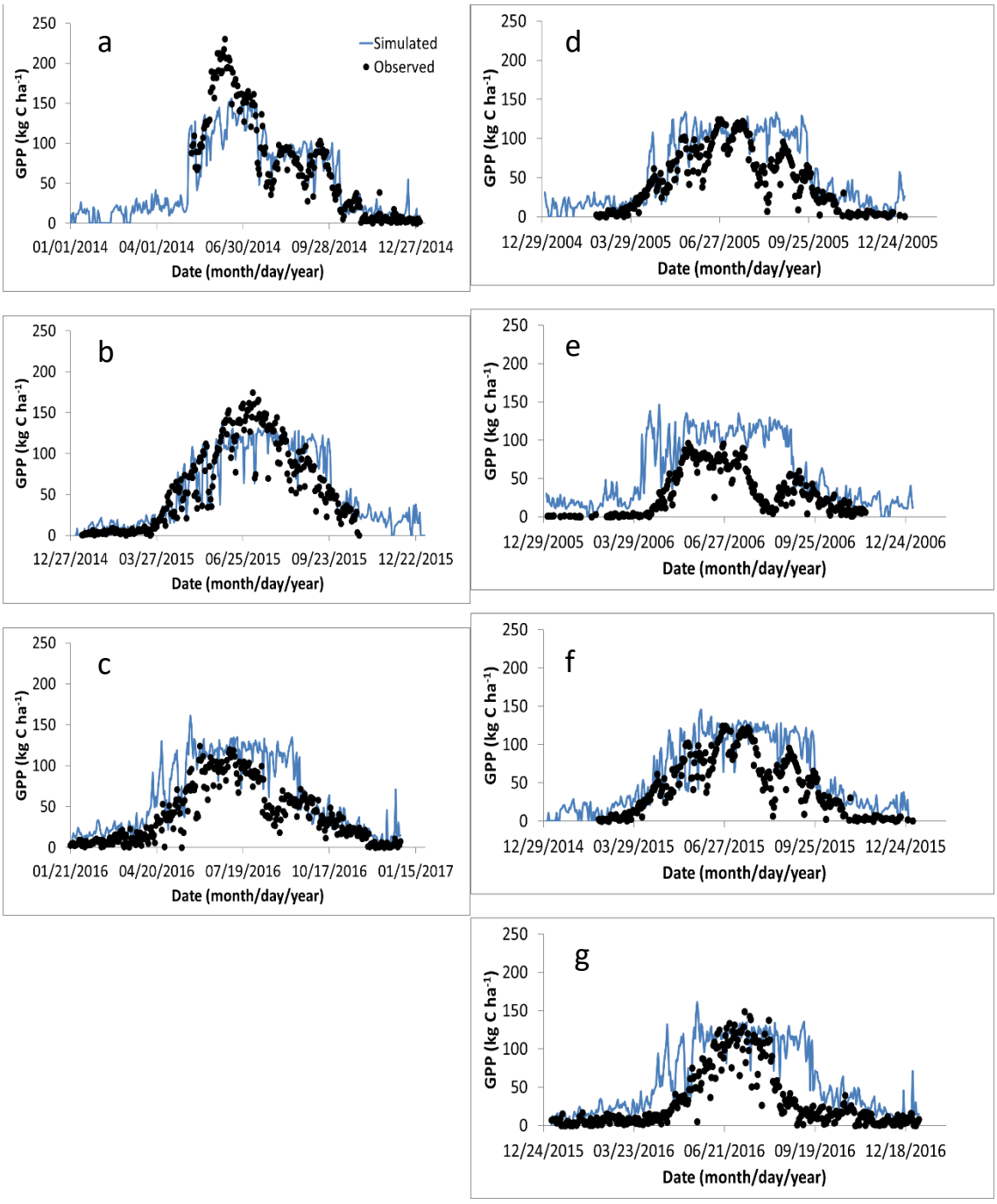

Figure 5.2 Seasonal dynamics of modelled simulated GPP and observed GPP from eddy covariance measurement of managed pasture (a-c) and native pasture (d-g).

When linear regression was applied to simulated and EC measured GPP values, the results showed varied coefficient of determination (R^2) and slope (Table 5.2). The overall

R^2 and slope values across sites and years were 0.73 and 0.84, respectively. However, the year 2006 in native pasture showed significant lower values of R^2 (0.5) and slope (0.48) whereas the highest R^2 (MP= 0.8, NP=0.8) and slope (MP= 0.99, NP= 0.95) was observed in the year 2015 at both sites.

Table 5.2 Coefficient of determination (R^2) for validation of the model results based on regression analysis between the observed and simulated GPP values.

		R^2	slope
MP	2014	0.76	1.13
	2015	0.8	0.99
	2016	0.72	0.64
NP	2005	0.74	0.76
	2006	0.5	0.48
	2015	0.8	0.95
	2016	0.76	0.9

5.3.2 Dynamics of Gross Primary Productivity (GPP) and Soil Organic Carbon (SOC) from 1999-2016: managed versus native pastures

The bar chart (Fig. 5.3) displays the simulated annual Gross Primary Productivity (GPP) and Soil Organic Carbon (SOC) from 1999 to 2016. As expected, the GPP and SOC of managed pasture were higher in years at the beginning of simulation (1999-2007) compared to the GPP and SOC of pasture under native condition. Both GPP and SOC at managed pasture site started to decline from 2009 and significantly decreased during drought spell of 2010-2012.The interannual variability in GPP and SOC was observed for

both managed and native pastures depending on the meterological conditions of the particular year. However, native pasture showed more resillience to rainfall variation than that by managed pasture. The productivity of the managed pasture was highest (22.31 thousands Kg C $ha^{-1}yr^{-1}$) in 2007 while the lowest (11.34 thousands Kg C $ha^{-1}yr^{-1}$) was observed in 1999. However, the highest (21.45 thousands Kg C $ha^{-1}yr^{-1}$) and lowest (10.26 thousands Kg C $ha^{-1}yr^{-1}$) productivity of native pasture was observed in 2016 and 19991,respectively (Fig. 5.3 a).

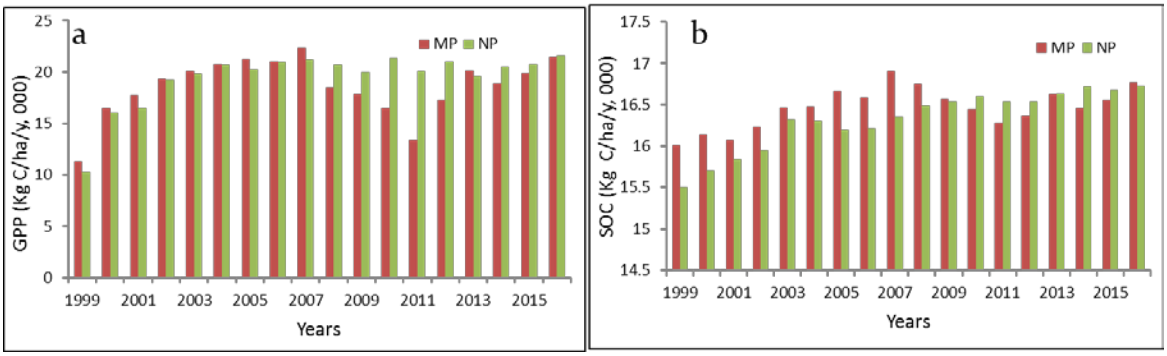

Figure 5.3. Interannual variability of Gross Primary Productivity (GPP) and soil organic carbon (SOC) at managed and native pasture sites.

The management activities (application of fertilizer) contributed higher soil organic carbon (SOC) in managed pasture sites at the first half of the study period (1999-2008). Similar to the GPP variation the managed pasture showed significant decline of SOC during the drought years (2010-2012) (Fig. 5.3 b). The addition of carbon to the soil in managed was greater (> 200 Kg C $ha^{-1}yr^{-1}$) for the first four years which decreased to around 7 Kg C $ha^{-1}yr^{-1}$ in 2012. The largest difference in SOC sequestration between the managed and native pasture was obtained in 2008, which showed about 289 Kg Kg C $ha^{-1}yr^{-1}$ was sequesterd moreby the managed pasture than did by native pasture. However, the

difference in SOC sequestration rate between managed and native pastures were variable depending upon the raifall amount.

5.3.3 Dynamics of N_2O and CH_4 fluxes from 1999-2016: managed versus native pastures

Although the magnitudes of N_2O fluxes varied largely between the years, the management activities in the managed pasture significantly contributed higher N_2O emissions in most of the years. About 1.7 Kg N ha^{-1} y^{-1} was released from the managed pasture in 2007 while it was only 0.8 Kg Kg N ha^{-1} y^{-1} from the native pasture. The lowest N_2O emissions was observed in 2001 from both pastures. Rainfall amount showed relationship to the magnitude of N_2O fluxes (Fig.5.4 a). In wet years (2007, 2013 and 2015) , both managed and native pastures showed higher emissions and the emissions was substantilly lowered in the dry years like 2003, 2006, and 2012 except 2011 where N_2O emissions from both pastures were relatively higher than other dry years.

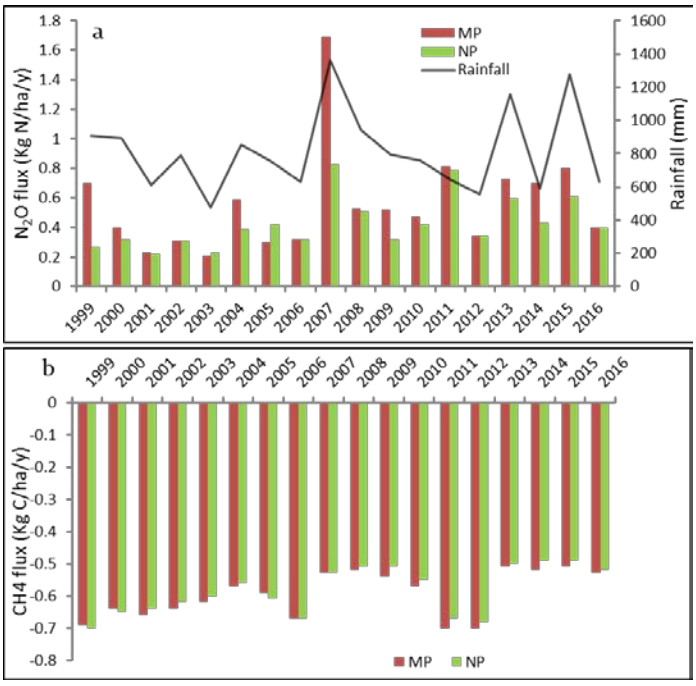

Figure 5.3. Total annual N_2O (a) and CH_4 fluxes (b) from managed and native pasture from 1999-2016. The black solid line represents the total annual rainfall in mm.

The methane fluxes in both pastures sites are negative indicating the net sink of methane gases during the study period. There was no any significant differences in the magnitude of CH4 fluxes between managed and netaive pastures, however small interannual variability was observed for both pastures (Fig. 5.4 b).

5.3.5 Seasonal dynamics of N_2O and CH_4 fluxes from managed and native pastures in dry and wet years

To understand the role of rainfall in N_2O and CH_4 emissions, the daily N_2O and CH_4 emissions from both managed and native pastures were simulated in wet (2007) and dry (2011) year and is presented in Figure 5.4. The signal of N_2O emissions was stronger from managed pasture regardless of the rainfall scenario, however the magnitude of emission was significantly higher in wet year than dry year. The signal of emission at about DOY=130 with amplified peak in 2007 was after the rainfall of 108 mm in DOY=128 (Fig. 5.5 a). The highest daily emission was about 0.13 Kg N ha^{-1} y^{-1} and 0.07 Kg N ha^{-1} y^{-1} from the improved and native pasture respectively in wet year (2007) but it was only about 0.09 Kg N ha^{-1} y^{-1} from both pastures in dry year (2011). This higher emissions signal of N_2O after the rainfall events indicated the significance of rainfall in N_2O emissions. Therefore, the application of fertilizer in managed pasture accompanied by the rainfall was more influential in terms of N_2O emissions. However, rainfall events did not show any impacts on the emissions of methane fluxes from both pastures. In both dry and wet years, the CH_4 fluxes from managed and native pastures did not vary and both pastures were sink of the CH_4 fluxes (Fig. 5.5 c,d).

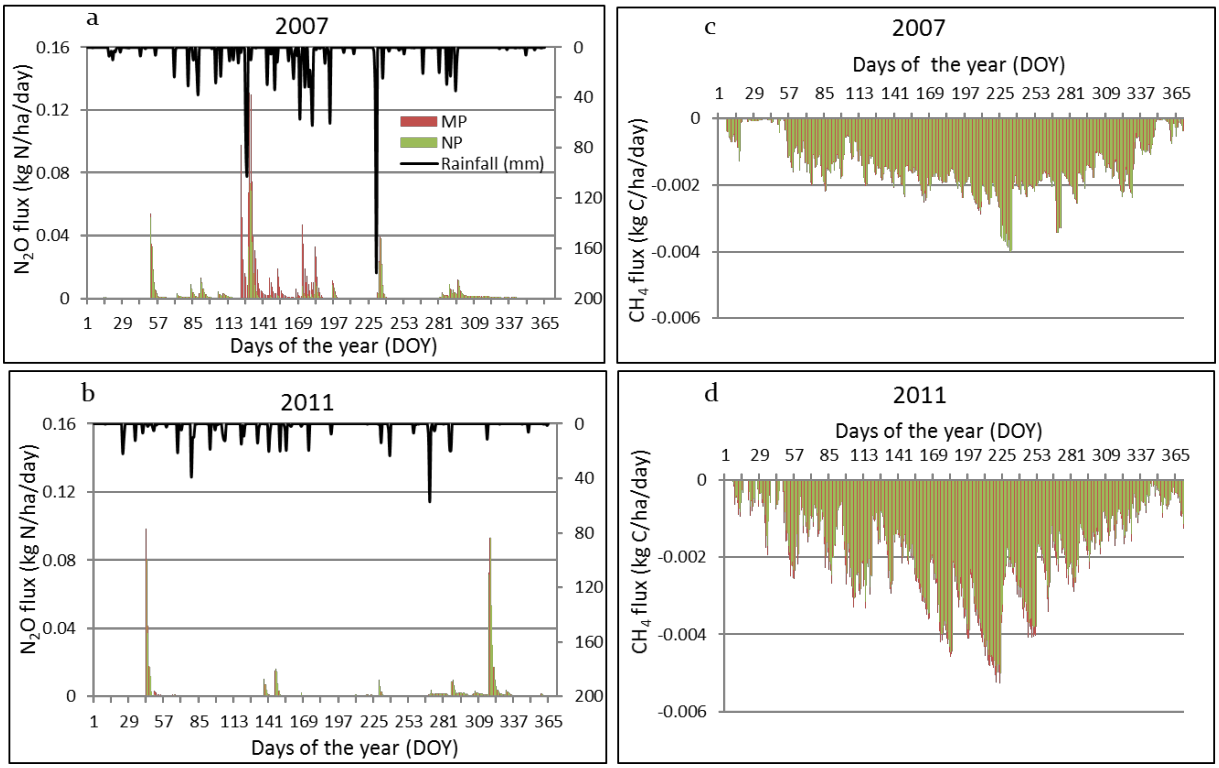

Figure 5.4 Daily dynamics of N2O and CH4 emissions from managed and native pastures in wet (2007) and dry (2011) year. The black bars represent the daily rainfall in mm.

5.3.6 Global warming potential (GWP) of soil organic carbon sequestration rate (SOC-R), N_2O and CH_4 and resulted net global warming potential (NGWP)

The global warming potential of soil organic carbon sequestration (GWP_{SOC-R}) was observed higher in the managed pasture than in the native pasture corresponded to the higher GPP. The highest (GWP_{SOC-R}) for managed pasture was observed in 2003 and the highest for native pasture was observed in 2007 (Fig 5.5 a) and there was large inter annual variation of GWP_{SOC-R} at both pasture sites dependent on the variation of SOC. The global warming potential of N_2O (GWP_{N2O}) is presented in figure 5.5, b. The GWP_{N2O} of managed pasture was significantly higher than that of native pasture most notably

on those wet years when the emissions were dependent on the rainfall events. For example, 2007 one of the wettest year had the highest (791 kg CO_2 -eq ha^{-1}) GWP $_{N2O}$ from the managed pasture and the N2O contributed about 389 kg CO_2 -eq ha^{-1} GWP from the native pasture in the same year. The net global warming potential (NGWP) calculated from GWP $_{SOC-R,}$ GWP $_{N2O,}$ and GWP $_{CH4}$ was observed positive for managed pasture and was significantly higher in the years with higher N_2O emissions. The NGWP for native pasture was negative in all years except 2004 (Fig 5.5 c).

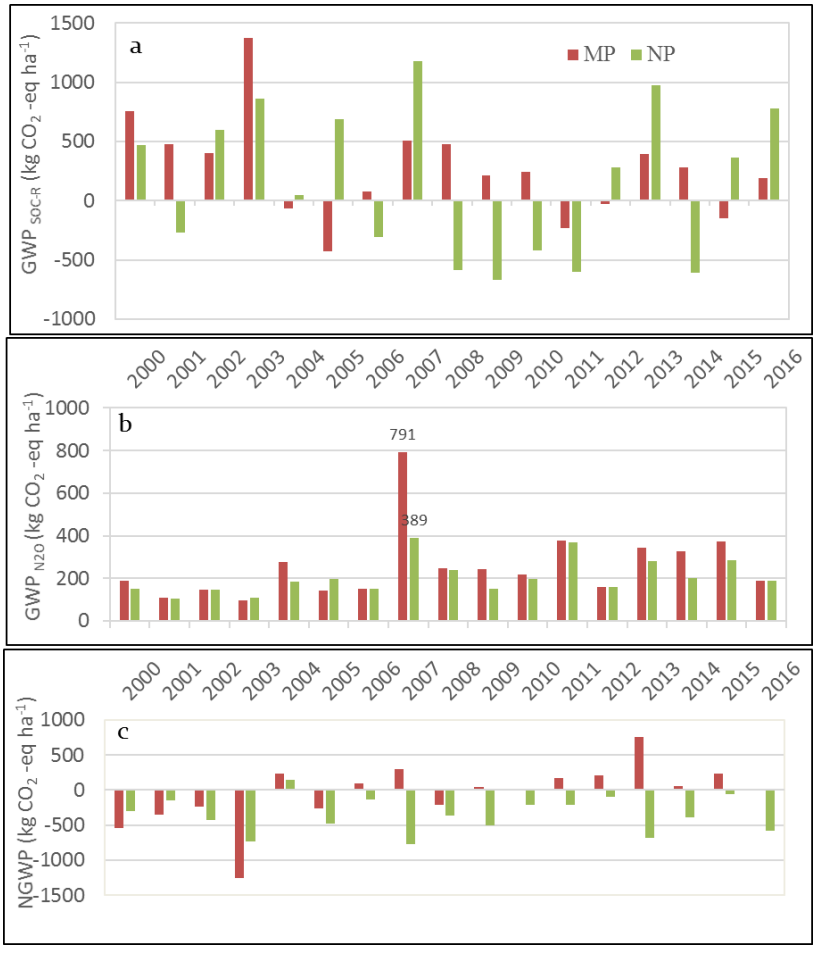

Figure 5.5 Yearly global warming potential (GWP) of soil organic carbon sequestration rate (SOC-R), N_2O and CH_4 and net global warming potential (NGWP) for managed and native pasture from 2000-2016.

5.4 Discussion

In the context of climate change and climatic variability many simulation studies from global climate models predicted rainfall in the future will either increase or decrease (Huntingford et al. 2003; Wang et al. 2005). Our results showed that the N_2O emissions was dependent on rainfall amount and distribution (Fig. 3.5). Higher rainfall contributed larger magnitudes of N_2O emissions in the managed pasture. At the same time, efforts in the future will be towards the increasing of grassland productivity by improving the pasture that demands the use of more chemical fertilizers. Many others studies in agriculture and grassland have showed the larger fluxes of greenhouse gases from the ecosystem as consistent with our study (Kessavalou et al. 1998; Mosier et al. 2006). However significant variation in N_2O emissions has been reported for temperate grasslands (Flechard et al. 2007; Rafique et al. 2011), native semi-arid grasslands (Du et al. 2006; Tian et al. 2010) and grasslands under varying soil conditions (Tian et al. 2010; Xu et al. 2008).The mean annual (1999-2016) N_2O emission rate of 0.43Kg N ha^{-1} in the native pasture was relatively higher from the mean emissions rate (0.09-0.16 Kg N ha^{-1}) reported from the Colorado shortgrass steppe between 1992-1994 (Mosier et al. 1996). However, the study reported increased N_2O emissions rates from the fertilized grassland from (0.21 – 0.83 Kg N ha^{-1}) which is similar to the mean rate we observed in our managed pasture (0.56 Kg N ha^{-1}). The considerable variations in the mean N_2O emissions (0.94, 0.16 and 0.1 Kg N ha^{-1}) from North American grassland has been observed in the previous studies based on different methods used such as process-based model (Tian et al. 2010), remote sensing model (Potter et al. 1996) and emprical model (Xu et al. 2008) respectively. The limited information on the N_2O rates from managed grassland of US has been available. However,

the syudies conducted in the grasslands of Europe, New Zealand and Australia showed significant increase in the emission rates of N_2O from fertilized pastures compared to native pastures(Burchill et al. 2014; Ding et al. 2004; Liu and Greaver 2009) .The inter-annual fluctuations on the emissions rate of N_2O was highly corresponded with the mean annual precipitation for example pluvial years (2007 and 2013) had the significant higher fluxes and the drought years (2006, 2011 and 2012) had significant lower fluxes, from both native and managed pastures due to the soil moisture a factor that regulate the soil denitrification processes (Conrad 1996). The control of rainfall on N_2O emissions consistent with our study has been reported in several other studies in the past (Butterbach-Bahl et al. 2013; Goldberg and Gebauer 2009; Ma et al. 2010).

The potential of pasture ecosystem to sink more atmospheric CO_2 by improving the pasture have been achieved in our study as in consistent with the arguments that managed grasslnd is one of the largest sink of atmospheric carbon via carbon sequestration (Ellis et al. 2010; Smith 2008) . The greater GPP in most of the years especially towrads the beginning of simulation provided the evidence that the productivity can be enhanced by improving the native pasture. However, the SOC sequestration rate was not consistent throught the period. Initial years sequestered the larger amounts of SOC while the potential of soil to sequester carbon in the soil decreased substantially, indicating the management of pasture by adding chemical fertilizers is not a sustainable mechanism to enhance the soil carbon sequestration potential. Therefore, in the long run this might be counterproductive for mitigating climate change due to the fact of higher green house gas emissions.

Pasture management such as application of fertilizers that change one type of GWP may also impact other GWP and therfore changes the NGWP (Mosier et al. 2006; Shang et al. 2011). In this study, addition of fertilizer in the pasture reduce the GWP by sequestration of more carbon into the soil and at the same time contributed to the larger amount of the N_2O emissions which offsetted the advantage gained from the increased SOC (Matson et al. 1998; Robertson et al. 2000). The GWP of the N_2O is greater than 298 factor equivalent to CO_2 which finally contributed for increased GWP therby resulting higher NGWP of managed pasture throught our study period (Fig 5.5 c). This is in agreement with the findings that the unmanaged ecosystem had lower GWP than the managed cropland during 1991-1999 in midwest US showing lower potentiality to mitigate the climate change due to higher GWP potential of N_2O emissions from the managed ecosystems (Robertson et al. 2000).

The results in this study indicate that the N_2O emissions from the managed pasture were controlled by the rainfall and nitrogen input. The significant contributions of the N_2O emissions to the NGWP from the managed pastures highlights the need for regular and long term measurement of the robust data from the manged pasture. This finding has the greater implications in the context of future volatility in raifall patterns has been predicted (Miraglia et al. 2009; Solomon 2007) and intensively managed pastures for increasing productivity productivity has been expected.

5.5 Conclusion

The management activities in pasture (managed pasture) increased the productivity that increased the roughages demands resulted by increased stocking density of cattle. The increased in productivity was measured in terms of GPP in managed pasture to that of native pasture particularly in years with good rainfall . Similarly, higher flux of N_2O from the managed pasture was resulted as the effect of fertilizer addition which amplified in magnitude in wet years than dry and normal years. The sesonal dynamics of N_2O flux was identified in correspondence with the rainfall distribution within the season. The advantage from increased SOC due to the fertilizer application, measured in terms of GWP was out weighed by the GWP calculated from the increased magnitude of N_2O fluxes in wet years thereby giving the positive NGWP. Therefore, pasture management policies should consider maintaining emissions level as minimum as possible while optimizing the productivity.

Chapter 6: Conclusions and Perspectives

Remote sensing indices have been widely used to study the ecosystem responses to climatic variability specially in drought assessment. The land use change and its impacts on change in carbon, water and energy flows from and to the ecosystems can be studied using the eddy covariance techniques. Similarly, various biogeochemical models are used to study the impacts of human management in emissions of greenhouse gases from the ecosystem. Therefore, this dissertation overall aims to understand the ecosystem responses to climatic variability and management practices using different approaches such as remote sensing, eddy covariance techniques and modelling.

Chapter 2 proposed a new approach of drought assessment, counting number of days with LSWI < 0 and based on this approach, an LSWI-based drought severity classification was developed. For this, 14 years of MODIS-derived VIs, Mesonet soil moisture and rainfall data at Marena and El Reno tallgrass prairie sites was used to study the impact of drought events on grassland phenology and growth through analyzing sensitivity differences of vegetation indices to drought. When three VIs were compared, LSWI decreased the most in drought years followed by EVI and NDVI, indicating that LSWI was the most sensitive indicator to the drought events. The number of days with LSWI < 0 was found higher during the summer droughts of 2006 and 2012, showing the ability of LSWI to track drought. LSWI values were more negative for the period of intensity drought categories (D2, D3 and D4) defined by USDM, demonstrating that LSWI could be used to describe the hydrological condition of the tallgrass prairie as an

effective additional VI for drought assessment. However, a more thorough evaluation of this approach as a drought monitoring tool for widely distributed grasslands and other vegetation types is required and will be the subject of future research.

Chapter 3 investigates the potential of the Land Surface Water Index (LSWI)-based algorithm developed in Chapter1, for agricultural drought monitoring under varying soil and land cover conditions of 113 Mesonet stations of Oklahoma. We compared LSWI and the number of days with negative LSWI (DNLSWI) to summer time precipitation, precipitation anomalies, and the U.S. Drought Monitor. Results of LSWI analysis for the period of 2000-2013 for 113 Mesonet stations across Oklahoma revealed valuable information within the context of drought tracking. A strong correlation and dynamics between LSWI-anomalies and summer rainfall anomalies comprises a fact that LSWI is sensitive to rainfall variations and can be used as an indicator of drought occurrence in an ecosystem. It is then deduced that DNLSWI had the close association with the vegetation condition under rainfall variations. There was a longitudinal sensitivity for low intensity droughts between eastern and western Oklahoma as shown by lower agreement of D0 and D1 drought with USDM in panhandle region (western Oklahoma). Results illustrated that drought intensity thresholds can be established by counting DNLSWI (in days) and used as a simple complementary tool in several drought applications for semi-arid and semi-humid regions of Oklahoma. However, larger discrepancies between USDM and the LSWI-based algorithm in arid regions of western Oklahoma suggest the requirement of further adjustment in the algorithm for its application in arid regions.

Chapter 4 aims to contrast CO_2 and H_2O fluxes between winter wheat and tallgrass prairie to provide insights on the impacts of conversion of tallgrass prairie to winter wheat on regional carbon and water budgets. Carbon dioxide and water vapor fluxes were measured using the eddy covariance system from two major ecosystems of the southern plains (winter wheat and tall grass prairie) in 2015 and 2016. The winter wheat site was a net sink of carbon for four months (February-May), whereas the tallgrass prairie site was a net sink of carbon for seven months (March-September). At the annual scale, the winter wheat site was a net source of carbon. In contrast, the tallgrass prairie site was a net sink of carbon. Similarly, the significant water loss due to evaporation from the fallow land (winter wheat-fallow rotation) when little carbon was fixed caused the winter wheat ecosystem to be less water efficient than the tallgrass prairie ecosystem despite higher growing season EWUE. Considering the large scale of land use conversion from prairie to winter wheat, our results indicate that the differences in magnitudes and patterns of CO_2 and H_2O fluxes between the two ecosystems can influence carbon and water budgets at the regional scale.

Chapter 5 tested the hypothesis that the application of fertilizers in the managed pasture would increase the primary productivity of the ecosystem for few years but this increase in carbon sink would be offsetted by the increasing rate of GHGs emissions in the long run. DeNitrification- DeComposition, a process-based model was used to simulate the emissions and consumption of gases within the ecosystem based on the interactions of local climate, local soils and on-site management practices. By combining field measurements

and modeling simulations, the effects of grassland management practices on the net C balance and GHGs emissions in the managed pasture amended with fertilizers was examined. Fertilizer application increased the plant production and generally leads to the increment of SOC pool whereas grazing decreased the SOC of the soil pool. Farm management practices alter the soil moisture, temperature, redox potential, and SOC and available N content. The change in these factors will determine the rate and direction of nitrification, denitrification and decomposition either collectively or simultaneously.

References

Albertson, F., Tomanek, G., & Riegel, A. (1957). Ecology of drought cycles and grazing intensity on grasslands of central Great Plains. *Ecological Monographs*, 27-44

Albertson, F., & Weaver, J. (1944). Nature and degree of recovery of grassland from the great drought of 1933 to 1940. *Ecological Monographs, 14*, 393-479

Amiro, B., Barr, A., Black, T., Iwashita, H., Kljun, N., McCaughey, J., Morgenstern, K., Murayama, S., Nesic, Z., & Orchansky, A. (2006). Carbon, energy and water fluxes at mature and disturbed forest sites, Saskatchewan, Canada. *Agricultural and forest meteorology, 136*, 237-251

Anthoni, P.M., Freibauer, A., Kolle, O., & Schulze, E.-D. (2004). Winter wheat carbon exchange in Thuringia, Germany. *Agricultural and forest meteorology, 121*, 55-67

Arndt, D.S., Basara, J.B., McPherson, R.A., Illston, B.G., McManus, G.D., & Demko, D.B. (2009). Observations of the overland reintensification of Tropical Storm Erin (2007). *Bulletin of the American Meteorological Society, 90*, 1079-1093

Aubinet, M., Grelle, A., Ibrom, A., Rannik, Ü., Moncrieff, J., Foken, T., Kowalski, A., Martin, P., Berbigier, P., & Bernhofer, C. (1999). Estimates of the annual net carbon and water exchange of forests: the EUROFLUX methodology. *Advances in ecological research, 30*, 113-175

Bajgain, R., Xiao, X., Basara, J., Wagle, P., Zhou, Y., Zhang, Y., & Mahan, H. (2017). Assessing agricultural drought in summer over Oklahoma Mesonet sites using the water-related vegetation index from MODIS. *International Journal of Biometeorology, 61*, 377-390

Bajgain, R., Xiao, X., Wagle, P., Basara, J., & Zhou, Y. (2015). Sensitivity analysis of vegetation indices to drought over two tallgrass prairie sites. *ISPRS Journal of Photogrammetry and Remote Sensing, 108*, 151-160

Barr, A.G., King, K., Gillespie, T., Den Hartog, G., & Neumann, H. (1994). A comparison of Bowen ratio and eddy correlation sensible and latent heat flux measurements above deciduous forest. *Boundary-Layer Meteorology, 71*, 21-41

Basara, J.B., & Christian, J.I. (2017). Seasonal and interannual variability of land–atmosphere coupling across the Southern Great Plains of North America using the North American regional reanalysis. *International Journal of Climatology*

Basara, J.B., & Crawford, K.C. (2002a). Linear relationships between root-zone soil moisture and atmospheric processes in the planetary boundary layer. *Journal of Geophysical Research: Atmospheres (1984–2012), 107*, ACL 10-11-ACL 10-18

Basara, J.B., & Crawford, K.C. (2002b). Linear relationships between root-zone soil moisture and atmospheric processes in the planetary boundary layer. *Journal of Geophysical Research: Atmospheres, 107*

Basara, J.B., Maybourn, J.N., Peirano, C.M., Tate, J.E., Brown, P.J., Hoey, J.D., & Smith, B.R. (2013a). Drought and associated impacts in the Great Plains of the United States-A review. *International Journal of Geosciences, 4*, 72

Basara, J.B., Maybourn, J.N., Peirano, C.M., Tate, J.E., Brown, P.J., Hoey, J.D., & Smith, B.R. (2013b). Drought and associated impacts in the Great Plains of the United States—A review

Belsky, A. (1986). Does herbivory benefit plants? A review of the evidence. *The American Naturalist, 127*, 870-892

Bhalme, H., Reddy, R., Mooley, D., & Murty, B.V.R. (1981). Solar activity and Indian weather/climate. *Proceedings of the Indian Academy of Sciences-Earth and Planetary Sciences, 90*, 245-262

Black, A., Brown, P., Halvorson, A., & Siddoway, F. (1981). Dryland cropping strategies for efficient water-use to control saline seeps in the northern Great Plains, USA. *Agricultural Water Management, 4*, 295-311

Boschetti, M., Nutini, F., Brivio, P.A., Bartholomé, E., Stroppiana, D., & Hoscilo, A. (2013). Identification of environmental anomaly hot spots in West Africa from time series of NDVI and rainfall. *ISPRS Journal of Photogrammetry and Remote Sensing, 78*, 26-40

Brock, F.V., Crawford, K.C., Elliott, R.L., Cuperus, G.W., Stadler, S.J., Johnson, H.L., & Eilts, M.D. (1995). The Oklahoma Mesonet: a technical overview. *Journal of Atmospheric and Oceanic Technology, 12*, 5-19

Brown, J.F., Wardlow, B.D., Tadesse, T., Hayes, M.J., & Reed, B.C. (2008). The Vegetation Drought Response Index (VegDRI): A new integrated approach for monitoring drought stress in vegetation. *GIScience & Remote Sensing, 45*, 16-46

Burba, G.G., & Verma, S.B. (2005). Seasonal and interannual variability in evapotranspiration of native tallgrass prairie and cultivated wheat ecosystems. *Agricultural and forest meteorology, 135*, 190-201

Burchill, W., Li, D., Lanigan, G.J., Williams, M., & Humphreys, J. (2014). Interannual variation in nitrous oxide emissions from perennial ryegrass/white clover grassland used for dairy production. *Global Change Biology, 20*, 3137-3146

Butterbach-Bahl, K., Baggs, E.M., Dannenmann, M., Kiese, R., & Zechmeister-Boltenstern, S. (2013). Nitrous oxide emissions from soils: how well do we understand the processes and their controls? *Phil. Trans. R. Soc. B, 368*, 20130122

Carlsson-Kanyama, A., & González, A.D. (2009). Potential contributions of food consumption patterns to climate change. *The American journal of clinical nutrition, 89*, 1704S-1709S

Ceccato, P., Flasse, S., & Gregoire, J.-M. (2002). Designing a spectral index to estimate vegetation water content from remote sensing data: Part 2. Validation and applications. *Remote sensing of Environment, 82*, 198-207

Ceccato, P., Flasse, S., Tarantola, S., Jacquemoud, S., & Grégoire, J.-M. (2001). Detecting vegetation leaf water content using reflectance in the optical domain. *Remote Sensing of Environment, 77*, 22-33

Chandrasekar, K., Sesha Sai, M., Roy, P., & Dwevedi, R. (2010). Land Surface Water Index (LSWI) response to rainfall and NDVI using the MODIS Vegetation Index product. *International Journal of Remote Sensing, 31*, 3987-4005

Chandrasekara, K., Saia, M.S., & Beheraa, G. (2011). Assessment of Early Season Agricultural Drought Through Land Surface Water Index (lswi) and Soil Water Balance Model. *ISPRS-International Archives of the Photogrammetry, Remote Sensing and Spatial Information Sciences, 3820*, 50-55

Change, I.P.O.C. (2007). Climate change 2007: The physical science basis. *Agenda, 6*, 333

Chen, D., Huang, J., & Jackson, T.J. (2005). Vegetation water content estimation for corn and soybeans using spectral indices derived from MODIS near-and short-wave infrared bands. *Remote Sensing of Environment, 98*, 225-236

Christian, J., Christian, K., & Basara, J.B. (2015a). Drought and Pluvial Dipole Events within the Great Plains of the United States. *Journal of Applied Meteorology and Climatology*

Christian, J., Christian, K., & Basara, J.B. (2015b). Drought and pluvial dipole events within the great plains of the United States. *Journal of Applied Meteorology and Climatology, 54*, 1886-1898

Claassen, R., Carriazo, F., Cooper, J.C., Hellerstein, D., & Ueda, K. (2011). Grassland to cropland conversion in the Northern Plains. *US Department of Agriculture, Economic Research Report*

Clark, D.B., Xue, Y., Harding, R.J., & Valdes, P.J. (2001). Modeling the impact of land surface degradation on the climate of tropical North Africa. *Journal of Climate, 14*, 1809-1822

Conant, R.T., & Paustian, K. (2002). Potential soil carbon sequestration in overgrazed grassland ecosystems. *Global Biogeochemical Cycles, 16*, 90-91-90-99

Conant, R.T., Paustian, K., Del Grosso, S.J., & Parton, W.J. (2005). Nitrogen pools and fluxes in grassland soils sequestering carbon. *Nutrient Cycling in Agroecosystems, 71*, 239-248

Conant, R.T., Paustian, K., & Elliott, E.T. (2001). Grassland management and conversion into grassland: effects on soil carbon. *Ecological Applications, 11*, 343-355

Conrad, R. (1996). Soil microorganisms as controllers of atmospheric trace gases (H2, CO, CH4, OCS, N2O, and NO). *Microbiological reviews, 60*, 609-640

Cooley, H., Riley, W., Torn, M., & He, Y. (2005). Impact of agricultural practice on regional climate in a coupled land surface mesoscale model. *Journal of Geophysical Research: Atmospheres, 110*

Coppedge, B.R., Engle, D.M., Fuhlendorf, S.D., Masters, R.E., & Gregory, M.S. (2001). Landscape cover type and pattern dynamics in fragmented southern Great Plains grasslands, USA. *Landscape Ecology, 16*, 677-690

Cramer, W., Kicklighter, D., Bondeau, A., Iii, B.M., Churkina, G., Nemry, B., Ruimy, A., Schloss, A., Intercomparison, T., & Model, P.O.T.P.N. (1999). Comparing global models of terrestrial net primary productivity (NPP): overview and key results. *Global Change Biology, 5*, 1-15

Crowley, T.J. (2000). Causes of climate change over the past 1000 years. *Science, 289*, 270-277

Dalgleish, H.J., & Hartnett, D.C. (2009). The effects of fire frequency and grazing on tallgrass prairie productivity and plant composition are mediated through bud bank demography. *Plant Ecology, 201*, 411-420

De Klein, C., Pinares-Patino, C., & Waghorn, G. (2008). Greenhouse gas emissions. *Environmental impacts of pasture-based farming'.(Ed. R McDowell) pp*, 1-33

Delgado, J.A., Nearing, M.A., Rice, C.W., & Donald, L. (2013). Conservation practices for climate change adaptation. *Advances in agronomy, 121*, 47-115

Dhuyvetter, K., Thompson, C., Norwood, C., & Halvorson, A. (1996). Economics of dryland cropping systems in the Great Plains: A review. *Journal of Production Agriculture, 9*, 216-222

Ding, W., Cai, Z., & Tsuruta, H. (2004). Cultivation, nitrogen fertilization, and set-aside effects on methane uptake in a drained marsh soil in Northeast China. *Global Change Biology, 10*, 1801-1809

Diodato, N., & Bellocchi, G. (2008). Modelling vegetation greenness responses to climate variability in a Mediterranean terrestrial ecosystem. *Environmental monitoring and assessment, 143*, 147-159

Dong, X., Xi, B., Kennedy, A., Feng, Z., Entin, J.K., Houser, P.R., Schiffer, R.A., L'Ecuyer, T., Olson, W.S., & Hsu, K.l. (2011). Investigation of the 2006 drought and 2007 flood extremes at the Southern Great Plains through an integrative analysis of observations. *Journal of Geophysical Research: Atmospheres, 116*

Du, R., Lu, D., & Wang, G. (2006). Diurnal, seasonal, and inter-annual variations of N 2 O fluxes from native semi-arid grassland soils of inner Mongolia. *Soil Biology and Biochemistry, 38*, 3474-3482

Ellis, E.C., Klein Goldewijk, K., Siebert, S., Lightman, D., & Ramankutty, N. (2010). Anthropogenic transformation of the biomes, 1700 to 2000. *Global ecology and biogeography, 19*, 589-606

Ellis, E.C., & Ramankutty, N. (2008). Putting people in the map: anthropogenic biomes of the world. *Frontiers in Ecology and the Environment, 6*, 439-447

Falge, E., Baldocchi, D., Olson, R., Anthoni, P., Aubinet, M., Bernhofer, C., Burba, G., Ceulemans, R., Clement, R., & Dolman, H. (2001). Gap filling strategies for defensible annual sums of net ecosystem exchange. *Agricultural and forest meteorology, 107*, 43-69

Farahani, H., Peterson, G., & Westfall, D. (1998a). Dryland cropping intensification: A fundamental solution to efficient use of precipitation. *Advances in agronomy (USA)*

Farahani, H., Peterson, G., Westfall, D., Sherrod, L., & Ahuja, L. (1998b). Soil water storage in dryland cropping systems: The significance of cropping intensification. *Soil Science Society of America Journal, 62*, 984-991

Fensholt, R., & Sandholt, I. (2003). Derivation of a shortwave infrared water stress index from MODIS near-and shortwave infrared data in a semiarid environment. *Remote Sensing of Environment, 87*, 111-121

Ferguson, C.R., & Wood, E.F. (2011). Observed land–atmosphere coupling from satellite remote sensing and reanalysis. *Journal of Hydrometeorology, 12*, 1221-1254

Field, C.B., Barros, V.R., Mach, K., & Mastrandrea, M. (2014). Climate change 2014: impacts, adaptation, and vulnerability. *Contribution of Working Group II to the Fifth Assessment Report of the Intergovernmental Panel on Climate Change*

Fischer, M.L., Billesbach, D.P., Berry, J.A., Riley, W.J., & Torn, M.S. (2007). Spatiotemporal variations in growing season exchanges of CO2, H2O, and sensible heat in agricultural fields of the Southern Great Plains. *Earth Interactions, 11*, 1-21

Fischer, M.L., Torn, M.S., Billesbach, D.P., Doyle, G., Northup, B., & Biraud, S.C. (2012). Carbon, water, and heat flux responses to experimental burning and drought in a tallgrass prairie. *Agricultural and forest meteorology, 166*, 169-174

Flanagan, P.X., Basara, J.B., & Xiao, X. (2017). Long-term analysis of the asynchronicity between temperature and precipitation maxima in the United States Great Plains. *International Journal of Climatology*

Flechard, C., Ambus, P., Skiba, U., Rees, R., Hensen, A., Van Amstel, A., Van Den Pol-Van Dasselaar, A., Soussana, J.-F., Jones, M., & Clifton-Brown, J. (2007). Effects of climate and management intensity on nitrous oxide emissions in grassland systems across Europe. *Agriculture, ecosystems & environment, 121*, 135-152

Foken, T. (2008). The energy balance closure problem: an overview. *Ecological Applications, 18*, 1351-1367

Ford, T.W., Quiring, S.M., Frauenfeld, O.W., & Rapp, A.D. (2015a). Synoptic conditions related to soil moisture-atmosphere interactions and unorganized convection in Oklahoma. *Journal of Geophysical Research: Atmospheres, 120*

Ford, T.W., Rapp, A.D., & Quiring, S.M. (2015b). Does afternoon precipitation occur preferentially over dry or wet soils in Oklahoma? *Journal of Hydrometeorology, 16*, 874-888

Gamon, J.A., Field, C.B., Goulden, M.L., Griffin, K.L., Hartley, A.E., Joel, G., Penuelas, J., & Valentini, R. (1995). Relationships between NDVI, canopy structure, and photosynthesis in three Californian vegetation types. *Ecological Applications*, 28-41

Gamon, J.A., Field, C.B., Roberts, D.A., Ustin, S.L., & Valentini, R. (1993). Functional patterns in an annual grassland during an AVIRIS overflight. *Remote sensing of Environment, 44*, 239-253

Gao, B.-C. (1996). NDWI—a normalized difference water index for remote sensing of vegetation liquid water from space. *Remote Sensing of Environment, 58*, 257-266

Garnett, T. (2009). Livestock-related greenhouse gas emissions: impacts and options for policy makers. *environmental science & policy, 12*, 491-503

Ghulam, A., Li, Z.-L., Qin, Q., & Tong, Q. (2007). Exploration of the spectral space based on vegetation index and albedo for surface drought estimation. *Journal of Applied Remote Sensing, 1*, 013529-013529-013512

Gillen, R.L., McCollum III, F.T., Tate, K.W., & Hodges, M.E. (1998). Tallgrass prairie response to grazing system and stocking rate. *Journal of Range Management*, 139-146

Gilmanov, T.G., Verma, S.B., Sims, P.L., Meyers, T.P., Bradford, J.A., Burba, G.G., & Suyker, A.E. (2003). Gross primary production and light response parameters of four Southern Plains ecosystems estimated using long-term CO2-flux tower measurements. *Global Biogeochemical Cycles, 17*

Gilmour, J., Clark, M., & Sigua, G. (1985). Estimating net nitrogen mineralization from carbon dioxide evolution. *Soil Science Society of America Journal, 49*, 1398-1402

Giltrap, D.L., Li, C., & Saggar, S. (2010). DNDC: A process-based model of greenhouse gas fluxes from agricultural soils. *Agriculture, ecosystems & environment, 136*, 292-300

Goldberg, S.D., & Gebauer, G. (2009). Drought turns a Central European Norway spruce forest soil from an N2O source to a transient N2O sink. *Global Change Biology, 15*, 850-860

Gu, Y., Hunt, E., Wardlow, B., Basara, J.B., Brown, J.F., & Verdin, J.P. (2008). Evaluation of MODIS NDVI and NDWI for vegetation drought monitoring using Oklahoma Mesonet soil moisture data. *Geophysical Research Letters, 35*

Guo, Z., & Dirmeyer, P.A. (2013). Interannual variability of land–atmosphere coupling strength. *Journal of Hydrometeorology, 14*, 1636-1646

Guo, Z., Dirmeyer, P.A., Koster, R.D., Sud, Y., Bonan, G., Oleson, K.W., Chan, E., Verseghy, D., Cox, P., & Gordon, C. (2006). GLACE: the global land–atmosphere coupling experiment. Part II: analysis. *Journal of Hydrometeorology, 7*, 611-625

Hartmann, T., Di Bella, C., & Oricchio, P. (2003). Assessment of the possible drought impact on farm production in the SE of the province of Buenos Aires, Argentina. *ISPRS Journal of Photogrammetry and Remote Sensing, 57*, 281-288

Haugland, M.J., & Crawford, K.C. (2005). The diurnal cycle of land–atmosphere interactions across Oklahoma's winter wheat belt. *Monthly weather review, 133*, 120-130

Heinsch, F.A., Zhao, M., Running, S.W., Kimball, J.S., Nemani, R.R., Davis, K.J., Bolstad, P.V., Cook, B.D., Desai, A.R., & Ricciuto, D.M. (2006). Evaluation of remote sensing based terrestrial productivity from MODIS using regional tower eddy flux network observations. *IEEE Transactions on Geoscience and Remote Sensing, 7*, 1908-1925

Herrmann, S.M., Anyamba, A., & Tucker, C.J. (2005). Exploring relationship between rainfall and vegetation dynamics in the Sahel using coarse resolution satellite data. *STATEMENT BY THE AUTHOR*, 79

Hickman, K.R., Hartnett, D.C., Cochran, R.C., & Owensby, C.E. (2004). Grazing management effects on plant species diversity in tallgrass prairie. *Journal of Range Management, 57*, 58-65

Hilker, T., Coops, N.C., Wulder, M.A., Black, T.A., & Guy, R.D. (2008). The use of remote sensing in light use efficiency based models of gross primary production: A review of current status and future requirements. *Science of the Total Environment, 404*, 411-423

Hoerling, M., Kumar, A., Dole, R., Nielsen-Gammon, J.W., Eischeid, J., Perlwitz, J., Quan, X.-W., Zhang, T., Pegion, P., & Chen, M. (2013). Anatomy of an extreme event. *Journal of Climate, 26*, 2811-2832

Hollinger, S., Isard, S., & Welford, M. (1993). A new soil moisture drought index for predicting crop yields. In, *Preprints, Eighth Conference on Applied Climatology* (pp. 187-190)

Huete, A., Didan, K., Miura, T., Rodriguez, E.P., Gao, X., & Ferreira, L.G. (2002). Overview of the radiometric and biophysical performance of the MODIS vegetation indices. *Remote Sensing of Environment, 83*, 195-213

Hui, D., Wan, S., Su, B., Katul, G., Monson, R., & Luo, Y. (2004). Gap-filling missing data in eddy covariance measurements using multiple imputation (MI) for annual estimations. *Agricultural and forest meteorology, 121*, 93-111

Hulse, J.H., & Escott, V.J. (1986). Drought–Inevitable and Unpredictable The Pattern and Consequences of Recurrent Drought. *Interdisciplinary Science Reviews, 11*, 346-358

Hunt, E.R., & Rock, B.N. (1989). Detection of changes in leaf water content using near-and middle-infrared reflectances. *Remote Sensing of Environment, 30*, 43-54

Hunt, E.R., Rock, B.N., & Nobel, P.S. (1987). Measurement of leaf relative water content by infrared reflectance. *Remote sensing of Environment, 22*, 429-435

Huntzinger, D.N., Post, W.M., Wei, Y., Michalak, A., West, T.O., Jacobson, A., Baker, I., Chen, J.M., Davis, K., & Hayes, D. (2012). North American Carbon Program (NACP) regional interim synthesis: Terrestrial biospheric model intercomparison. *Ecological Modelling, 232*, 144-157

Illston, B.G., Basara, J.B., Fiebrich, C.A., Crawford, K.C., Hunt, E., Fisher, D.K., Elliott, R., & Humes, K. (2008). Mesoscale monitoring of soil moisture across a statewide network. *Journal of Atmospheric and Oceanic Technology, 25*, 167-182

Jackson, R., Slater, P., & Pinter, P. (1983). Discrimination of growth and water stress in wheat by various vegetation indices through clear and turbid atmospheres. *Remote sensing of Environment, 13*, 187-208

Jackson, T.J., Chen, D., Cosh, M., Li, F., Anderson, M., Walthall, C., Doriaswamy, P., & Hunt, E.R. (2004). Vegetation water content mapping using Landsat data derived normalized difference water index for corn and soybeans. *Remote Sensing of Environment, 92*, 475-482

Jensen, J.R. (2009). *Remote sensing of the environment: An earth resource perspective 2/e*. Pearson Education India

Ji, L., & Peters, A.J. (2003). Assessing vegetation response to drought in the northern Great Plains using vegetation and drought indices. *Remote Sensing of Environment, 87*, 85-98

Jones, M., & Donnelly, A. (2004). Carbon sequestration in temperate grassland ecosystems and the influence of management, climate and elevated CO2. *New Phytologist, 164*, 423-439

Joo, E., Hussain, M.Z., Zeri, M., Masters, M.D., Miller, J.N., Gomez-Casanovas, N., DeLucia, E.H., & Bernacchi, C.J. (2016). The influence of drought and heat stress on long term carbon fluxes of bioenergy crops grown in the Midwestern US. *Plant, cell & environment*

Katul, G.G., Oren, R., Manzoni, S., Higgins, C., & Parlange, M.B. (2012). Evapotranspiration: A process driving mass transport and energy exchange in the soil-plant-atmosphere-climate system. *Reviews of Geophysics, 50*

Keohane, N.O., & Olmstead, S.M. (2016). Introduction. *Markets and the Environment* (pp. 1-10): Springer

Kimes, D., Markham, B., Tucker, C., & McMurtrey, J. (1981). Temporal relationships between spectral response and agronomic variables of a corn canopy. *Remote Sensing of Environment, 11*, 401-411

Kogan, F. (1995). Application of vegetation index and brightness temperature for drought detection. *Advances in Space Research, 15*, 91-100

Kogan, F. (2002). World droughts in the new millennium from AVHRR-based vegetation health indices. *Eos, Transactions American Geophysical Union, 83*, 557-563

Kogan, F., Stark, R., Gitelson, A., Jargalsaikhan, L., Dugrajav, C., & Tsooj, S. (2004). Derivation of pasture biomass in Mongolia from AVHRR-based vegetation health indices. *International Journal of Remote Sensing, 25*, 2889-2896

Kolberg, R., Kitchen, N., Westfall, D., & Peterson, G. (1996). Cropping intensity and nitrogen management impact of dryland no-till rotations in the semi-arid western Great Plains. *Journal of Production Agriculture, 9*, 517-521

Koster, R.D., Dirmeyer, P.A., Guo, Z., Bonan, G., Chan, E., Cox, P., Gordon, C., Kanae, S., Kowalczyk, E., & Lawrence, D. (2004). Regions of strong coupling between soil moisture and precipitation. *Science, 305*, 1138-1140

Lal, R. (2004). Soil carbon sequestration to mitigate climate change. *Geoderma, 123*, 1-22

Lark, T.J., Salmon, J.M., & Gibbs, H.K. (2015). Cropland expansion outpaces agricultural and biofuel policies in the United States. *Environmental Research Letters, 10*, 044003

Lashof, D.A., & Ahuja, D.R. (1990). Relative contributions of greenhouse gas emissions to global warming

Li, C. (2007). Quantifying greenhouse gas emissions from soils: Scientific basis and modeling approach. *Soil Science and Plant Nutrition, 53*, 344-352

Li, C., Frolking, S., & Frolking, T.A. (1992). A model of nitrous oxide evolution from soil driven by rainfall events: 1. Model structure and sensitivity. *Journal of Geophysical Research: Atmospheres, 97*, 9759-9776

Li, C., Frolking, S., & Harriss, R. (1994). Modeling carbon biogeochemistry in agricultural soils. *Global Biogeochemical Cycles, 8*, 237-254

Lillesand, T., Kiefer, R.W., & Chipman, J. (2014). *Remote sensing and image interpretation*. John Wiley & Sons

Liu, L., & Greaver, T.L. (2009). A review of nitrogen enrichment effects on three biogenic GHGs: the CO2 sink may be largely offset by stimulated N2O and CH4 emission. *Ecology letters, 12*, 1103-1117

Liu, L., Hong, Y., Bednarczyk, C.N., Yong, B., Shafer, M.A., Riley, R., & Hocker, J.E. (2012). Hydro-climatological drought analyses and projections using meteorological and hydrological drought indices: a case study in Blue River Basin, Oklahoma. *Water resources management, 26*, 2761-2779

Liu, W., & Kogan, F. (1996). Monitoring regional drought using the vegetation condition index. *International Journal of Remote Sensing, 17*, 2761-2782

Lloyd, J., & Taylor, J. (1994). On the temperature dependence of soil respiration. *Functional ecology*, 315-323

Luo, G., Han, Q., Zhou, D., Li, L., Chen, X., Li, Y., Hu, Y., & Li, B.L. (2012). Moderate grazing can promote aboveground primary production of grassland under water stress. *Ecological Complexity, 11*, 126-136

Lyon, D.J., Nielsen, D.C., Felter, D.G., & Burgener, P.A. (2007). Choice of summer fallow replacement crops impacts subsequent winter wheat. *Agronomy journal, 99*, 578-584

Ma, B., Wu, T., Tremblay, N., Deen, W., Morrison, M., McLaughlin, N., Gregorich, E., & Stewart, G. (2010). Nitrous oxide fluxes from corn fields: on-farm assessment of the amount and timing of nitrogen fertilizer. *Global Change Biology, 16*, 156-170

Maki, M., Ishiahra, M., & Tamura, M. (2004). Estimation of leaf water status to monitor the risk of forest fires by using remotely sensed data. *Remote Sensing of Environment, 90*, 441-450

Mallya, G., Zhao, L., Song, X., Niyogi, D., & Govindaraju, R. (2013). 2012 midwest drought in the United States. *Journal of Hydrologic Engineering, 18*, 737-745

Matson, P.A., Naylor, R., & Ortiz-Monasterio, I. (1998). Integration of environmental, agronomic, and economic aspects of fertilizer management. *Science, 280*, 112-115

McCorkle, T.A., Williams, S.S., Pfeiffer, T.A., & Basara, J.B. (2016). Atmospheric contributors to heavy rainfall events in the Arkansas-Red River Basin. *Advances in Meteorology, 2016*

McGee, E., Peterson, G., & Westfall, D. (1997). Water storage efficiency in no-till dryland cropping systems. *Journal of Soil and Water Conservation, 52*, 131-136

McKee, T.B., Doesken, N.J., & Kleist, J. (1993). The relationship of drought frequency and duration to time scales. In, *Proceedings of the 8th Conference on Applied Climatology* (pp. 179-183): American Meteorological Society Boston, MA

McPherson, R.A., Fiebrich, C.A., Crawford, K.C., Kilby, J.R., Grimsley, D.L., Martinez, J.E., Basara, J.B., Illston, B.G., Morris, D.A., & Kloesel, K.A. (2007). Statewide monitoring of the mesoscale environment: A technical update on the Oklahoma Mesonet. *Journal of Atmospheric and Oceanic Technology, 24*, 301-321

McPherson, R.A., & Stensrud, D.J. (2005). Influences of a winter wheat belt on the evolution of the boundary layer. *Monthly weather review, 133*, 2178-2199

McPherson, R.A., Stensrud, D.J., & Crawford, K.C. (2004). The impact of Oklahoma's winter wheat belt on the mesoscale environment. *Monthly weather review, 132*, 405-421

Meyers, T.P. (2001). A comparison of summertime water and CO 2 fluxes over rangeland for well watered and drought conditions. *Agricultural and forest meteorology, 106*, 205-214

Miraglia, M., Marvin, H., Kleter, G., Battilani, P., Brera, C., Coni, E., Cubadda, F., Croci, L., De Santis, B., & Dekkers, S. (2009). Climate change and food safety: an emerging issue with special focus on Europe. *Food and chemical toxicology, 47*, 1009-1021

Mitchell, J., Johns, T., Gregory, J., & Tett, S. (1995). *Climate response to increasing levels of greenhouse gases and sulphate aerosols*.

Mizzell, H.P., & Lakshmi, V. (2003). Integration of Science and Policy During the Evolution of South Carolina's Drought Program. *Water: Science, Policy, and Management: Challenges and Opportunities*, 311-339

Moffat, A.M., Papale, D., Reichstein, M., Hollinger, D.Y., Richardson, A.D., Barr, A.G., Beckstein, C., Braswell, B.H., Churkina, G., & Desai, A.R. (2007). Comprehensive comparison of gap-filling techniques for eddy covariance net carbon fluxes. *Agricultural and forest meteorology, 147*, 209-232

Mosier, A., Parton, W., Valentine, D., Ojima, D., Schimel, D., & Delgado, J. (1996). CH4 and N2O fluxes in the Colorado shortgrass steppe: 1. Impact of landscape and nitrogen addition. *Global Biogeochemical Cycles, 10*, 387-399

Mosier, A.R., Halvorson, A.D., Reule, C.A., & Liu, X.J. (2006). Net global warming potential and greenhouse gas intensity in irrigated cropping systems in northeastern Colorado. *Journal of Environmental Quality, 35*, 1584-1598

Narasimhan, B., & Srinivasan, R. (2005). Development and evaluation of Soil Moisture Deficit Index (SMDI) and Evapotranspiration Deficit Index (ETDI) for agricultural drought monitoring. *Agricultural and Forest Meteorology, 133*, 69-88

Nemani, R.R., & Running, S.W. (1989). Estimation of regional surface resistance to evapotranspiration from NDVI and thermal-IR AVHRR data. *Journal of Applied meteorology, 28*, 276-284

Ní Choncubhair, Ó., Osborne, B., Finnan, J., & Lanigan, G. (2016). Comparative assessment of ecosystem C exchange in Miscanthus and reed canary grass during early establishment. *GCB Bioenergy*

Nicholson, S.E. (1989). LONG-TERM CHANGES IN AFRICAN RAINFALL. *Weather, 44*, 46-56

Nicholson, S.E. (2000). The nature of rainfall variability over Africa on time scales of decades to millenia. *Global and planetary change, 26*, 137-158

Ogle, S.M., Ojima, D., & Reiners, W.A. (2004). Modeling the impact of exotic annual brome grasses on soil organic carbon storage in a northern mixed-grass prairie. *Biological Invasions, 6*, 365-377

Oldeman, L. (1994). The global extent of soil degradation. *Soil resilience and sustainable land use, 9*

Otkin, J.A., Anderson, M.C., Hain, C., Mladenova, I.E., Basara, J.B., & Svoboda, M. (2013). Examining rapid onset drought development using the thermal infrared–based evaporative stress index. *Journal of Hydrometeorology, 14*, 1057-1074

Otkin, J.A., Shafer, M., Svoboda, M., Wardlow, B., Anderson, M.C., Hain, C., & Basara, J. (2015). Facilitating the use of drought early warning information through interactions with agricultural stakeholders. *Bulletin of the American Meteorological Society, 96*, 1073-1078

Owensby, C.E., Ham, J.M., & Auen, L.M. (2006). Fluxes of CO 2 from grazed and ungrazed tallgrass prairie. *Rangeland Ecology & Management, 59*, 111-127

Palmer, W.C. (1965). *Meteorological drought*. US Department of Commerce, Weather Bureau Washington, DC, USA

Peters, A.J., Walter-Shea, E.A., Ji, L., Vina, A., Hayes, M., & Svoboda, M.D. (2002). Drought monitoring with NDVI-based standardized vegetation index. *Photogrammetric engineering and remote sensing, 68*, 71-75

Peterson, G., Schlegel, A., Tanaka, D., & Jones, O. (1996). Precipitation use efficiency as affected by cropping and tillage systems. *Journal of Production Agriculture, 9*, 180-186

Pettorelli, N., Vik, J.O., Mysterud, A., Gaillard, J.-M., Tucker, C.J., & Stenseth, N.C. (2005). Using the satellite-derived NDVI to assess ecological responses to environmental change. *Trends in ecology & evolution, 20*, 503-510

Pielke, R.A., Marland, G., Betts, R.A., Chase, T.N., Eastman, J.L., Niles, J.O., & Running, S.W. (2002). The influence of land-use change and landscape dynamics on the climate system: relevance to climate-change policy beyond the radiative effect of greenhouse gases. *Philosophical Transactions of the Royal Society of London A: Mathematical, Physical and Engineering Sciences, 360*, 1705-1719

Potter, C.S., Matson, P.A., Vitousek, P.M., & Davidson, E.A. (1996). Process modeling of controls on nitrogen trace gas emissions from soils worldwide. *Journal of Geophysical Research: Atmospheres, 101*, 1361-1377

Qin, Y., Xiao, X., Dong, J., Zhou, Y., Zhu, Z., Zhang, G., Du, G., Jin, C., Kou, W., & Wang, J. (2015). Mapping paddy rice planting area in cold temperate climate region through analysis of time series Landsat 8 (OLI), Landsat 7 (ETM+) and MODIS imagery. *ISPRS Journal of Photogrammetry and Remote Sensing, 105*, 220-233

Rafique, R., Hennessy, D., & Kiely, G. (2011). Nitrous oxide emission from grazed grassland under different management systems. *Ecosystems, 14*, 563-582

Ramankutty, N., Evan, A.T., Monfreda, C., & Foley, J.A. (2008). Farming the planet: 1. Geographic distribution of global agricultural lands in the year 2000. *Global Biogeochemical Cycles, 22*

Reichstein, M., Falge, E., Baldocchi, D., Papale, D., Aubinet, M., Berbigier, P., Bernhofer, C., Buchmann, N., Gilmanov, T., & Granier, A. (2005). On the separation of net ecosystem exchange into assimilation and ecosystem respiration: review and improved algorithm. *Global Change Biology, 11*, 1424-1439

Reichstein, M., Tenhunen, J.D., Roupsard, O., Ourcival, J.m., Rambal, S., Miglietta, F., Peressotti, A., Pecchiari, M., Tirone, G., & Valentini, R. (2002). Severe drought effects on ecosystem CO2 and H2O fluxes at three Mediterranean evergreen sites: revision of current hypotheses? *Global change biology, 8*, 999-1017

Riebsame, W.E. (1990). The United States Great Plains. *The earth as transformed by human action: Global and regional changes in the biosphere over the past 300 years*, 561-575

Robertson, G.P., Paul, E.A., & Harwood, R.R. (2000). Greenhouse gases in intensive agriculture: contributions of individual gases to the radiative forcing of the atmosphere. *Science, 289*, 1922-1925

Ruiz-Barradas, A., & Nigam, S. (2013). Atmosphere–land surface interactions over the Southern Great Plains: Characterization from pentad analysis of DOE ARM field observations and NARR. *Journal of Climate, 26*, 875-886

Santanello Jr, J.A., Peters-Lidard, C.D., Kennedy, A., & Kumar, S.V. (2013). Diagnosing the nature of land–atmosphere coupling: a case study of dry/wet extremes in the US Southern Great Plains. *Journal of Hydrometeorology, 14*, 3-24

Santanello Jr, J.A., Peters-Lidard, C.D., Kumar, S.V., Alonge, C., & Tao, W.-K. (2009). A modeling and observational framework for diagnosing local land–atmosphere coupling on diurnal time scales. *Journal of Hydrometeorology, 10*, 577-599

Santanello Jr, J.A., Roundy, J., & Dirmeyer, P.A. (2015). Quantifying the land–atmosphere coupling behavior in modern reanalysis products over the US Southern Great Plains. *Journal of Climate, 28*, 5813-5829

Schmidt, M., Reichenau, T.G., Fiener, P., & Schneider, K. (2012). The carbon budget of a winter wheat field: An eddy covariance analysis of seasonal and inter-annual variability. *Agricultural and forest meteorology, 165*, 114-126

Schuman, G., Janzen, H., & Herrick, J. (2002). Soil carbon dynamics and potential carbon sequestration by rangelands. *Environmental pollution, 116*, 391-396

Searchinger, T., Heimlich, R., Houghton, R.A., Dong, F., Elobeid, A., Fabiosa, J., Tokgoz, S., Hayes, D., & Yu, T.-H. (2008). Use of US croplands for biofuels increases greenhouse gases through emissions from land-use change. *Science, 319*, 1238-1240

Shafer, B., & Dezman, L. (1982). Development of a Surface Water Supply Index (SWSI) to assess the severity of drought conditions in snowpack runoff areas. In, *Proceedings of the Western Snow Conference* (pp. 164-175)

Shahid, S., & Behrawan, H. (2008). Drought risk assessment in the western part of Bangladesh. *Natural Hazards, 46*, 391-413

Shang, Q., Yang, X., Gao, C., Wu, P., Liu, J., Xu, Y., Shen, Q., Zou, J., & Guo, S. (2011). Net annual global warming potential and greenhouse gas intensity in Chinese double rice-cropping systems: a 3-year field measurement in long-term fertilizer experiments. *Global Change Biology, 17*, 2196-2210

Shukla, J., & Mintz, Y. (1982). Influence of land-surface evapotranspiration on the earth's climate. *Science, 215*, 1498-1501

Smith, P. (2008). Land use change and soil organic carbon dynamics. *Nutrient Cycling in Agroecosystems, 81*, 169-178

Smith, P., Powlson, D.S., Smith, J.U., Falloon, P., & Coleman, K. (2000). Meeting Europe's climate change commitments: quantitative estimates of the potential for carbon mitigation by agriculture. *Global Change Biology, 6*, 525-539

Solomon, S. (2007). *Climate change 2007-the physical science basis: Working group I contribution to the fourth assessment report of the IPCC*. Cambridge University Press

Solomon, S., Plattner, G.-K., Knutti, R., & Friedlingstein, P. (2009). Irreversible climate change due to carbon dioxide emissions. *Proceedings of the national academy of sciences, 106*, 1704-1709

Song, J., Willmott, C.J., & Hanson, B. (1997). Simulating the surface energy budget over the Konza Prairie with a mesoscale model. *Agricultural and forest meteorology, 87*, 105-118

Song, Y., & Ma, M. (2011). A statistical analysis of the relationship between climatic factors and the Normalized Difference Vegetation Index in China. *International Journal of Remote Sensing, 32*, 3947-3965

Sönmez, F.K., Koemuescue, A.U., Erkan, A., & Turgu, E. (2005). An analysis of spatial and temporal dimension of drought vulnerability in Turkey using the standardized precipitation index. *Natural Hazards, 35*, 243-264

Steiner, J.L., Schneider, J.M., Pope, C., Pope, S., Ford, P., Steele, R.F., & Anderson, T. (2015). Southern Plains assessment of vulnerability and preliminary adaptation and mitigation strategies for farmers, ranchers, and forest land owners

Steinfeld, H., Gerber, P., Wassenaar, T., Castel, V., Rosales, M., & De Haan, C. (2006). *Livestock's long shadow*. FAO Rome

Stocker, T. (2014). *Climate change 2013: the physical science basis: Working Group I contribution to the Fifth assessment report of the Intergovernmental Panel on Climate Change*. Cambridge University Press

Suyker, A.E., & Verma, S.B. (2001). Year-round observations of the net ecosystem exchange of carbon dioxide in a native tallgrass prairie. *Global Change Biology, 7*, 279-289

Suyker, A.E., Verma, S.B., & Burba, G.G. (2003). Interannual variability in net CO2 exchange of a native tallgrass prairie. *Global Change Biology, 9*, 255-265

Svoboda, M., LeComte, D., Hayes, M., Heim, R., Gleason, K., Angel, J., Rippey, B., Tinker, R., Palecki, M., & Stooksbury, D. (2002). The drought monitor. *Bulletin of the American Meteorological Society, 83*, 1181-1190

Tadesse, T., Brown, J.F., & Hayes, M.J. (2005). A new approach for predicting drought-related vegetation stress: Integrating satellite, climate, and biophysical data over the US central plains. *ISPRS Journal of Photogrammetry and Remote Sensing, 59*, 244-253

Tadesse, T., Wardlow, B.D., Brown, J.F., Svoboda, M.D., Hayes, M.J., Fuchs, B., & Gutzmer, D. (2015). Assessing the Vegetation Condition Impacts of the 2011 Drought across the US Southern Great Plains Using the Vegetation Drought Response Index (VegDRI). *Journal of Applied Meteorology and Climatology, 54*, 153-169

Thebault, A., Mariotte, P., Lortie, C.J., & MacDougall, A.S. (2014). Land management trumps the effects of climate change and elevated CO2 on grassland functioning. *Journal of Ecology, 102*, 896-904

Tian, H., Xu, X., Liu, M., Ren, W., Zhang, C., Chen, G., & Lu, C. (2010). Spatial and temporal patterns of CH4 and N2O fluxes in terrestrial ecosystems of North America during 1979-2008: application of a global biogeochemistry model. *Biogeosciences, 7*, 2673

Tian, Y., Zhou, L., Romanov, P., Yu, B., & Ek, M. (2013). Comparison of Amazon and Central Africa tropical vegetation dynamics using SEVIRI data from 2009 to 2011. In, *EGU General Assembly Conference Abstracts* (p. 6535)

Tubiello, F.N., Lin, G., Druitt, J., & Marino, B.D. (1999). Ecosystem-level evapotranspiration and water-use efficiency in the desert biome of Biosphere 2. *Ecological Engineering, 13*, 263-271

Tucker, C.J. (1980). Remote sensing of leaf water content in the near infrared. *Remote Sensing of Environment, 10*, 23-32

Turner, B.L., & Meyer, W.B. (1994). Global land-use and land-cover change: an overview. *Changes in land use and land cover: a global perspective, 4*

Twine, T.E., Kustas, W., Norman, J., Cook, D., Houser, P., Meyers, T., Prueger, J., Starks, P., & Wesely, M. (2000). Correcting eddy-covariance flux underestimates over a grassland. *Agricultural and forest meteorology, 103*, 279-300

U.S. Department of Agriculture. (2011). U.S. Agriculture and Forestry Greenhouse Gas Inventory: 1990- 2008 (C. C. P. Office, Trans.) (Vol. Technical Bulletin No., 1930, pp. 159): U.S. Department of Agriculture, Office of the Chief Economist.

Van Rooy, M. (1965). A rainfall anomaly index independent of time and space. *Notos, 14*, 43-48

Vick, E.S., Stoy, P.C., Tang, A.C., & Gerken, T. (2016). The surface-atmosphere exchange of carbon dioxide, water, and sensible heat across a dryland wheat-fallow rotation. *Agriculture, ecosystems & environment, 232*, 129-140

Wagle, P., & Kakani, V.G. (2014). Growing season variability in evapotranspiration, ecosystem water use efficiency, and energy partitioning in switchgrass. *Ecohydrology, 7*, 64-72

Wagle, P., Kakani, V.G., & Huhnke, R.L. (2015a). Net ecosystem carbon dioxide exchange of dedicated bioenergy feedstocks: Switchgrass and high biomass sorghum. *Agricultural and forest meteorology, 207*, 107-116

Wagle, P., Xiao, X., Scott, R.L., Kolb, T.E., Cook, D.R., Brunsell, N., Baldocchi, D.D., Basara, J., Matamala, R., & Zhou, Y. (2015b). Biophysical controls on carbon and water vapor fluxes across a grassland climatic gradient in the United States. *Agricultural and forest meteorology, 214*, 293-305

Wagle, P., Xiao, X., & Suyker, A.E. (2015c). Estimation and analysis of gross primary production of soybean under various management practices and drought conditions. *ISPRS Journal of Photogrammetry and Remote Sensing, 99*, 70-83

Wagle, P., Xiao, X., Torn, M.S., Cook, D.R., Matamala, R., Fischer, M.L., Jin, C., Dong, J., & Biradar, C. (2014). Sensitivity of vegetation indices and gross primary production of tallgrass prairie to severe drought. *Remote Sensing of Environment, 152*, 1-14

Wan, Z., Wang, P., & Li, X. (2004). Using MODIS land surface temperature and normalized difference vegetation index products for monitoring drought in the southern Great Plains, USA. *International Journal of Remote Sensing, 25*, 61-72

Wang, G., & Eltahir, E.A. (2000). Role of vegetation dynamics in enhancing the low-frequency variability of the Sahel rainfall. *Water Resources Research, 36*, 1013-1021

Wang, J., Price, K., & Rich, P. (2001). Spatial patterns of NDVI in response to precipitation and temperature in the central Great Plains. *International Journal of Remote Sensing, 22*, 3827-3844

Wayne Polley, H., Frank, A.B., Sanabria, J., & Phillips, R.L. (2008). Interannual variability in carbon dioxide fluxes and flux–climate relationships on grazed and ungrazed northern mixed-grass prairie. *Global Change Biology, 14*, 1620-1632

Weaver, C.P., & Avissar, R. (2001). Atmospheric disturbances caused by human modification of the landscape. *Bulletin of the American Meteorological Society, 82*, 269-281

Weaver, S.J., Baxter, S., & Harnos, K. (2016). Regional Changes in the Interannual Variability of US Warm Season Precipitation. *Journal of Climate, 29*, 5157-5173

Weghorst, K. (1996). The reclamation drought index: Guidelines and practical applications. In, *North American Water and Environment Congress & Destructive Water* (pp. 637-642): ASCE

Weiying, C., Qianguang, X., & Yongwei, S. (1994). Application of the anomaly vegetation index to monitoring heavy drought in 1992. *Remote Sensing of Environment, 9*, 106-112

Wilhite, D.A., & Glantz, M.H. (1985). Understanding: the drought phenomenon: the role of definitions. *Water international, 10*, 111-120

Wilson, K., & Baldocchi, D. (2001). Comparing independent estimates of carbon dioxide exchange over 5 years at a deciduous forest in the southeastern United States. *Journal of Geophysical Research. D. Atmospheres, 106*, 34

Wilson, K., Goldstein, A., Falge, E., Aubinet, M., Baldocchi, D., Berbigier, P., Bernhofer, C., Ceulemans, R., Dolman, H., & Field, C. (2002). Energy balance closure at FLUXNET sites. *Agricultural and forest meteorology, 113*, 223-243

Wright, C.K., & Wimberly, M.C. (2013). Recent land use change in the Western Corn Belt threatens grasslands and wetlands. *Proceedings of the National Academy of Sciences, 110*, 4134-4139

Xiao, X., Boles, S., Liu, J., Zhuang, D., & Liu, M. (2002). Characterization of forest types in Northeastern China, using multi-temporal SPOT-4 VEGETATION sensor data. *Remote Sensing of Environment, 82*, 335-348

Xu, X., Tian, H., & Hui, D. (2008). Convergence in the relationship of CO2 and N2O exchanges between soil and atmosphere within terrestrial ecosystems. *Global Change Biology, 14*, 1651-1660

Yang, L., Wylie, B.K., Tieszen, L.L., & Reed, B.C. (1998). An analysis of relationships among climate forcing and time-integrated NDVI of grasslands over the US northern and central Great Plains. *Remote Sensing of Environment, 65*, 25-37

Zeri, M., Anderson-Teixeira, K., Hickman, G., Masters, M., DeLucia, E., & Bernacchi, C.J. (2011). Carbon exchange by establishing biofuel crops in Central Illinois. *Agriculture, ecosystems & environment, 144*, 319-329

Zhang, G., Xiao, X., Dong, J., Kou, W., Jin, C., Qin, Y., Zhou, Y., Wang, J., Menarguez, M.A., & Biradar, C. (2015). Mapping paddy rice planting areas through time series analysis of MODIS land surface temperature and vegetation index data. *ISPRS Journal of Photogrammetry and Remote Sensing, 106*, 157-171

Zhang, N., Hong, Y., Qin, Q., & Liu, L. (2013). VSDI: a visible and shortwave infrared drought index for monitoring soil and vegetation moisture based on optical remote sensing. *International Journal of Remote Sensing, 34*, 4585-4609

Zhang, X., & Nearing, M. (2005). Impact of climate change on soil erosion, runoff, and wheat productivity in central Oklahoma. *Catena, 61*, 185-195

Zhou, Y., Xiao, X., Wagle, P., Bajgain, R., Mahan, H., Basara, J.B., Dong, J., Qin, Y., Zhang, G., & Luo, Y. (2017a). Examining the short-term impacts of diverse management practices on plant phenology and carbon fluxes of Old World bluestems pasture. *Agricultural and forest meteorology, 237*, 60-70

Zhou, Y., Xiao, X., Zhang, G., Wagle, P., Bajgain, R., Dong, J., Jin, C., Basara, J.B., Anderson, M.C., & Hain, C. (2017b). Quantifying agricultural drought in tallgrass prairie region in the US Southern Great Plains through analysis of a water-related vegetation index from MODIS images. *Agricultural and forest meteorology, 246*, 111-122